universität wien

DIPLOMARBEIT

Titel der Diplomarbeit

„Absence of glucosylation on N-linked glycans: consequences for ER-associated degradation (ERAD)“

Verfasser

Fikret Rifatbegović

angestrebter akademischer Grad

Magister der Naturwissenschaften (Mag.rer.nat.)

Wien, im Juli 2012

Studienkennzahl lt. Studienblatt:	A 490
Studienrichtung lt. Studienblatt:	Diplomstudium Molekulare Biologie
Betreuerin / Betreuer:	Ao. Univ.-Prof. DI Dr. N. Erwin Ivessa

Content

1. Introduction

1.1. Endoplasmic Reticulum

The endoplasmic reticulum (ER) is an organelle found in all eukaryotic cells. It has many functions including protein folding and modification, quality control of proteins, biogenesis of organelles and Ca^{2+} homeostasis (Kleizan & Braakman, 2004). ER is the central part of the secretory pathway and it has evolved into a staging ground for secretory protein synthesis. The secretory proteins are mostly synthesized by polyribosomes bound to the ER membrane. Through a translocation channel (Sec61), the proteins are co-translationally transported to the ER lumen, or inserted into the ER membrane (Benyair, et al., 2011).

The ER is a unique compartment where a set of covalent protein modifications take place, including the removal of the signal sequence and glycosyl-phosphatidylinositol (GPI) anchor addition (Anelli & Sitia, 2008). Further, the ER lumen provides a safe environment for protein folding, due to the oxidative conditions which facilitate the disulfide bond formation, and it is loaded with molecular chaperones which facilitate protein folding and prevent the formation of aggregates (Brodsky & Skach, 2011).

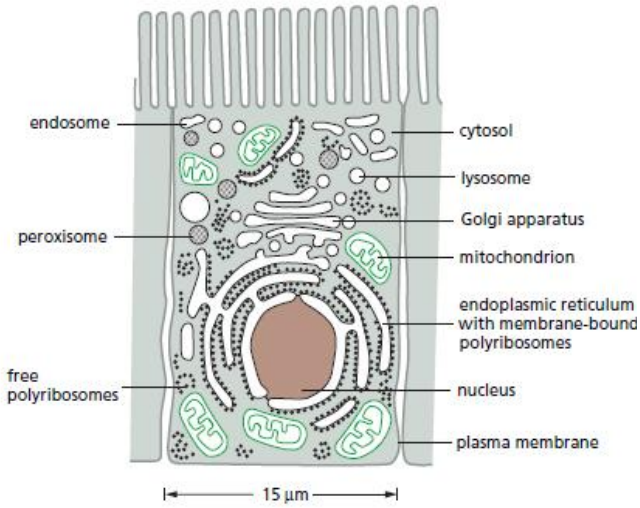

Figure 1. Intracellular compartments (Alberts, et al., 2004)
The major intracellular compartments of an animal cell are the cytosol, endoplasmic reticulum (ER), Golgi apparatus, mitochondria, endosomes and lysosomes. The ER encloses about half of the total membrane area. The majority of the ER membrane is ribosome bound, forming the rough ER. The part of ER which is oriented to the Golgi apparatus typically lacks ribosomes: smooth ER. This part represents the exit site of secretory proteins (Alberts, et al., 2004).

The ER is organized into a netlike labyrinth of branching tubules and flattened sacs (see figure 1). Its membrane constitutes more than half of the total membrane of an average animal cell. The tubules and sacs are connected, and their membranes are continuous with the outer nuclear membrane. The membrane is enclosing the so called ER lumen where protein folding and modification take place (Alberts, et al., 2008).

ER subcompartment	Main functions
Rough ER	Protein synthesis and folding
Smooth ER	Lipid synthesis, calcium storage
Nuclear envelope	Delineates nucleus
MAM	ER/mitochondria calcium homeostasis, apoptotic calcium signaling, lipid transfer
ERQC	Export of unfolded proteins to the proteasome
ERES	Export of proteins from ER to Golgi
PAM	Calcium import from extracellular space, sterol trafficking to plasma membrane
Russell bodies	Segregation of protein aggregates
Lipid droplets	Storage of triacylglycerides

Table 1. ER subcompartments and their functions (Lynes & Simmen, 2011)

Two main ER membrane regions can be distinguished: rough endoplasmic reticulum (rough ER) and smooth endoplasmic reticulum (smooth ER). The rough ER is the place of ribosomal attachment and protein biosynthesis, whereas the smooth ER lacks bound ribosomes. The smooth ER represents the exit site of proteins; ER exit sites (ERES). However, in specialized cells the smooth ER has additional functions (Alberts, et al., 2008). The smooth ER can form interfaces with other compartments like lysosomes; the Golgi-ER-lysosome compartment (GERL) and mitochondria; the ER-mitochondria interface (MAM). In addition, there are other smooth ER domains, including the plasma domain (PAM) and the ER quality control compartment (ERQC). On ERES, where the export of proteins is mediated, an intermediate compartment is generated; ER-Golgi intermediate compartment (ERGIC) (Lynes & Simmen, 2011). An overview of ER subcompartments is shown in table 1.

1.2. Protein synthesis in the ER

The synthesis of mammalian secretory and membrane proteins begins in the cytosol (Kleizan & Braakman, 2004). Then these proteins are bound by the signal recognition particle (SRP), which recognizes the proteins ER signal sequence and temporarily stops their elongation. These complexes are directed together with the ribosomes to the ER via the SRP receptor (SRP-R), where the synthesis continues (Alberts, et al., 2004). The ribosomes and protein translocation channels (translocons) mediate the production of secretory proteins. These translocons are made up of more than 20 polypeptides and are associated with the translocones associated protein complex (TRAP), translocating chain associated membrane protein (TRAM), oligosaccharyltransferase (OST), signal peptidase, SRP-R and accessory proteins (Lynes & Simmen, 2011). The growing polypeptide chains co-translationally enter the

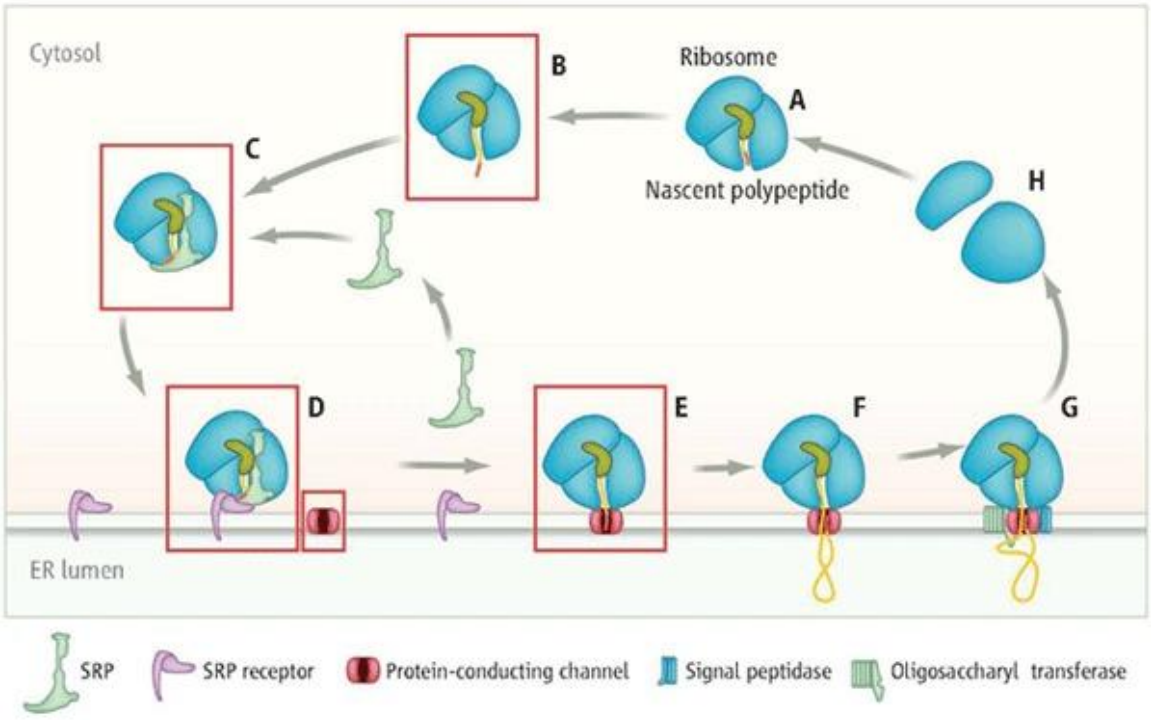

Figure 2. Cotranslational synthesis of proteins on the ER membrane (Kampmann & Blobel, 2009)
(A) Protein synthesis of ER resident and secretory proteins begins in the Cytosol. (B) The destination of proteins depends on the signal sequence which is synthesized in the polypeptide. Proteins without a signal sequence remains in the cytosol. (C) ER signal sequences are recognized by the Signal Recognition Particle (SRP) which binds to the polypeptide and the ribosomes, and temporally stops the synthesis. (D) The SRP-polypeptide-ribosome complex is recognized by the SRP receptor which is located on the ER membrane. This receptor recruits the complex to the translocon. After recruitment, the SRP and SRP receptor dissociate from the ribosome-polypeptide-translocon complex. (E, F, G) The growing polypeptide enters the ER lumen. (H) The ribosomes dissociate and bind to new transcripts (Kampmann & Blobel, 2009).

ER through the Sec61αβγ complex in an unfolded state (see figure 2) (Hebert, et al., 2009). Folding of these polypeptides starts immediately once the growing chain emerges in the ER lumen (Bagola, et al., 2011). The co-translational folding of proteins allows a sequential folding of the proteins, which greatly increases the folding efficiency (Kleizen & Braakman, 2004).

While entering the ER lumen, the polypeptides encounter a network of chaperones, which minimize aggregation, facilitate the formation of native structures and ensure oligomeric assembly. This network of chaperone systems involves i) non-covalent interactions with Hsp40, Hsp70 (Grp78/BiP/Kar2) and Hsp90 (Grp94) chaperones, ii) lectin based chaperones like calnexin (CNX) and calreticulin (CRT), and iii) protein disulfide isomerases (PDI) (Brodsky & Skach, 2011).

1.3. Glycosylation of proteins

The majority of secretory proteins are N-linked glycoproteins. During translocation across the ER membrane into the ER lumen, a precursor oligosaccharide is

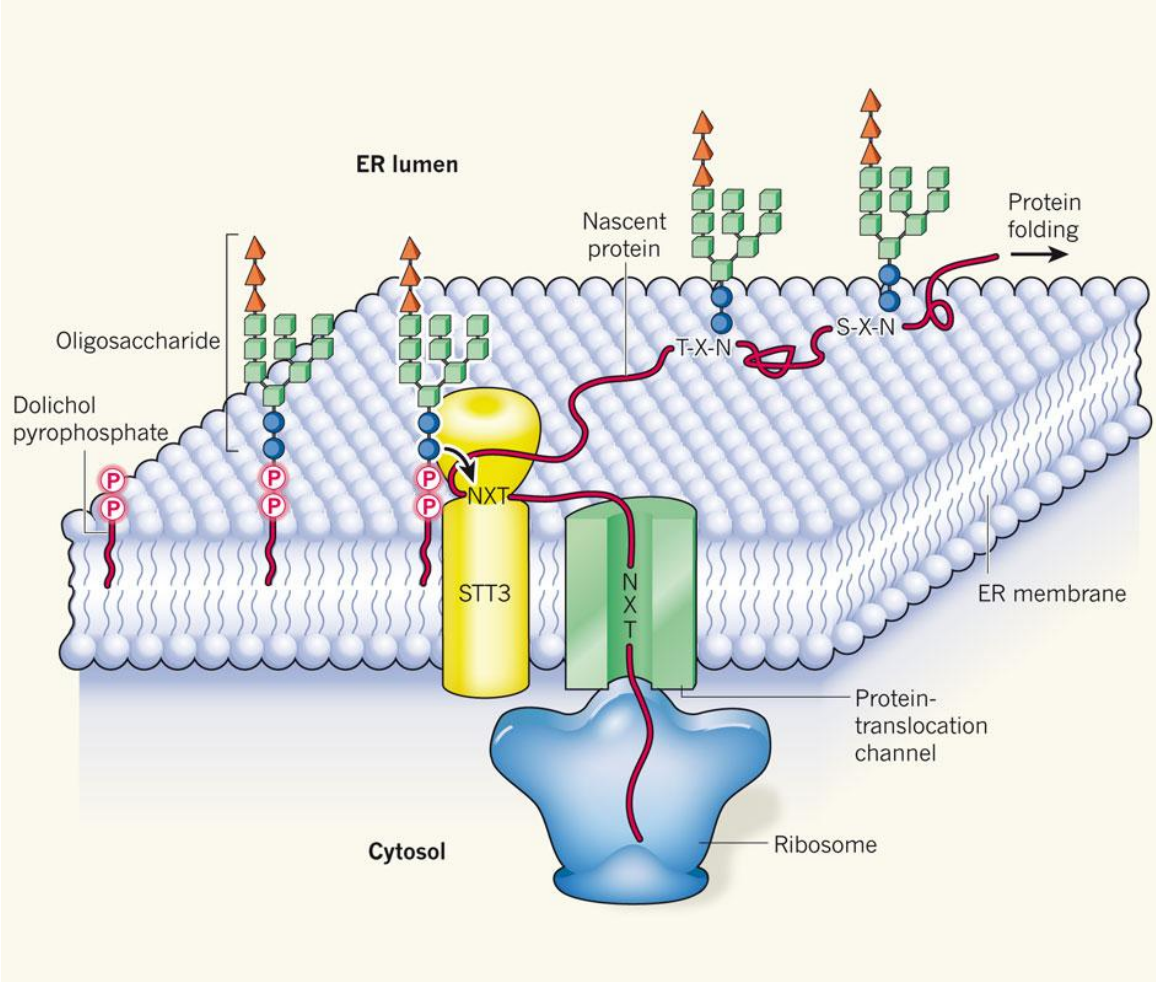

Figure 3. Protein glycosylation in the ER (Gilmore, 2011)
Most of the secretory proteins are N-glycosylated. The glycosylation is mediated by OST, a protein complex which transfers a precursor oligosaccharide from dolichol pyrophosphate to a consensus sequence of the growing polypeptide chain. Most commonly the polypeptide is transferred to a N-X-S or N-X-T sequence (Alberts, et al., 2008).

transferred to the NH_2 group of an asparagine, which is part of the consensus sequence asparagine-X-serine/threonine, where X can be any amino acid except proline (Alberts, et al., 2008). This central reaction of the pathway is mediated by OST which is a protein complex located in the membrane of the ER (see figure 3). The preformed oligosaccharide is transferred from a lipid linked oligosaccharide (LLO) donor (Mohorko, et al., 2011).

$Glc_3Man_9GlcNAc_2$ is the preferred substrate of eukaryotic OST (see figure 4). However, it was shown that different oligosaccharides can also serve as a substrate for the OST. The minimal glycan substrate of OST that still leads to a N-glycosidic linkage is the dolichol-linked monosaccharide Dol-PP-GlcNAc (Mohorko, et al., 2011). For long time it was unclear why such a large oligosaccharide precursor

($Glc_3Man_9GlcNAc_2$) is used for protein N-glycosylation, if it will later be extensively trimmed (Lederkremer, 2009). Nowadays it is known that the addition of such a complex N-glycan provides a molecular tag that can promote the folding, maturation, and quality control of a precursor. A defect N-glycosylation machinery can cause pathological consequences. (Wilson & Roebuck, 2008).

1.3.1. Oligosaccharyltransferase (OST)

The human OST is a heptameric complex containing the subunits ribophorin I, ribophorin II, OST48, OST4, Stt3p, N33/Tusc3 and IAP, and DAD1 (see figure 5) (Mohorko, et al., 2011). The catalytic center of the OST complex lies within the Stt3 subunit. In mammals, two STT3 isoforms exist: Stt3A and Stt3B (Wilson & Roebuck, 2008). Stt3 is the largest and most conserved polypeptide of the OST complex (Mohorko, et al., 2011). In the multimeric OST, some of the additional subunits fine-tune the glycosylation process (Schwarz & Aebi, 2011).

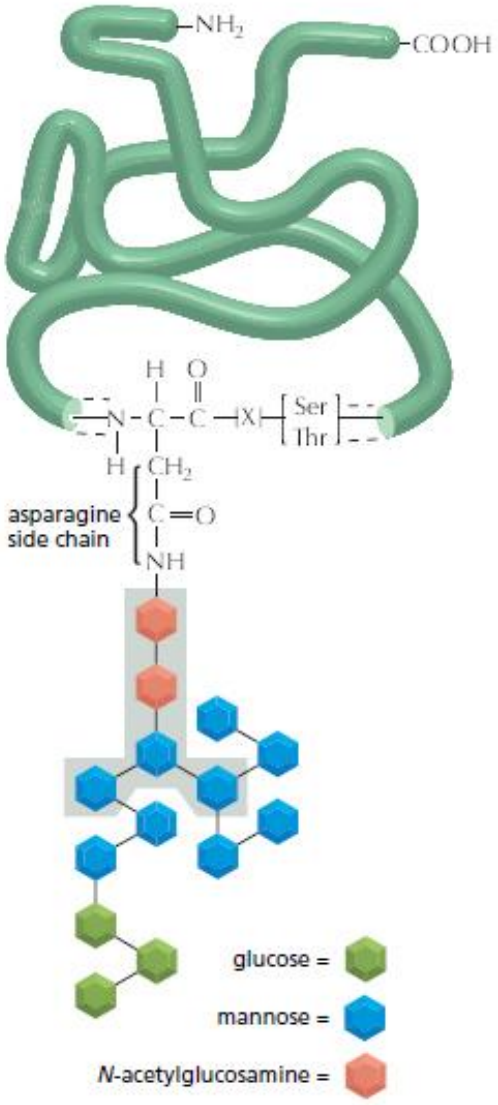

Figure 4. The N-linked glycan (Alberts, et al., 2004) The precursor oligosaccharide is composed of three glucose molecules (green), nine mannose molecules (blue) and two N-acetylglucosamins (red): $Glc_3Man_9GlcNAc_2$. In the ER the glycans are extensively trimmed and therefore in many glycoproteins only the core region of the glycans survives (highlighted with the gray box) (Alberts, et al., 2008).

1.3.2. Ribophorin I

Ribophorin I and II were the first identified subunits of the mammalian OST complex. It was initially proposed that ribophorin I recruits the dolichol bound glycan to the OST, and later studies suggested that ribophorin I might form part or all of the OST active site, although this now seems unlikely (High & Wilson, 2007). Ribophorin I is highly conserved among various species. The human ribophorin I sequence shows more than 90% similarity with homologous proteins in vertebrates (Mohorko, et al., 2011).

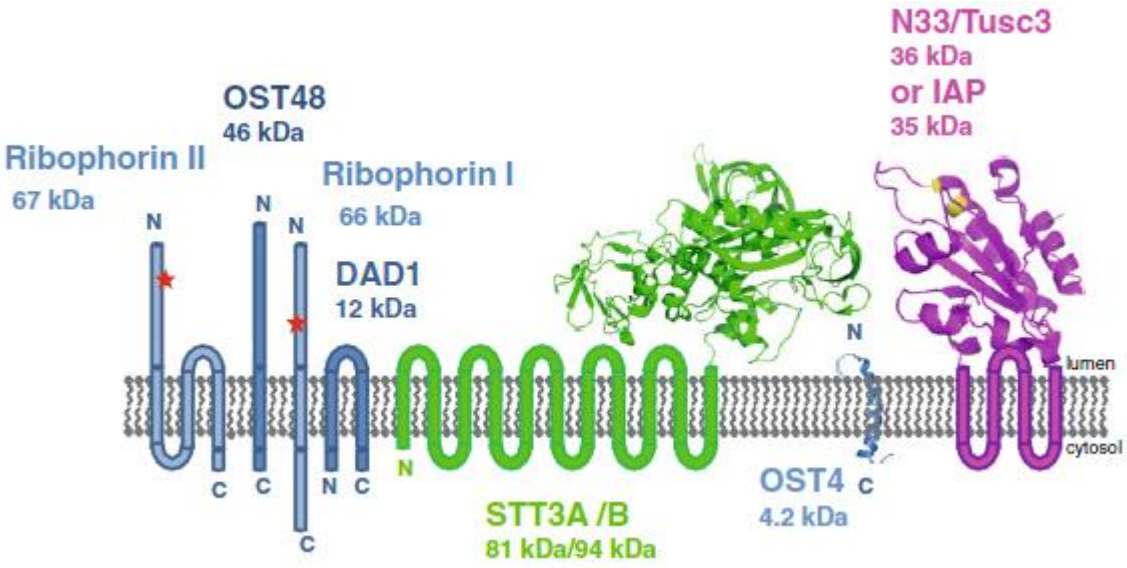

Figure 5. Human oligosaccharyltransferase complex (OST).
The human OST is a heptameric complex with following subunits: ribophorin I, ribophorin II, OST48, OST4, Stt3p, N33/Tusc3 and IAP, and DAD1. Some of the subunits have more isoforms, and therefore there are four variants of the human OST (Mohorko, et al., 2011).

Ribophorin I is a 68-kDa transmembrane protein with a single transmembrane helix, a large luminal domain and a smaller C-terminal cytosolic domain (Chotwiwatthanakun, et al., 2008). The parts of both ribophorins oriented towards the cytosol most probably provide binding sites for translating ribosomes. Interactions between ribophorins and ribosomes were detected in cross linking experiments, and it was shown that antibodies against the C-terminal cytosolic domain of ribophorin I prevent ribosome targeting to the ER membrane and in this way inhibit protein translocation (Mohorko, et al., 2011). Ribophorin I probably improves the efficiency of N-glycosylation of selected substrates (Wilson & High, 2007), but it is not essential for glycosylation per se (Mohorko, et al., 2011).

1.4. The secretory pathway

The secretory pathway ensures that newly synthesized proteins are delivered through the ER to their final destinations in the cell. It is also necessary for proteins to fold and to be modified (Reynaud & Simpson, 2002). The transported cargo includes membrane proteins, soluble proteins and secreted proteins. These proteins have a signal sequence in common which directs them to the ER where they are entering the secretory pathway (see above) (Bethune, et al., 2006).

The central organelle of the secretory pathway is the ER where proteins are synthesized and prepared for their further journey. However, the secretory pathway also includes other organelles which are all collectively described as the

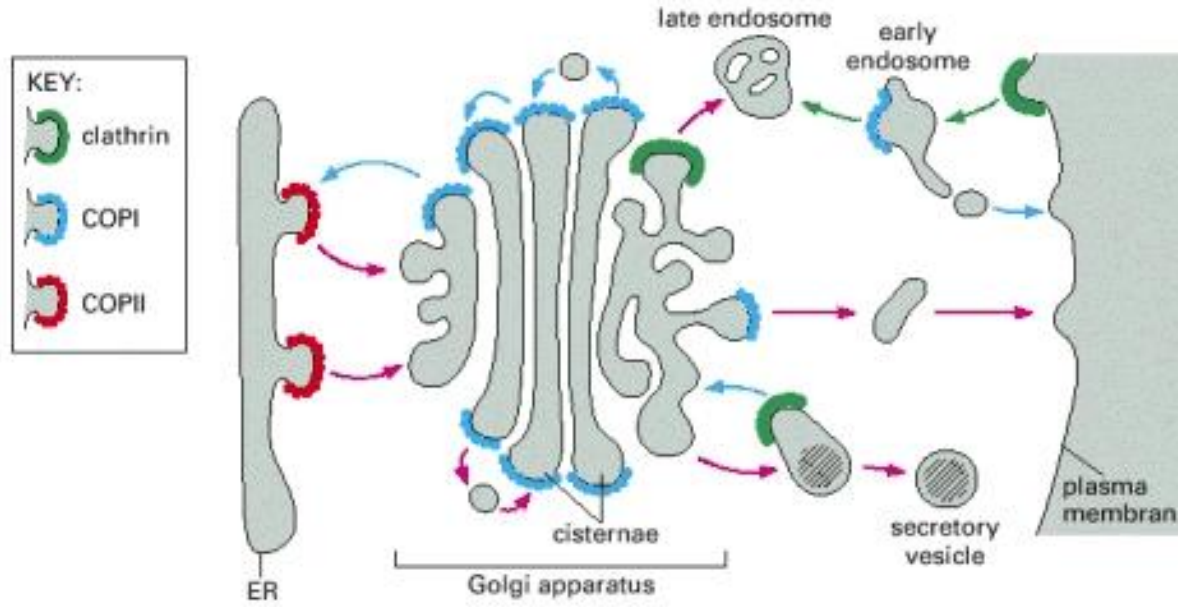

Figure 6. The different pathways of the coated vesicles (Alberts, et al., 2004)
Clathrin coated vesicles are present in the late secretory pathway. They transport their cargo from the plasma membrane to the early endosomes, and between endosomes and the Golgi apparatus. COPI and COPII coated vesicles are part of the early secretory pathway. COPI coated vesicles transport their cargo within the Golgi, and from the Golgi to the ER. The anterograde transport (from ER to the Golgi) is mediated by the COPII coated vesicles. (Lodish, et al., 2004).

endomembrane system. These compartments are interconnected by vesicular traffic (see figure 6) (Glick, 2002). During the vesicular transport, the transport vesicles supply the compartments with the appropriate proteins and lipids. This process is tightly regulated by the cell, and it is vectorial; vesicles generated from a donor compartment will only fuse with the cognate acceptor membrane (Spang, 2008).

So far three types of transport vesicles have been characterized in detail: i) coat protein complex I (COPI) - coated vesicles, ii) coat protein complex II (COPII) – coated vesicles and clathrin-coated vesicles (Gerdes, 2008). These vesicles are generated and fused by a number of processes in which different players are involved: GTPases, SNARE proteins and the cargo itself (see table 2) (Spang, 2008). A general scheme of coated vesicle formation is shown in figure 7. The clathrin coated vesicles transport their cargo from the plasma membrane and between endosomal and Golgi compartments. The COPI and COPII coated vesicles transport their cargo in the early secretory pathway: COPII coated vesicles transport their cargo from the ER exit sites to the Golgi (anterograde transport); COPI coated vesicles transport their cargo mainly within the Golgi apparatus and from the *cis*-Golgi to the ER (retrograde transport) (Lodish, et al., 2004). The transport vesicles and the appropriate pathways are briefly described below.

1.4.1. COPII – coated vesicles: export from the ER

Properly folded proteins are packed and transported further in the secretory pathway via COPII transport vesicles which, in most cell types, bud from the ER exit sites (ERES) (Glick, 2002). The ERES, which are relatively immobile structures, face out towards assemblies of vesicular-tubular structures called ER-Golgi intermediate compartment (ERGIC) clusters. These structures are cargo-rich compartments which mediate the trafficking of secretory proteins between ER and Golgi (Hughes & Stephens, 2008). The ERGIC compartment is defined by the presence of ERGIC-53, which is a mannose - dependent lectin (Bethune, et al., 2006).

To ERES, the GTPase Sar1 has to be recruited. This is done with the help of the guanine nucleotide exchange factor (GEF) Sec12. Further, a complex on the ER membrane is assembled by Sar1, the GTPase activating protein (GAP) Sec23, the cargo recruiter Sec24 and the cargo (Spang, 2008). Sec23 stimulates the hydrolysis of Sar1p-GTP to Sar1p-GDP which leads to the budding from the donor membrane (Murshid & Presley, 2004).

1.4.2. COPI – coated vesicles: retrograde transport

After the cargo leaves the ER membrane, it is found in the ERGIC. This compartment contains COPII and COPI markers: it is a interface between COPII and COPI mediated transport. From ERGIC, the cargo is transported to the *cis*-Golgi. This transport is probably COPI independent (Bethune, et al., 2006). The cargo moves from the *cis* site successively to the medial and *trans* cistern. During this journey, the proteins are additionally modified (Glick, 2002). The anterograde transport within the Golgi-apparatus seems to be COPI dependent, as well as the retrograde transport of material back to the ER. In the trans-Golgi network the cargo is sorted for targeting to the final destinations: lysosomes, endosomes and the plasma membrane (Bethune, et al., 2006).

Vesicle type	Coat proteins	Associated GTPase	Main functions
COPII	Sec23/Sec24 and Sec13/Sec31 complexes, Sec16	Sar1	ER to *cis*-Golgi
COPI	Coatomers containing seven different COP subunits	ARF	*Cis*-Golgi to ER, later to earlier Golgi cistern
Clathrin and adapter proteins	Clathrin + AP1 complexes	ARF	*Trans*-Golgi to endosome
	Clathrin + AP2 complexes	ARF	Plasma membrane to endosome
	Clathrin + GGA	ARF	*Trans*-Golgi to endosome
	Clathrin (?) + AP3 complexes	ARF	Golgi to lysosome, melanosome, or platelet vesicles

Table 2. Coated vesicles involved in protein trafficking (Lodish, et al., 2004)

Like COPII, the COPI coat is organized by a small GTPase. However, in this case the GTPase is ADP-ribosylation factor 1 (Arf1) instead of Sar1. The vesicle formation is not restricted to one compartment region, but can be formed at multiple distinct membranes along the early secretory pathway. The recruitment of Arf1 is mediated by a number of GEFs which all have a specific domain in common: Sec7 (Spang, 2008). GBF1 is the major GEF involved in COPI vesicle biogenesis (Beck, et al., 2009). Through the GEF activity, the Arf1 conformation is changed and in consequence an amphipathic helix is exposed, which allows a stable association of Arf1 with the membrane (Bethune, et al., 2006). Once Arf1 is membrane-bound, it can interact with SNARE proteins, GAPs and the cargo proteins. The GTP hydrolysis is not efficient at this time, but the GAP activity mediates the interaction with SNARE proteins. The main cargo recruiter is coatomer (derived from coat protomer) which acts to deform the membrane. Coatomer is a 550 kDa protein complex of seven subunits (Yu, et al., 2012), from which at least three bind to different cargo motifs (Spang, 2008). Additionally, the coatomer also recruits transmembrane proteins from the p24 family. They bind directly to the coatomer and increase the efficiency of vesicle formation (Beck, et al., 2009). Another critical component of the COPI vesicles is

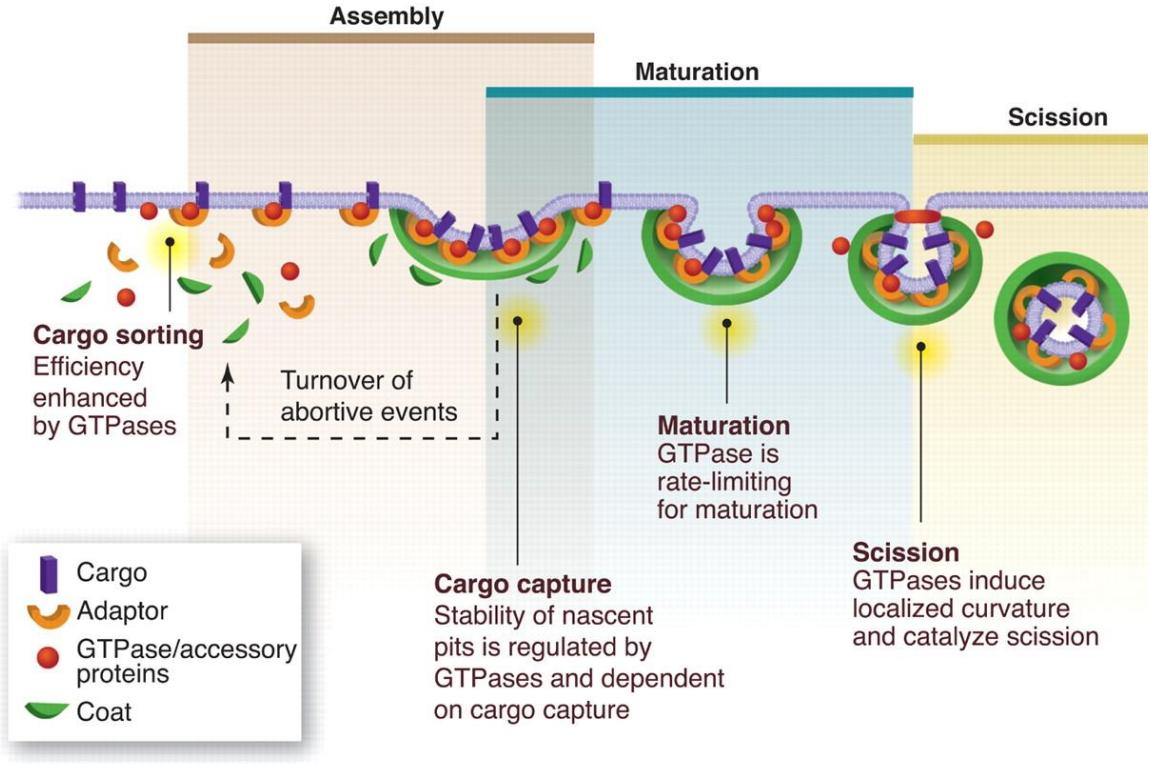

Figure 7. General scheme of coated vesicle formation (Pucadyil & Schmid, 2009)
This process involves the initial assembly of coat subunits on the membrane, during which cargo recognition and sorting takes place, followed by maturation, during which the coat and underlying membrane acquire curvature. Scission of the coated bud finally generates a coated vesicle (Pucadyil & Schmid, 2009).

brefeldin-A ADP-ribosylated substrate (BARS), which is critical for the fission step (Hsu & Yang, 2009).

After the formation of COPI-coated vesicles, but before the fusion with the target membrane, the vesicles have to be uncoated. This process is catalyzed by Arf1 GTPase-activating proteins (Beck, et al., 2009). After uncoating, the vesicles are ready for fusion with the target membrane. Therefore, the vesicles are guided to the proper target with SNARE proteins and other factors (Kartberg, et al., 2005).

1.4.3. Clathrin-coated vesicles: late secretory pathway

Clathrin-coated vesicles are formed during endocytosis and in the late secretory pathway (vesicles which leave the *trans*-Golgi) (Buxbaum & Engelbert, 2007). The major protein of the clathrin-coated vesicles is clathrin itself. The subunits of clathrin form a three legged structure called triskelion. These structures assemble into a convex framework to form coated pits on the cytosolic surface of membranes (Alberts, et al., 2008).

Like COPI, the GTP binding protein is the monomeric Arf1, which cycles between the inactive (GDP-bound) and active (GTP-bound) form (Lodish, et al., 2004). A number of adaptor proteins (AP1, AP2, AP3, AP4 and GGAs) function with Arf1 to generate the vesicle at the *trans*-Golgi and the endosomes (Spang, 2008).

1.5. Quality Control in the ER

The ER quality control of proteins is a topic of relatively recent interest. However, quality control in biological processes has long been a subject of intensive study (Määttänen, et al., 2010). For proteins, proof reading occurs at the level of transcription, translation, folding and assembly (Ellgaard & Helenius, 2003). After synthesis, proteins must rapidly fold to perform their biological activity. Folding takes place in three main sub-cellular compartments: cytosol, ER and mitochondria. Each organelle is equipped with a specific set of chaperones and folding enzymes optimized to work in the local conditions (Anelli & Sitia, 2008). An overview of the ER quality control is shown in figure 8.

The presence of quality control in the ER is essential for several reasons. By preventing the premature exit of folding intermediates and incompletely assembled proteins from the ER, quality control extends the exposure of the substrates to the

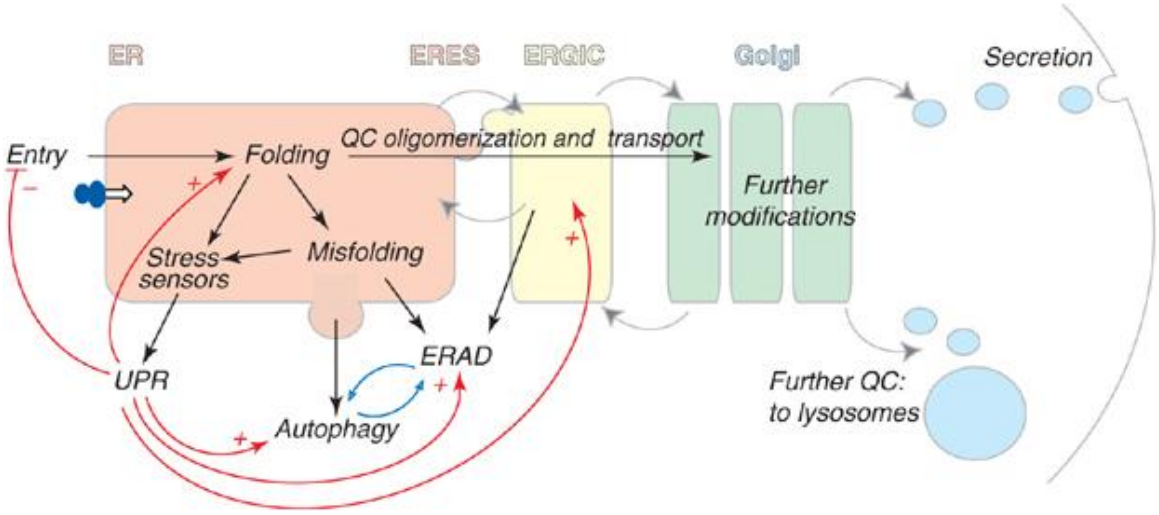

Figure 8. Quality control in the early secretory pathway (Anelli & Sitia, 2008)
A quality control machinery in the ER decides the fate of newly synthesized secretory proteins. If they are properly folded, that is if they obtain their native structure, the proteins will continue their journey through the secretory pathway. However, misfolded proteins are recognized in the ER and are retrotranslocated to the cytosol (ERAD). Accumulation of misfolded proteins can also induce the unfolded protein response (UPR) (Anelli & Sitia, 2008).

folding machinery in the ER lumen and thereby improves the chance of correct maturation. This ensures that proteins are not dispatched to terminal compartments when they are still incompletely folded and therefore potentially damaging to the cell (Ellgaard & Helenius, 2003). The quality control of secretory proteins requires the retention of nascent, unfolded proteins which are synthesized into the lumen of the ER and must be retained until proper folding is achieved (Benyair, et al., 2011).

The majority of the proteins traversing the secretory pathway in eukaryotic cells are N-glycosylated glycoproteins. An elaborate quality control mechanism ensures that only correctly folded and processed glycoproteins exit the ER. In recent years it has become clear that the timing of this interval is linked to trimming of the sugar tree. (Avezov, et al., 2008).

Association of nascent glycoproteins with the lectin chaperone calnexin (CNX), or its soluble homolog calreticulin (CRT), and examination by the folding sensor UDP glucose glycoprotein glucosyltransferase (UGGT) play a central role in ER retention, proper folding, and sensing of terminally misfolded glycoproteins. It appears that all misfolded glycoproteins are sent to ERAD through what is known as the CNX cycle (Benyair, et al., 2011).

1.5.1. ER chaperones

Molecular chaperones are present in different cellular compartments, but they are particularly important in the ER because of the high protein density in its lumen. The abundance of molecular chaperones in the ER ensures that exposed hydrophobic patches of misfolded proteins, nascent proteins and proteins in intermediate forms of folding are concealed. However, the ER lumen is not only populated by a variety of folding chaperones (Hsp70, Hsp90 and Hsp40 members), but also with lectin chaperones and various proteins essential for disulfide bond formation (Benyair, et al., 2011). An incomplete list of the ER machinery is shown in table 3.

A central question in the ER quality control processes is: How are the incorrect components recognized and discriminated from the correct ones? In the secretory

Class	Name	Localization	Function
Chaperones	BiP/GRP78	ER	Folding assistant/unfolding; regulation of IRE1, PERK and ATF6 in ER signaling; Translocon gating and regulation
	GRP94	ER	Folding assistant
	ORP150	ER	Folding assistant, hypoxia
	HERP	ER membrane	ERAD
	SEL1L	ER membrane	ERAD
Co-chaperones	Sil1/BAP	ER	ATP exchange factor
	ERdjs	ER	BiP cofactors
Lectins	CNX	ER membrane	Folding
	CRT	ER soluble	Folding
	ERGIC-53	ERGIC	Transport F5, F8, CatZ, CatC, IgM polymers
	VIPL	ER	Transport
	VIP-36	Cis-Golgi	Transport
	EDEM1, 2, 3	ER subregion	ERAD
	OS9	ER membrane	ERAD
	Erlectin/XTP3-B	ER membrane	ERAD
Enzymes redox	Ero1α	ER + ERGIC	Oxidase
	Ero1β	ER	Oxidase
	PDI	ER	Oxidase, isomerase, reductase
	ERp57	ER	Isomerase, oxidase (?)
	ERp72	ER	Unclear
	ERp44	ERGIC-*cis*-Golgi	Thiol-mediated retention/IP3 R1 regulation
Sugar processing	Glucosidase I	ER	Sugar processing
	Glucosidase II	ER	Sugar processing
	ER Man I	ER	Sugar processing
	ER Man II	ER	Sugar processing
	UGGT	ER	Folding sensor and sugar processing
	Man IA, IB, IC	Golgi	Sugar processing

Table 3. Incomplete list of ER factors (Anelli & Sitia, 2008)

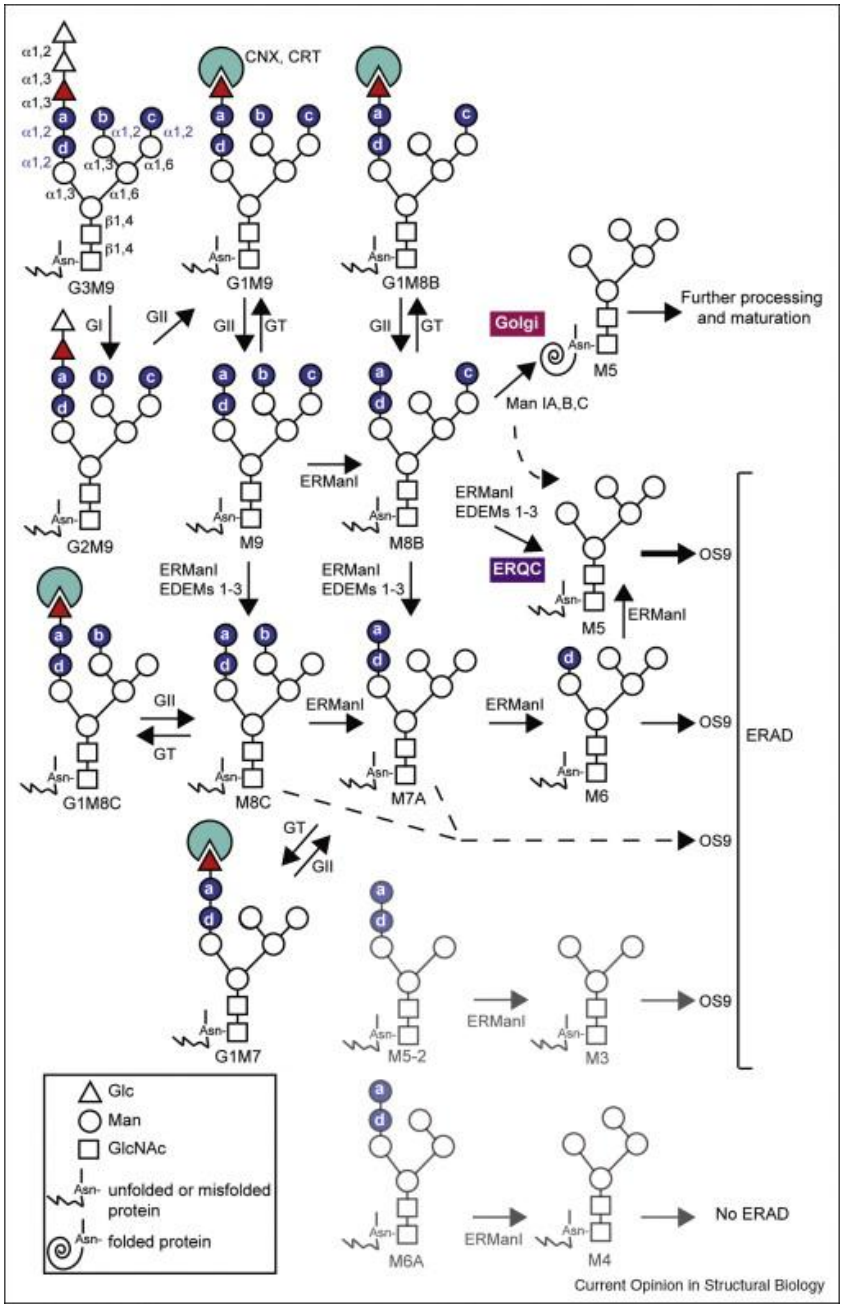

Figure 9. Glycoprotein trimming and the consequences (Lederkremer, 2009).
The precursor oligosaccharide (G3M9), attached to Asn on the nascent polypeptide chain is trimmed by removal of the non-reducing terminal glucose residue by glucosidase I (GI) toG2M9 and of the second glucose by glucosidase II (GII) to G1M9, allowing binding of calnexin (CNX) or calreticulin (CRT). CNX folding cycles then start, where the glycoprotein is deglucosylated by GII and reglucosylated by UDPGlc:glycoprotein glucosyltransferase (GT). If the glycoprotein is properly folded, it is no longer recognized as a substrate by GT and it exits to the Golgi where it is further trimmed of all its α1,2 linked mannose residues (blue) by Golgi mannosidases IA, IB and IC to Man5GlcNAc2 (M5). If the glycoprotein cannot fold successfully, it is delivered to the ER-derived quality control compartment (ERQC) and further trimmed to M6 and M5 by ERManI with the assistance of the EDEMs 1-3, and possibly of recycled Golgi α1,2 mannosidases (Lederkremer, 2009).

pathway the folding status of glycoproteins passing through the ER is marked by the composition of the N-glycan. The different glycoforms are recognized by specialized lectins (Määttänen, et al., 2010). A number of ER lectins are specific to a wide range of glycan specificities. The most important ER lectins are CNX and the closely related luminal variant CRT. Both have specificity for Glc1Man9GlcNAc2 N-glycan that can be

generated by the action of glucosidase II on the Glc2Man9GlcNAc2 after processing of Glc3Man9GlcNAc2 by glucosidase I (Määttänen, et al., 2010). The trimming of N-glycans is illustrated in figure 9.

1.5.1.1. Calreticulin (CRT)

CNX and CRT are conserved from plants through fungi to mammals, although their cycles of operation may differ between species (Benyair, et al., 2011). CRT is a soluble 46-kDa protein of the ER lumen. It consists of three distinct structural domains with different functions: the N-terminal domain which is highly conserved between species and plays an important role in chaperone activity, the P-domain which is proline rich and also takes part in the chaperone activity, and finally the C-terminal domain which is responsible for Ca2+ buffering activity (Wang, et al., 2012).

The main function of CRT is in the CRT/CNX cycle (in the ER lumen) where it interacts with CNX and an ER oxidoreductase of 57-kDa (ERp57). However, immunogold labeling studies indicate that CRT is also found outside the ER, and there are implications that CRT plays a role in a variety of processes that occur outside the ER lumen, including the cell surface, cytoplasm and within the nucleus (Michalak, et al., 2009).

1.5.1.2. Calnexin (CNX)

CNX is a 90 kDa type I ER membrane protein, with the most part located within the ER lumen (Williams, 2006). CNX shares 42-78% sequence identity with CRT, with the highest homology in the proline rich calcium binding P-domain. It is composed of a luminal domain (highly homologous to CRT), a transmembrane domain and a short cytosolic domain of 88 amino acids. Like CRT, it mainly acts as a chaperone preventing the export of incorrectly or incompletely folded glycoproteins. It also helps to prevent rapid degradation (Bedard, et al., 2005).

The carbohydrate binding domain of CNX is located in the globular domain, consisting of a number of ß sheets. The globular domain also contains a Ca2+ binding site (Benyair, et al., 2011). Like CRT, CNX is predominantly located in the ER but can also be found at the cell surface of a number of cells (Bedard, et al., 2005).

1.5.2. CNX cycle

Immediately after protein glycosylation (Glc3Man9GlcNAc2) in the ER, the glycan processing begins. In the first step, the glucosidase I (GI) cleaves the outermost

glucose, which occurs very rapidly, since it can be detected concomitantly with glycan transfer. This glycan composition prevents reassociation with the OST (Pearse & Hebert, 2010). The first hydrolysis is followed by sequential removal of the remaining two glucose residues by glucosidase II (GII) (D'Alessio, et al., 2010).

GII is a heterodimeric protein consisting of α and β subunits. The β subunit contains a mannose 6-phosphate receptor homology (MRH) domain, which is suggesting a pathway in which the β subunit initially binds to the mannose residue of one oligosaccharide while the α subunit cleaves the glucose residues of another oligosaccharide. Following this cleavage (if at least two N – linked glycans are present in the glycoprotein), the β subunit may bind to the monoglucosylated oligosaccharide and allow the α subunit to process the glycoprotein until a non-glucosylated substrate is produced (Benyair, et al., 2011). Since there is only a single active site within GII, it is a slow digestion, which is the result of reorientation of the active site of the α subunit (Pearse & Hebert, 2010).

Until recently, it was not known if there are ER proteins that interact with the intermediate Glc2Man9GlcNAc2 glycoprotein. However, recent studies have identified malectin, an ER membrane bound Glc2 specific lectin (Pearse & Hebert, 2010). Malectin seems to inhibit secretion of misfolded proteins and to modulate the second step trimming by GII (Benyair, et al., 2011). It is a potential new component in the ER QC, but it is not fully understood which role it plays (Määttänen, et al., 2010).

Once GI and GII remove the two outermost glucose residues, the Glc1Man9GlcNAc2 glycoprotein can be recognized by CNX and/or CRT (Williams, 2006). The transmembrane CNX interacts with both, membrane bound and soluble substrates, whereas the soluble CRT is more frequently associated with soluble substrates (Benyair, et al., 2011). These chaperones bind to the glycoprotein substrates in a Ca2+ dependent fashion (Pearse & Hebert, 2010). The binding of CNX and/or CRT to unfolded, monoglucosylated proteins grants such proteins time to achieve their native conformation by slowing folding events and allowing them to occur in a controlled manner. After binding to the substrate, they also recruit the oxidoreductase ERp57, which is an ER resident protein disulfide isomerase family

member. The trimeric complex CNX/CRT-ERp57-substrate promotes formation of disulfide bonds in the substrate protein (Jessop, et al., 2009). ERp57 binds to one of the lectin chaperones through an interaction of a positively charged patch on a thioredoxin domain, and the negatively charged tip of the chaperone P domain (Pearse & Hebert, 2010). The importance of the CNX/CRT-ERp57 interaction was shown in experiments with a point mutation, which abrogates this interaction and greatly diminishes the ability of ERp57 to form mixed disulfides with proteins in the ER (Määttänen, et al., 2010). The formation of disulfide bonds and their isomerization enhance the proper glycoprotein folding (Williams, 2006).

The glycoproteins remain in the CNX cycle as long as they are monoglucosylated: they are released by the second GII cleavage of the terminal glucose molecule. This most likely occurs irrespective of the folding state of the protein and prevents its renewed association with one of the two lectin chaperones (Ellgaard & Frickel, 2003). By abolishing the substrate-chaperone interaction, properly folded glycoproteins can pursue their transit through thesecretory pathway (Stigliano, et al., 2011). Released misfolded proteins are retained in the ER by entering the CNX cycle again (Williams, 2006).

The central protein in this pathway is UGGT. UGGT is a unique 175 kDa soluble ER protein (Kleizen & Braakman, 2004) which specifically glucosylates non-native, non-glucosylated proteins (Stigliano, et al., 2011). Still, the structure is not fully analyzed, but UGGT is most probably a homodimer with the catalytic region at the C-terminus and the sensor domain at the N-terminus (Määttänen, et al., 2010). The misfolded proteins become re-glucosylated by UGGT, which leads to a new round of CNX/CRT binding (Dalbey & Von Heijne, 2002). UGGT recognizes the N-linked core of the Man3GlcNAc2 glycoprotein and senses the exposed hydrophobic regions found in unfolded or misfolded proteins (Benyair, et al., 2011). It has been shown that UGGT cannot only detect misfoldings on a domain level, but also local folding defects (Ellgaard & Frickel, 2003).

UGGT and GII are opposite players and their activities hold glycoproteins in the CNX cycle. Theoretically, misfolded or/and unfolded glycoproteins could re-enter the CNX cycle over and over again, and in this way be retained in the ER lumen. This, however,

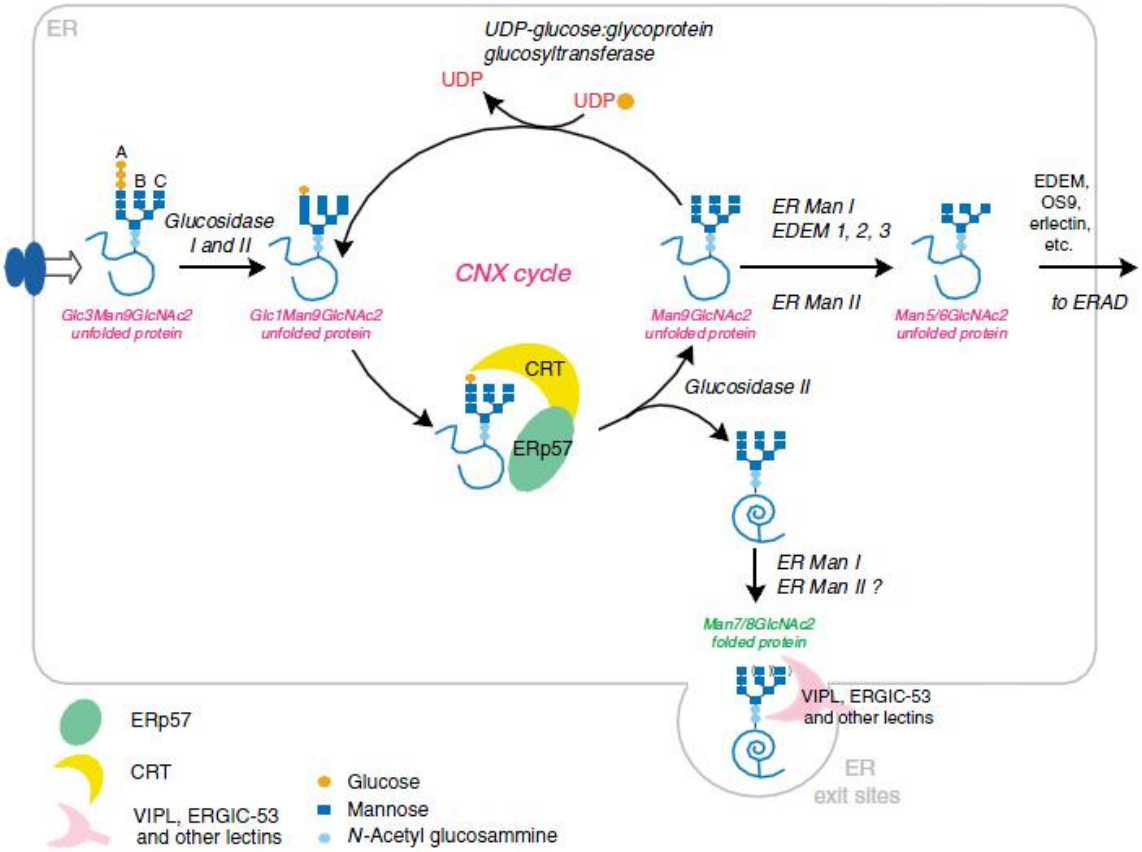

Figure 10. The CNX cycle (Anelli & Sitia, 2008)
The CNX/CRT cycle. After transfer of the preformed core oligosaccharide (Glc3Man9GlcNAc2) onto nascent proteins, glucosidase I and II sequentially remove the two terminal glucoses from the A branch. The monoglucosylated Glc1Man9GlcNAc2 unfolded protein can now interact with the lectin chaperones CNX and CRT. In association with the oxidoreductase ERp57, CNX and CRT prevent aggregation and facilitate glycoprotein folding. Removal of the last glucose by glucosidase II (Man9GlcNAc2) interrupts the interaction of the protein with CNX/CRT. If the protein has attained its native structure, it can now proceed along the secretory pathway by bulk flow or by interaction with specific lectin transporters such as ERGIC-53 or VIPL. If unfolding persists, the glycoprotein is recognized by UGGT, which places a single glucose back onto the A branch, causing the protein to enter the CNX/CRT cycle again. Mannose trimming causes exit from the CNX/CRT cycle. Misfolded proteins can be recognized by specific lectins (EDEMs, OS9, etc) and targeted to degradation (Anelli & Sitia, 2008).

would bring about an accumulation of glycoproteins in the ER and cause pathological consequences. Therefore, a timing mechanism is necessary to remove terminally misfolded glycoproteins from the ER avoid accumulation (Benyair, et al., 2011). The crucial step of removing the glycoproteins from the CNX cycle is another trimming of the glycan: the cleavage of the α1,2 linked mannose residues. This crucial step is done by ER mannosidases and is the initial step of the ER associated degradation (ERAD) of the misfolded proteins (Lederkremer, 2009). In mammalian cells, the glycoproteins can be trimmed from Man9GlcNAc2 to Man5GlcNAc2 or Man6GlcNAc2 (M6 or M5 species). Due to the lack of the mannose residue, which is the acceptor for the glucose

transfer by GII, the glycoproteins can escape from the CNX cycle (Frenkel, et al., 2003). An overview of the CNX cycle and its key players is shown in figure 10.

1.5.3. ER-associated degradation (ERAD)

Proteins that are unable to pass the ER quality control are identified and destroyed by the ER-associated degradation (ERAD) machinery. Therefore the terminally misfolded proteins are identified and retrotranslocated to the cytosol where they are degraded by the proteasome (Brodsky & Skach, 2011). The general principle of ERAD is illustrated in figure 11.

The ERAD substrates can be categorized in three groups, depending on the localization of the lesion: i) ERAD-L substrates contain lesions in their luminal domain, ii) ERAD-C substrates contain lesions in the cytosolic domain and iii) ERAD-M substrates contain lesions in the transmembrane domain. Depending on the substrate, the ERAD pathway can vary in the factor composition, but the principles appear to be similar (Benyair, et al., 2011). A list of established ERAD factors is shown in table 4.

1.5.3.1. Recognition of irreparably misfolded proteins

In the case of N-glucosylated proteins, the glycans do not only play an important role in glycoprotein entering or leaving the CNX cycle in which the proteins have time to fold, but they also can serve as degradation signals (Ushioda & Nagata, 2011).

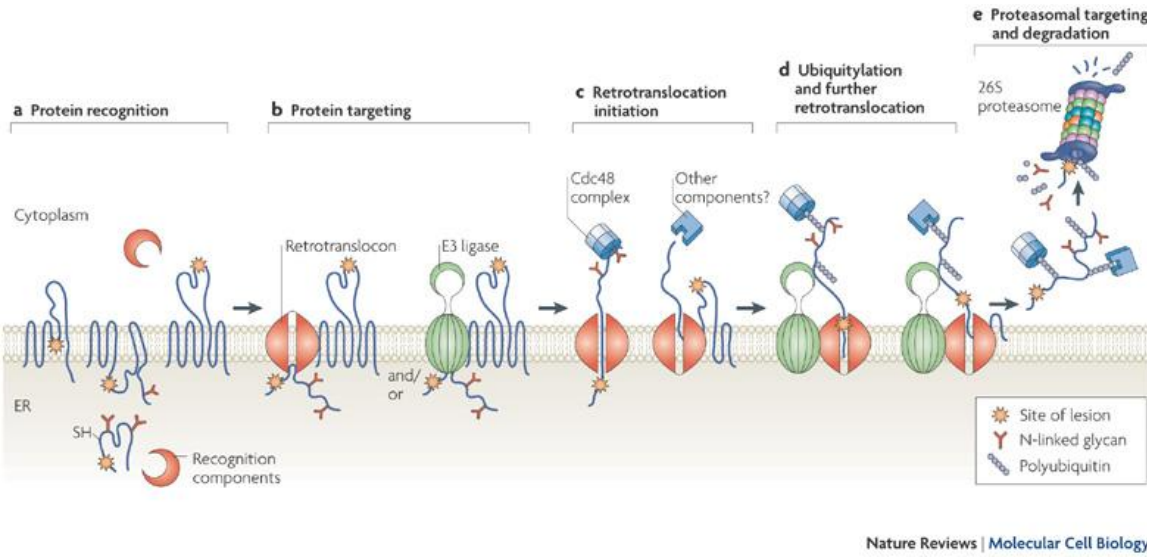

Figure 11. Overview of the ERAD pathway (Vembar & Brodsky, 2008)
After terminally misfolded proteins have been recognized (a), they are targeted to the retrotranslocon (b). After the retrotranslocation initiation (c), the substrates are polyubiquitinated by ubiquitin ligases (d). Once retrotranslocated, the substrates are targeted to the proteasome (e) (Vembar & Brodsky, 2008)

Yeast	Mammals	Localization	Function
Hrd1	Hrd1/synoviolin	Integral ER membrane	Ubiquitin ligase
/	Gp78/AMFR	Integral ER membrane	Ubiquitin ligase
Doa10	Teb4/MARCH6	Integral ER membrane	Ubiquitin ligase
/	TRC8	Integral ER membrane	Ubiquitin ligase
/	RNF/RMA1	Integral ER membrane	Ubiquitin ligase
/	RFP2	Integral ER membrane, cytosolic	Ubiquitin ligase
/	CHIP	cytosolic	Ubiquitin ligase
/	Parkin	cytosolic	Ubiquitin ligase
Hrd3	SEL1L	Integral ER membrane	Substrate recruitment factor for Hrd1
Yos9	OS9, XTP3-B	ER lumen, associated with Hrd3/Sel1L	Substrate recruitment factor for Hrd1
Ubc6	Ubc6, Ubc6ep	Integral ER membrane	Ubiquitin conjugating enzyme
Ubc7	Ube2g2	Cytosolic; associated with ER membrane	Ubiquitin conjugating enzyme
Cue1	/	Integral ER membrane	Recruits and activates Ubc7
Usa1	HERP	Integral ER membrane	Scaffolding protein for the Hrd1 ligase
Der1	Derlin 1,2,3	Integral ER membrane	Components of a dislocation channel (?)
Ubx2	Erasin/UBXD2	Integral ER membrane	Recruits Cdc48/p97 to the ERAD ligases
Cdc48/Npl4/Ufd1	p97/Npl4/Ufd1	Cytosolic	Ubiquitin specific AAA-ATPase

Table 4. ERAD factors in yeast and mammals (Benyair, et al., 2011).

Properly folded proteins do not re-enter the CNX cycle, but continue their journey through the secretory pathway. However, one of central questions is how cells recognize that N-glycosylated proteins are irreparably misfolded, and prevent their re-entering in the CNX cycle. Intensive work has been dedicated to this issue, but there is still no clear answer to the question as yet (Caramelo & Parodi, 2008). Due to the slow catalytic activity of ER mannosidases, a mannose timer hypothesis was postulated: the action of ER mannosidases is delayed, and therefore only glycoproteins with prolonged CNX/CRT association are targeted to ERAD (Määttänen, et al., 2010).

1.5.3.2. Labeling of terminally misfolded proteins for ERAD

Once the misfolded and/or unfolded proteins are recognized, trimming of the glycan and the removal of α(1,2)-bonded mannose residues generate a recognition code for the ERAD machinery. It is known that ER mannosidase I (ERManI) plays a central role in the sequential trimming of the glycan, but nowadays it is known that the trimming is done by other mannosidases and mannosidase-like proteins as well: the EDEMs 1-3, Golgi α(1,2)-mannosidases, and members of the glycosyl hydrolase 47 family (Bagola, et al., 2011) (Benyair, et al., 2011).

At low concentrations, ERManI removes only mannose-b (see figure 9). However, it has been shown that ERManI can be concentrated in the ER-derived quality control compartment (ERQC), which is located around the centrosomes in mammalian cells, and therefore becomes capable of removing all four α(1,2)-mannoses (Lederkremer, 2009). The concentration of Golgi α(1,2)-mannosidases in the ER is low, but can be increased by their over-expression which accelerates ERAD, indicating that in the ER even Golgi mannosidases are involved in glycoprotein trimming (Hosokawa, et al., 2007). For the EDEMs it is not fully understood, whether they act only as cofactors of ERManI, or if they are true mannosidases (Benyair, et al., 2011).

1.5.3.3. Recognition of substrates by the ERAD machinery

The glycans generated by trimming actions of various glycosidases are recognized by crucial ERAD protein factors like Yos9 in yeast or OS-9 and XTP3-B in mammals. These factors deliver the misfolded proteins to the ERAD pathway (Bagola, et al., 2011). Yos9 is a lectin-like protein with a mannosidase receptor homology (MRH) domain. It is assumed that Yos9 acts as a gatekeeper by scanning the glycoproteins and allows only Man7GlcNAc2 proteins to enter the ERAD pathway (Stolz & Wolf, 2010). However, beside the proofreading function, Yos9 also associates with the membrane embedded ubiquitin ligase complex Hrd1p-Hrd3p (Hosokawa, et al., 2010) and BiP (Vembar & Brodsky, 2008). Hrd1p is a prototypical ERAD E3 ubiquitin ligase. These proteins are the central organizers of all ERAD pathways (see figure 12). Hrd3 can bind misfolded proteins independently of Yos9. This binding is not due to recognition of the characteristic glycans, but due to the binding of hydrophobic

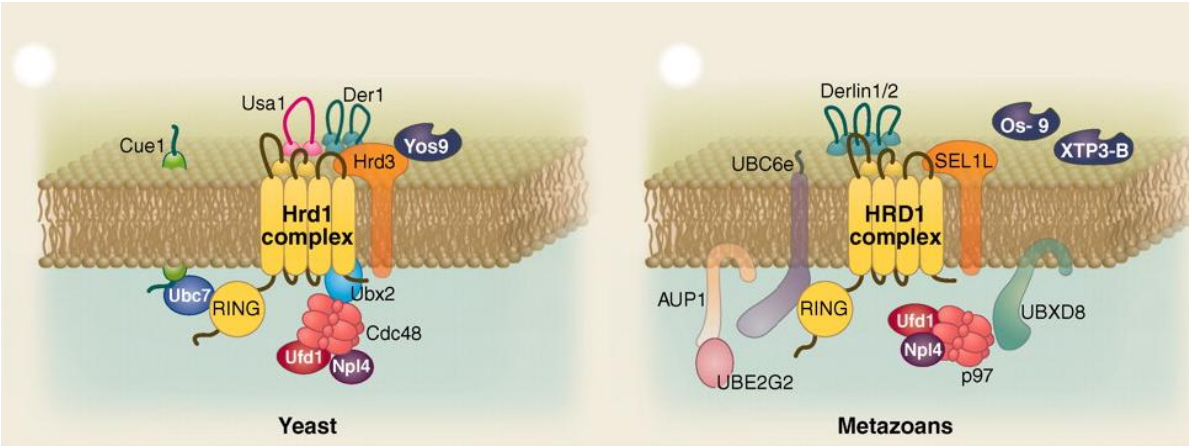

Figure 12. The core Hrd1p/HRDP1 complex in yeast/mammals (Smith, et al., 2011)
E3 ubiquitin ligases are the central organizers of all ERAD pathways. The prototype of the E3 ligase in yeast is the Hrd1 complex, and in mammals the HRD1 complex (Stolz & Wolf, 2010).

protein patches. Hrd3 is most probably necessary to bind non-glucosylated misfolded proteins and deliver them to the ERAD pathway (Stolz & Wolf, 2010). The function of E3 ubiquitin ligases will be discussed later in detail.

1.5.3.4. Retrotranslocation: identity of the channel

In a not fully understood mechanism, the ERAD machinery translocates the misfolded proteins into the cytosol (a process termed retrotranslocation), where they are eliminated by proteolysis (Stolz & Wolf, 2010). It is still speculated about the nature of the channel that allows the substrate to leave the ER lumen, and about the driving force for the directional transport (Bagola, et al., 2011). Many studies implicate that retrotranslocation into the cytoplasm depends on the Sec61 channel, which is known to be necessary for the forward translocation (from cytosol into the ER lumen). In fact, mutations in the SEC61 gene reduce the proteasome binding to the channel. It has, however, thus far not been experimentally demonstrated that Sec61 alone supports the retrotranslocation (Ng, et al., 2007), but this has not been established yet (Benyair, et al., 2011). There are also alternative protein candidates for the retrotranslocation channel, like the derlin family (Vembar & Brodsky, 2008). Another hypothesis implies a non-protein dependent retrotranslocation mechanism: it was found that ER stress stimulates lipid droplets formation, which transports the misfolded proteins from the ER to the cytosol (Fei, et al., 2009). However, this hypothesis has been refuted by a recent study in which it was shown that the droplet formation is dispensable for the dislocation of ERAD substrates (Olzmann & Kopito, 2011). Sec61 is the only ER protein with the obvious ability to transport proteins across the membrane, and therefore it is reasonable to assume that it can promote translocation in both directions. It is also known that some proteins are retrotranslocated independently of Sec61 (Bagola, et al., 2011).

Prior to the degradation in the cytosol, most misfolded proteins are first ubiquitinated. For this process the actions of E1 ubiquitin-activating enzymes, E2 ubiquitin-conjugating enzymes and E3 ubiquitin ligases are necessary (Vembar & Brodsky, 2008). However, the polyubiquitination of ERAD substrates is also a prerequisite for their retrotranslocation into the cytosol. It has been shown that mutant ubiquitin variants cause accumulation of ERAD substrates in the ER. The function of polyubiquitination for the retrotranslocation is still not fully understood,

but probably the ubiquitination is necessary to recruit factors that facilitate the retrotranslocation of the misfolded proteins (Bagola, et al., 2011). However, some misfolded proteins do not seem to require polyubiquitination for retrotranslocation, and these proteins are found in the cytosol when the proteasomes are inhibited. This is unusual for most of the ERAD substrates, which remain in the ER if the proteasome machinery is abrogated, due to the blocking of retrotranslocation, as it is coupled to proteasomal degradation (Benyair, et al., 2011).

1.5.3.5. Ubiquitination and retrotranslocation

Ubiquitin is a 76-residue polypeptide, which is highly conserved in all eukaryotes. Usually it is covalently linked via its C-terminal glyine to lysine or N – terminal methionine residues on the target proteins. It also can be conjugated to other ubiquitin molecules, generating polyubiquitinated proteins (Bagola, et al., 2011).

Dislocation of misfolded proteins to the cytosol is tightly coupled to substrate ubiquitination and proteasomal degradation. Many studies have shown that the dislocation of misfolded proteins across the ER membrane into the cytosol is regulated by luminal, transmembrane and cytosolic complexes build around ER ubiquitin ligases (Hebert, et al., 2009).

The ubiquitination itself is a highly regulated process that includes E1 ubiquitin-activating enzymes, E2 ubiquitin-conjugating enzymes and E3 ubiquitin ligase enzymes (Tsai & Weissman, 2011). The E1 ubiquitin-activating enzyme prepares the C-terminal glycine of ubiquitin for binding by forming a thioester bond. The activated ubiquitin is transferred to the E2 ubiquitin-conjugating enzyme. Finally, the E3 ubiquitin ligase enzyme transfers the activated ubiquitin from the E2 enzyme to the protein substrate (Benyair, et al., 2011). E3 is of central importance, because it is necessary for the recognition of substrates, which have to be labeled for degradation, and further it catalyzes substrate ubiquitination and organizes the complexes necessary for translocation (Smith, et al., 2011).

Two E3 multi-spanning membrane proteins are implicated in the yeast ERAD pathway: Hrd1p and Doa10p. In mammals there is a whole series of E3 proteins acting in the ERAD pathway. Both, Doa10p and Hrd1p ligases, contain the catalytic RING domains. They have different preferences for unique membrane associated E2

enzymes: the Doa10p dependent ubiquitination requires Ubc6 and Ubc7 E2 enzymes, whereas Hrd1 requires the Ubc7 E2 enzyme (Vembar & Brodsky, 2008). Hrd3p is a yeast dual function protein; it acts as an adaptor protein, which is also part of the E3 complex, and a regulator of Hrd1p activity. Hrd3p and its mammalian homolog SEL1L are the best characterized adaptor proteins that bind to potential ERAD substrates, recruiting them to the E3 ligase. Hrd3p is also a regulatory protein that inhibits the auto-ubiquitination of Hrd1p. Additionally, a second protein also regulates Hrd1p: Usa1p. This protein regulates the oligomerization of Hrdp1, which may be essential for its activity (Smith, et al., 2011).

Another member of the yeast E3 complex is Der1p, a member of the derlin protein family. Der1p is a multi-pass transmembrane protein that also acts as an adaptor. Further, it is speculated, whether derlins form the translocation channels itself, or if they participate in a complex containing the dislocation channel (Hebert, et al., 2009).

Once the misfolded glycoproteins have become polyubiquitinated, they have to be extracted from the membrane into the cytosol. In this process the cell-division cycle-48 complex (Cdc48) plays an important role in both, yeast and mammals. In yeast, the Cdc48 complex is composed of a hexameric AAA ATPase, which is Cdc48, and two additional factors: Ufd1 and Npl4. The homolog of Cdc48 in mammals is p97, and the homologs for Ufd1 and Npl4 are UFD1 and NPL4 (Vembar & Brodsky, 2008). In some cases also the proteasome lid plays a role in this key cytosolic event of substrate extraction (Smith, et al., 2011). The Cdc48-Ufd1p-Npl4p complex is involved in many cellular processes like cell cycle progression, transcription factor processing and homeotypic membrane fusion (Bagola, et al., 2011). Probably it also generates the driving force for the protein extraction, due to its AAA-ATPase activity (Gauss, et al., 2006). Finally, the Cdc48 complex is thought to transport ERAD substrates to the cytosol and to prevent their aggregation (Bagola, et al., 2011). The ERAD substrates are recruited to the Cdc48 complex by a family of proteins containing an ubiquitin regulatory X domain (UBX). The 80-amino acid long UBX domain also regulates the activity of Cdc48 and its homolog p97. The main member of this family involved in ERAD is Ubx2 in yeast, and Erasin (Ubxd2) in mammals (Benyair, et al., 2011).

1.5.3.6. Shuttling to the proteasomes

Once the proteins are retrotranslocated and ubiquitinated, the cdc48/p97 complex recruits a peptide N-glycanase that removes the N-linked glycans (Smith, et al., 2011). In some cases, this seems not to be an essential step and in this cases the proteins are degraded by the proteasomes while still glycosylated (Benyair, et al., 2011).

The task of shuffling the misfolded proteins to the proteasome is thought to be carried out by proteins that contain an ubiquitin-like domain (UBL) and an ubiquitin-associated domain (UBA) (Raasi & Wolf, 2007). Two yeast factors in this class are Rad23 and Dsk2. However, it is not clear yet, if these factors are just static members of the Cdc48 complex, or if they act as mobile escorts (Vembar & Brodsky, 2008).

1.5.3.7. Substrate recognition by the proteasome

The mammalian proteasome is a 26S multisubunit enzyme consisting of the catalytic core particle (20S complex) and the regulatory particle (19S complex) (Benyair, et al., 2011). The regulatory particle (RP) contains ATPase domains, which provide energy for degradation, and an ubiquitin binding subunit. The regulatory activities of the RP are: i) recognition of the misfolded, retrotranslocated proteins, ii) removal of the polyubiquitin chain, iii) unfolding the proteins and iv) driving the protein to the protease chamber of the catalytic particle (Raasi & Wolf, 2007).

1.5.4. Unfolded protein response

If for some reason the ERAD pathway is overloaded, the retrotranslocation of unfolded or misfolded proteins is delayed, and they can accumulate in the ER. This accumulation leads to the ER stress which initiates the unfolded protein response (Kaser, et al., 2011). Cells usually respond to stressful conditions by changing their expression pattern. As a consequence, molecular chaperones are usually overexpressed which is essential for folding and oligomerization of polypeptides. In stressful situations, these proteins facilitate stabilization in a sense that they try to refold the misfolded proteins (Flores-Diaz, et al., 2004).

Generally, the UPR represents a collection of highly conserved signaling pathways which collectively monitor the conditions in the ER. If due to the UPR the cells fail to establish a homeostasis, the UPR is able to induce apoptosis (Walter & Ron, 2011).

As already mentioned, the UPR is a highly conserved biological process. In yeast, the UPR is managed by the IRE1-Hac1p pathway. The key players in this pathway are the

bifunctional transmembrane inositol requiring enzyme 1 (IRE1) and a transcription factor named Hac1p. IRE1 acts as a sensor molecule and a ribonuclease. If misfolded or unfolded proteins accumulate in the ER, IRE1 is activated by oligomerization in the ER membrane. When activated, IRE1 displays an endoribonuclease activity in the cytosol, which cleaves the Hac1p transcript. This splice product encodes a transcription factor which moves to the nucleus and regulates the expression of specific genes, which are necessary for the maintenance of homeostasis (Kaser, et al., 2011).

1.5.4.1. Mammalian UPR

In mammalian cells, the UPR is more complex. Until today, three different branches of the UPR have been identified. These branches operate in parallel and each of them is defined by a class of transmembrane factors (Walter & Ron, 2011). The branches are mediated by three ER membrane receptors: i) activating transcription factor 6 (ATF6), ii) double-stranded RNA-activated protein kinase-like endoplasmic reticulum kinase (PERK) and iii) inositol requiring kinase 1 (IRE1) (Chakrabarti, et al., 2011).

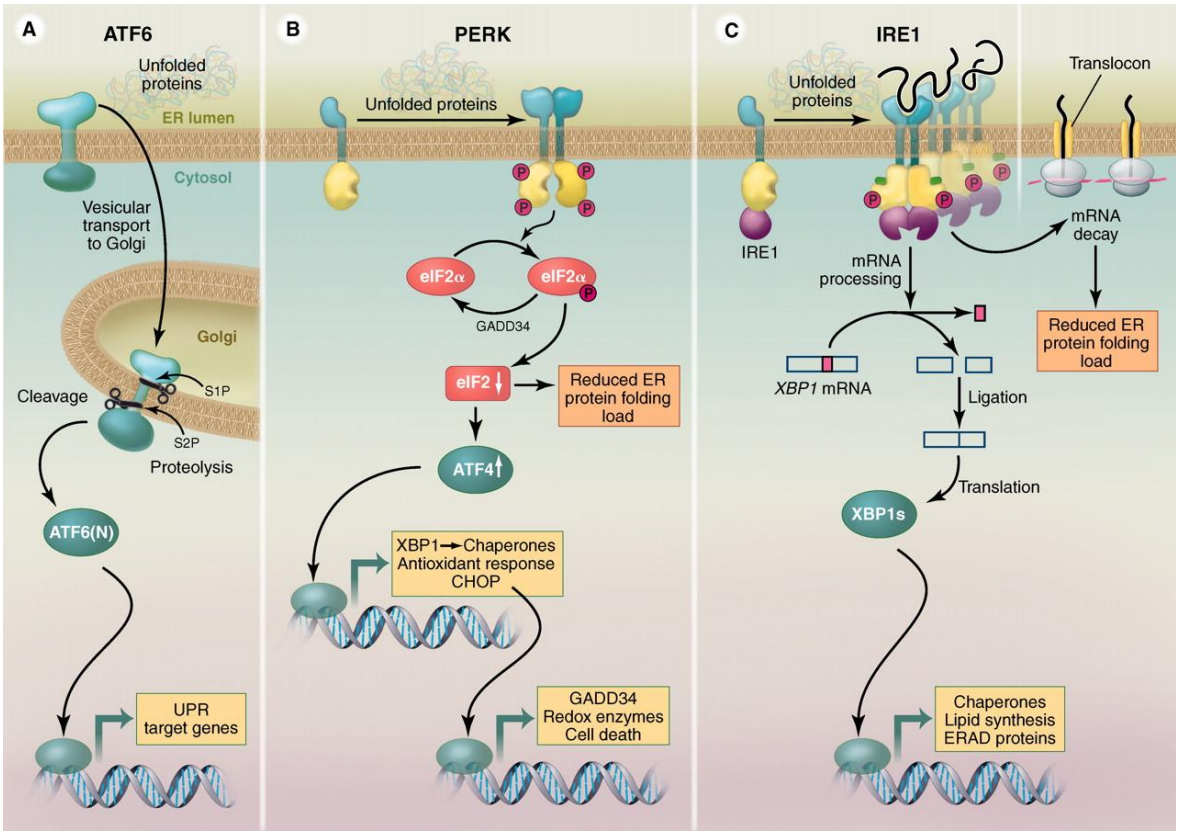

Figure 13. Three UPR branches in mammalian cells (Walter & Ron, 2011).
Each pathway uses a different mechanism of signal transduction: ATF6 by regulated proteolysis, PERK by translational control, and IRE1 by nonconventional mRNA splicing (Walter & Ron, 2011).

Similar to the yeast UPR, the activated branches produce transcription factors which regulate the expression of some UPR target genes (Walter & Ron, 2011). The three UPR branches are illustrated in figure 13.

BiP (Grp78), which is a critical member of the Hsp70 family, is a chaperone that recognizes and binds to misfolded and unfolded proteins. It does not only act as a folding chaperone, but it also regulates the activation of three different UPR branches. In absence of ER stress (low levels of unfolded/misfolded proteins in the ER), BiP is bound to ATF6, PERK and IRE1. Under these conditions, the three UPR transducers are inactivated (Chakrabarti, et al., 2011). BiP physically inhibits the dimerisation of Ire1 and PERK, and in this way it inhibits their activity. Accumulation of unfolded or misfolded proteins in the ER lumen disturbs the BiP-Ire1 and BiP-PERK interaction. As a consequence, the dimerisation and activation of PERK/Ire1 molecules are permitted and the UPR pathways are activated. BiP also regulates the activity of ATF6, but in a different way: it prevents the movement of ATF6 to the Golgi. However, increased levels of unfolded or misfolded proteins prevent the interaction between BiP and ATF6, allowing ATF6 to move to the Golgi and activate the third UPR pathway (Diehl, et al., 2011).

ATF6 pathway

ATF6 is initially synthesized as an ER transmembrane protein. While bound to BiP, it remains inactivated in the ER membrane. However, upon accumulation of misfolded or unfolded proteins, it is released from BiP and escapes to the Golgi via transport vesicles. In the Golgi, it is sequentially processed by the site-1 (S1P) and site-2 (S2P) protease. Afterwards, the cytosolic fragment is released and moves to the nucleus, where it acts as a transcription factor which activates, together with other transcription factors and co-regulators, the expression of BiP, PDI and Grp94 (Walter & Ron, 2011). The ATF6 induced gene expression is also cytoprotective (Chakrabarti, et al., 2011).

PERK pathway

After dissociation from BiP, upon accumulation of misfolded and unfolded proteins in the ER, PERK is activated due to oligomerization and autophosphorylation (Walter & Ron, 2011). Further, the activated receptor also phosphorylates the initiation factor

eIF2α and the bZIP transcription factor Nrf2 (Schröder & Kaufman, 2005). The phosphorylation of eIF2α leads to three downstream effects. In the first place, it leads to a global attenuation of translation initiation. As a consequence, the protein import into the ER is decreased, and therefore the removal of proteins accumulated in the ER is facilitated (Chakrabarti, et al., 2011). However, expression of some specific proteins is induced if eIF2α is phosphorylated. ATF4, a transcription factor, is one of these proteins. The induced ATF4 positively regulates the expression of cell protective and pro-apoptotic factors (Walter & Ron, 2011).

IRE1 pathway

IRE1 is a 100 kDa ER transmembrane protein, containing an endoribonuclease and a serine-threonine kinase domain. Its N-terminus is located in the ER lumen where BiP is bound under normal conditions. However, increasing amounts of unfolded and misfolded proteins in the ER remove BiP and allow IRE1 dimerisation (Chakrabarti, et al., 2011). As a consequence of dimerisation, IRE1 autophosphorylates and activates itself. The activated IRE1 cleaves the XBP-1 transcript at two specific positions removing an intron. This alternative splicing generates a mRNA which is translated to XBP-1 which is a transcription factor. It seems that XBP-1 in mammals plays a special

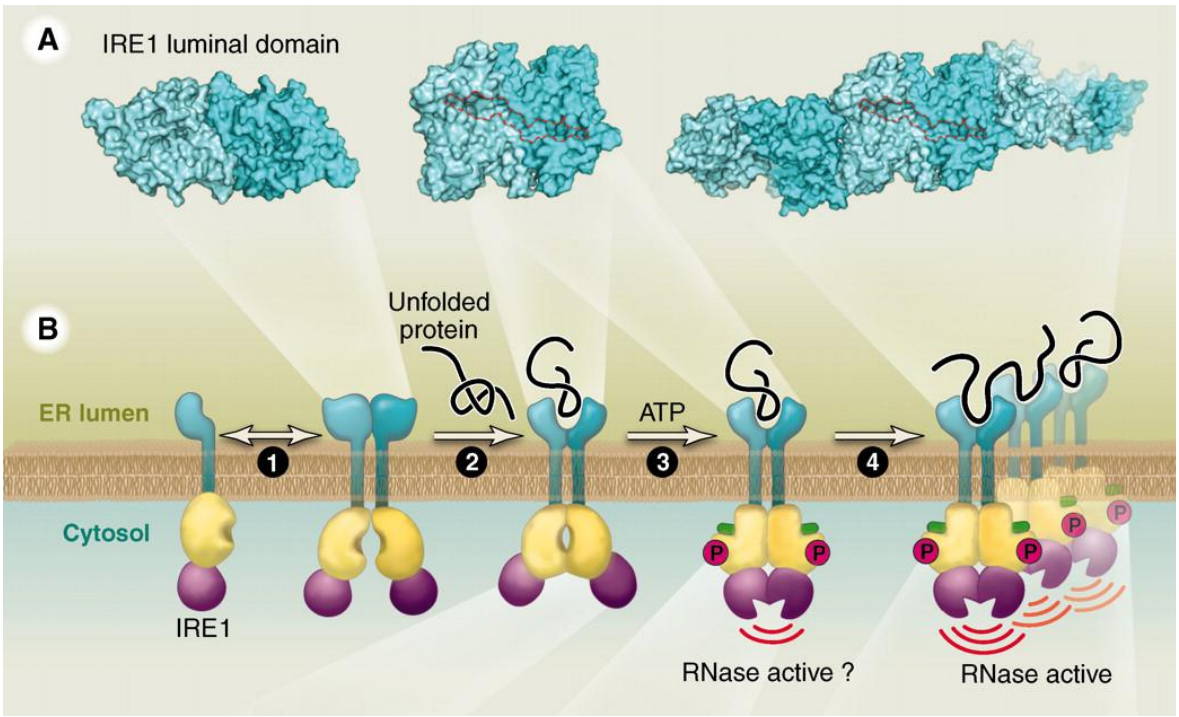

Figure 14. A speculative model of IRE1 activation (Walter & Ron, 2011)
The figure depicts multiple structures of the IRE1 luminal ER stress–sensing domain (A). IRE1 may be activated in response to an accumulation of unfolded proteins in the ER lumen (B) (Walter & Ron, 2011)

role in regulation of lipid biosynthetic enzymes and ERAD components (Walter & Ron, 2011). A model of IRE1 activation is shown in figure 14.

1.5.4.2 UPR induced apoptosis

In most cases the UPR has cytoprotective effects. However, if UPR fails to establish the ER homeostasis, it can induce programmed cell death (apoptosis). The mechanisms for UPR induced apoptosis are still poorly understood, but one possibility is that the relative timing of the three UPR pathways can shift the balance between the cyto-protection and apoptosis (Walter & Ron, 2011). There is also strong evidence that Ca^{2+} release from the ER mediates apoptosis as well as the activation of caspases (Diehl, et al., 2011).

Recent studies indicate that UPR can also induce autophagy, which is a cellular reboot mechanism, unlike apoptosis which is a terminal death program (Chakrabarti, et al., 2011).

1.5.4.3. Effect of glucose starvation on the UPR

The N – glycosylation of secretory proteins is an essential step which, as already described, is necessary for protein folding (CNX cycle) and the quality control (Wilson & High, 2007). However, due to glucose starvation, the level of UDP-Glc which is a precursor necessary for protein N – glycosylation is decreased and thus glycosylation is disturbed. Similar conditions have been shown to induce the overexpression of stress proteins in bacteria, which are required for survival. It has been shown that also glucose starvation induces at least one stress protein. However, some studies have demonstrated that an UDP-glucose deficiency in mammals causes an overexpression of some glucose/oxygen-regulated proteins, independently of the ER stress elements (Flores-Diaz, et al., 2004).

These findings should be seen in the context of the practical part of this diploma thesis, that in part was done with mammalian cells which have a defective UDPG:PP, and therefore have a permanent low level of UDP-Glc.

1.6. Diseases of glycosylation

Diseases of glycosylation are rare inherited disorders known as congenital disorders of glycosylation (CDG) (Hennet, 2012) which affect glycoprotein biogenesis (Freeze & Aebi, 2005). Nowadays nearly 70 genetic disorders are known to be caused by

Gene	Gene locus MIM #	Function	Disease
Nucleotide – sugar biosynthesis			
PMM2	601785	Phosphomannomutase (Man-6-P > Man-1-P)	PMM2-CDG (CDG-Ia)
MPI	154550	Phosphomannose Isomerase (Fru-6-P > Man-6-P)	MPI-CDG (CDG-Ib)
GFPT1	138292	Glutamine: fructose-6-phosphate amidotransferase	Congenital myasthenic syndrome
GNE	603284	UDP-N-acetylglucosamine 2-epimerase	Herediatry inclusion body myopathy
GALK	604313	Gal kinase	Galactosemia
GALT	606999	Gal-1-P uridylyltransferase	Galactosemia
GALE	606953	UDP-Gal 4-epimerase	Galactosemia
Dolichol biosynthesis			
DHDDS	608172	Cis-prenol synthase	Retinitis pigmentosa
SRD5A3	611715	Polyprenol reductase	SRD5A3-CDG (CDG-Iq)
TMEM15	610746	Dol kinase	TMEM15-CDG (CDG-Im)
N-glycosylation			
TUSC3/N33	601385	Oligosaccharyltransferase	Autosomal recessive mental retard.
IAP/MAGT1	300715	Oligosaccharyltransferase	X – linked mental retardation
GCS1	601336	α1-2 glucosidase	GCS-CDG (CDG-IIa)
MAN1B1	604346	ER α1-2 mannsidase-I	Autosomal recessive mental retard.
MGAT2	602616	β1-2 GlcNAc-transferase	MGAT2-CDG (CDG-IIa)
B4GALT1	137060	β1-4 Gal-transferase	B4GALT1-CDG (CDG-IId)
ST3GAL3	606494	α2-3 Sia-transferase	Autosomal recessive mental retard.

Table 5. Diseases of glycosylation (Hennet, 2012).

impaired synthesis of glycoproteins (Freeze, et al., 2012). Most disorders are due to defects in the N-glycosylation, O-glycosylation or both (Jaeken, et al., 2009). CDGs are classified into the type I (CDG-I) and type II (CDG-II) disorders (Freeze, 2007). CDG-I are more common (Woods, et al., 2012), and they include all disorders of N-glycosylation site occupancy, while CDG-II include all other disorders of N-glycosylation, O- glycosylation and glycolipid biosynthesis (Hennet, 2012). Most of the disorders are caused by autosomal recessive mutations (Jaeken, 2011).

As the number of known glycosylation disorders is increasing, a new CDG nomenclature is applied which was suggested by Jaeken and colleagues (Jaeken, et al., 2009). The meanwhile established nomenclature focuses on the name of the mutated gene followed by the "CDG" abbreviation (Hennet, 2012). A list of gene defects responsible for the main disorders is shown in table 5.

CDGs show a broad clinical spectrum, and they can affect nearly all organs and systems. Nowadays, treatment is available only for few CDGs, including MPI-CDG, SLC35C1-CDG and PIGM-CDG (Jaeken, 2011). However, defects in the glucosidase I

gene (GSC1), ER mannosidase I gene (MAN1B1) and other components of the N – glycosylation processing machinery are accompanied with a severe pathology. A selection of CDGs is briefly described below.

1.6.1. PMM2 – CDG

Phosphomannomutase 2 (PMM2) is a cytosolic enzyme which catalyzes the conversion of Man-6-P to Man-1-P (Haeuptle & Hennet, 2009). Mutations in the *PMM2* gene (OMIM ID: 601785) represent the most frequent type of CDG with an incidence of about 1:50.000, affecting the biosynthesis of N-glycans, O-glycans and GPI anchors (Hennet, 2012).

PMM2 – CDG is mainly associated with psychomotor retardation, developmental delay, epilepsy, ataxia and other neurologic symptoms (Haeuptle & Hennet, 2009).

1.6.1. MPI – CDG

MPI – CDG is caused by a mutation in the mannose phosphate isomerase (MPI) gene *MPI* (OMIM ID: 154550) (Haeuptle & Hennet, 2009). MPI is necessary for Man-6-P generation and a deficiency of MPI results in unoccupied N-glycosylation sites on glycoproteins (Sharma, et al., 2011).

MPI – CDG patients commonly show the following symptoms: diarrhea, vomiting, gastrointestinal bleeding, hepatomegaly and hepatic fibrosis (Hennet, 2012). High doses of mannose make this lethal disease treatable (Jaeken, 2011).

1.6.2. GSC1-CDG

So far, one case o glucosidase I (GSC1) deficiency was reported (OMIM ID: 601336). Due the importance of glucosidase I for N – linked glycoprotein trimming, this mutation causes a loss of N-glycan trimming and is accompanied with a severe pathology with the following symptoms: dysmorphism, hypotonia. So far no efficient therapy is known and the disorder causes death of the affected infants (Hennet, 2012).

1.6.3. MAN1B1-CDG

The *MAN1B1* gene encodes ER mannosidase I, an enzyme which is involved in the maturation of N-linked glycans in the ER. As described earlier, this enzyme is also necessary for the timing and disposal of misfolded proteins through the ERAD pathway. However, mutations in this gene cause abnormal trimming and, as a

consequence, disorders of the ERAD pathway (OMIM ID: 604346). MAN1B1 – CDG patients show intellectual disabilities, such as delayed speech and mild dysmorphic features (Hennet, 2012).

1.7. Truncated versions of ribophorin I as an ERAD substrate

During this diploma thesis, the ERAD pathway was studied using two truncated variants of ribophorin I *(see 1.3.2. Ribophorin I)*. One version of the truncated polypeptide consists of only the 332 N-terminal amino acids (RI332) of the mature protein, thus lacking the transmembrane and cytoplasmic domains of wild type ribophorin I. Hence, the soluble protein corresponds to most of its wild type luminal domain (de Virgilio, et al., 1998). As RI332 is a misfolded protein, it is targeted to ERAD and is rapidly degraded. The second truncated variant used in this study contains also the 332 N-terminal amino acids of wild type ribophorin I, but in addition harbors a 6HA tag (RI332-6HA) at its C-terminus. This truncated variant is also rapidly degraded by the proteasome (Ermonval, et al., 2001), which makes it a favorable ERAD substrate model. Using HeLa cell transformants it was shown that during the process of RI332 degradation trimming intermediates of the N-linked glycan occur and that retrotranslocation of the protein to the cytoplasm and degradation by the proteasome are highly coupled processes (Kitzmüller, et al., 2003).

The cDNA of both variants of the truncated ribophorin I were inserted into the pZeoSV vector (Invitrogen) during former studies, allowing for a selection of cells expressing one of the two truncated proteins in the Chinese hamster fibroblast cell lines G3 and QC.

2. Materials

2.1. Chemicals and reagents

2 - mercaptoethanol (>98%)	Sigma
Acetic acid (99% – 100%)	AppliChem
Ammonium Persulfate	Bio Rad
Bromphenol blue	AppliChem
CHAPS	Fluka
CHAPS	Sigma Aldrich
Complete (Protease inhibitor cocktail tablets)	Roche
Cysteine	Sigma
D(+) – Galactose	Sigma
ddH2O	-
Developer (G153 B)	AGFA
Developer (G153)	AGFA
EN3HANCE	Perkin Elmer
EtOH 96%	Brenntag
Fluorescent mounting medium	Dako
G-418 Sulphate (Geneticin)	Gibco
G-418 Sulphate (Geneticin)	PAA
Glycine	AppliChem
HCl (60%)	Amresco
Immersion oil	Zeiss
Isobutanol	Merck
KCl	AppliChem
MEM NEAA (non essential amino acids) 100x	Invitrogen
Methanol (dried, max. 0.003% H_2O)	Merck
Methanol (pure)	Brenntag
Methionine	Sigma
Milk powder (low fat)	Maresi
N, N, N'N' – Tetramethylethylendiamin (TEMED)	Merck
NaCl	Sigma
NEC-811 Protein MW Markers, [^{14}C] methylated	Perkin Elmer

NEG-072 Expre^{35}s^{35}s, [^{35}S] Protein Labeling Mix	Perkin Elmer
Penicillin/Streptomycin (10.000 U/ml/10.000µg/ml)	Gibco
Precision Plus Protein Standards	Bio Rad
Protein A Sepharose CL-4B	GE Healthcare
Rapid fixer (G354)	AGFA
Sodium Dodecyl Sulfate (SDS)	AppliChem
TRIS	Amresco
Triton X 100	Amresco
Trypsin – EDTA 5% (10x)	Gibco
Tween 20	Amresco

2.2. Buffers and solutions

CHAPS lysis buffer

1% CHAPS	Fulka/Sigma
4% Complete Protease Inhibitor	Roche
95% HBS	

CHAPS wash buffer

0,5% CHAPS	Fulka/Sigma
1% Complete Protease Inhibitor	Roche
98,5% HBS	

Fixation solution

10% (v/v) Acetic acid	AppliChem
30% (v/v) Methanol	Brenntag
ddH2O	-

HBS

50mM HEPES NaOH pH 7,6	USB
200mM NaCl	Sigma

Immunofluorescence blocking solution

1% milk powder	Instant
99% PBS	

PBS

137mM NaCl	Sigma
2,5mM KCl	AppliChem
10mM Na2HPO4	Merck
1,7 mM KH2PO4	Merck

Running buffer

25mM Tris	
192mM Glycine	AppliChem
0,1% SDS	AppliChem

Transfer buffer

25mM Tris	
192mM Glycin	AppliChem

Sample buffer

50mM Tris	
0,1% Bromphenol Blue	AppliChem
2% SDS	Amresco
10% Glycerol	Sigma
3% β mercaptoethanol	Sigma

SDS wash buffer

95mM NaCl	Sigma Aldrich
25mM Tris/HCl pH 7,4	Amresco
3mM EDTA	Sigma
1,25% Triton X	Amresco

0,2% SDS	AppliChem
1% Complete Protease Inhibitor	Roche

SDS lysis buffer

95mM NaCl	Sigma Aldrich
25mM TrisHCl pH 7,4	Amresco
3mM EDTA	Sigma
1% SDS	AppliChem
4% Complete Protease Inhibitor	Roche

SDS PAGE 10% (for four gels)

Separation gel

5,34ml dH2O	
3,33ml solution I	
1,26ml solution IIA	
54µl 20% SDS	Amresco
5µl TEMED	Merck
50µl 10% APS	BioRad

Stackig gel

3,6ml dH2O	
0,75ml solution I	
0,63ml solution II B	
25µl 20% SDS	Amresco
5µl TEMED	Merck
25µl 10% SDS	BioRad

Solution I (PAGE)

30% Acrylamide	USB

0,6% Bis acrylamide	USB

Solution IIA (PAGE)

3M Tris/HCl pH 8,9

Solution IIB (PAGE)

0,5M Tris/HCl pH 6,7

Triton X-100 buffer (10ml)

1ml 2M Tris/Maleat pH 6,5	Merck
10µl 2M CaCl2	Sigma
400µl Complete Protease Inhibitor	Roche
140µl Triton X-100	Amresco

Trypsin – EDTA solution

90% PBS	
10% Trypsin – EDTA (10x)	Gibco

Western blot blocking solution

5% milk powder	Instant
94,8% PBS	
0,2 Tween 20	Amresco

2.3. Cell culture media

Growth medium (hamster cells)

RPMI – 1640 (500ml) - L-glutamine + D-glucose	Gibco
1% Glutamine (200mM)	Gibco
1% Pen (10.000 U/ml)/ Strep (10.000µg/ml)	Gibco

10% Fetal calf serum (FCS)	Gibco
400µg/ml G418 sulfate (Geneticin)	Gibco
1,25ml/500ml Zeocin (100mg/ml)	Invitrogen

Growth medium (HeLa cells)

MEM Low glucose - Glutamine	Gibco
7% FCS	Gibco
1% L-glutamine	Gibco
1% Pen (10.000 U/ml)/ Strep (10.000µg/ml)	Gibco
400µg/ml G418 sulfate (Geneticin)	Gibco

High galactose medium (hamster cells)

RPMI – 1640 + L-glutamine - D-glucose	Gibco
1% Glutamine	Gibco
1mM glucose	Sigma
5mM galactose	Sigma
1% MEM NEAA (100x)	Gibco
1% Pen (10.000 U/ml)/ Strep (10.000µg/ml)	Gibco
400µg/ml G418 sulfate (Geneticin)	Gibco
1,25ml Zeocin (100mg/ml)	Invitrogen

High glucose medium (hamster cells)

RPMI – 1640 + L-glutamine - D-glucose	Gibco
1% Glutamine	Gibco
6mM glucose	Sigma
1% MEM NEAA (100x)	Gibco

1% Pen (10.000 U/ml)/ Strep (10.000µg/ml)	Gibco
400µg/ml G418 sulfate (Geneticin)	Gibco
1,25ml Zeocin (100mg/ml)	Invitrogen

Pulse – chase media

Starvation medium (hamster cells)

RPMI – 1640 - L-glutamine - L-methionine - L-cysteine - L-cystine	Gibco
1% Glutamine	Gibco

Pulse medium (hamster cells)

Starvation medium

NEG-072 Expre^{35}s^{35}s, [^{35}S] Protein Labeling Mix (11 mCi/ml)	Perkin Elmer

Chase medium (hamster cells)

Growth medium (hamster cells)

5mM methionine (unlabeled)

5mM cysteine (unlabeled)

2.4. Cell lines

During the practical work, mainly hamster cell lines were used. For some experiments, HeLa cells were used in order to check antibody reactivity.

All hamster cell lines originated from a chinese hamster mutant cell line (DonQ), described in former studies (Flores-Diaz, et al., 2004). DonQ cells have a recessive mutation in the UDP-glucose pyrophosphorylase (UDPG:PP) gene, which was induced by chemical mutagenesis (ethyl methanesulfonate). Consequently, these cells have a low level of UDP-glucose, and therefore, glucosylation is affected. In further studies, DonQ cells were transfected with i) a vector carrying the cDNA of a w/t bovine UDPG:PP cDNA, and ii) a empty vector. Thus, two cell lines were generated: i) the G3

cell line (expressing the w/t UDPG:PP protein) and ii) the QC cell line (carrying only a genomic mutant UDPG:PP gene). These cells were obtained from Dr. Stuart E.H. Moore (INSERM U773CRB3, Paris, France). A second stable transfection generated G3 and QC cells carrying the cDNA of a i) short, untagged, ribophorin I (RI – 332), and ii) short, HA tagged, ribophorin I (RI – 332 – 6HA). These short versions of ribophorin I lack the transmembrane domain, which makes them soluble. They serve as luminal misfolded model proteins.

Finally, four different cell lines, generated and isolated in former studies, were used during the practical work: i) G3-RI332 i) G3-RI332-6HA iii) QC-RI332 and iv) QC-RI332-6HA. The clones used are designated in the Results section where appropriate.

2.5. Antibodies

Primary antibodies					
Name	**Manufacture**	**Type**	**Recognizes**	**Host animal**	**Application and dilution**
Anti-BiP C-20	Santa Cruz	Polyclonal	BiP (GRP78) in ER	Goat	Western blot (1:600)
Anti-Calnexin	Abcam	Monoclonal	Calnexin in ER	Mouse	Immunofluorescence (1:50)
Anti-Calnexin	Ivessa et al.	Polyclonal	Calnexin in ER	Rabbit	Immunofluorescence (1:200) Western blot (1:10000)
Anti-Calreticulin	Bioreagents	Polyclonal	Calreticulin in ER	Rabbit	Western blot (1:2000)
Anti-RI lum	Ivessa et al.	Polyclonal	Ribophorin I	Rabbit	Immunofluorescence (1:200) Pulse – chase (1:10) Western blot (1:5000)
CTR433	Bornens et al.	Monoclonal	CTR433 in Golgi apparatus	Mouse	Immunofluorescence (1:40)
ERGIC-53	Alexis Biochemicals	Monoclonal	ERGIC	Mouse	Immunofluorescence (1:1000)
ERGIC-53	ENZO	Monoclonal	ERGIC	Mouse	Immunofluorescence (1:1000)
ERGIC-53	Santa Cruz	Polyclonal	ERGIC	Rabbit	Immunofluorescence (1:50)
Ero1 - Lα	Santa Cruz	Monoclonal	Oxidoreductin-1-Lα in ER	Mouse	Immunofluorescence (1:100)
Giantin	Abcam	Polyclonal	Golgi apparatus	Rabbit	Immunofluorescence (1:2000)
HA.11	Covance	Monoclonal	Tagged RI332-6HA (HA epitope)	Mouse	Immunofluorescence (1:50) Pulse – chase (1:30) Western blot (1:5000)
Monoclonal Anti α Tubulin	Sigma Aldrich	Monoclonal	α tubulin	Mouse	Western blot (1:15000)
Rabbit polyclonal to LMAN1	Abcam	Polyclonal	ERGIC	Rabbit	Immunofluorescence (1:50)
Secondary antibodies					
Name	**Manufacture**	**Host animal**	**Recognizes**	**Application and dilution**	
Alexa Fluor 488	Invitrogen	Goat	Rabbit antibodies	Immunofluorescence (1:200) – green fluorescence	
Alexa Fluor 594	Invitrogen	Goat	Mouse antibodies	Immunofluorescence (1:200) – red fluorescence	
Goat anti rabbit (HRP)	Accurate Chemical	Goat	Rabbit antibodies	Western blot (1:20000)	
Goat anti mouse (HRP)	Accurate Chemical	Goat	Mouse antibodies	Western blot (1:20000)	
Rat anti goat (HRP)	Accurate Chemical	Rat	Goat antibodies	Western blot (1:50000)	

Table 6. Overview of primary and secondary antibodies

2.6. Inhibitors (drugs)

Inhibitors				
Name	**Final concentration**	**Solvent**	**Target**	**Company**
Deoxymannojirimycin hydrochloride (DMJ)	2mM	ddH2O	ER mannosidase	TRC
Z-Leu-Leu-Leu-H (ZLLL)	50µM	DMSO	Proteasome	Peptides
Kifunensine (KIF)	2µg/ml	ddH2O	ER mannosidase	TRC
Castanospermine (CST)	1mM	ddH2O	Glucosidases I & II	TRC

Table 7. Overview of the inhibitors and their final concentrations

2.7. Equipments

Acrodisc PF syringe filter (0,8/0,2µm)	Pall
Analysis scale H110	Sartorius
Cell culture dishes (100mm x 20mm)	IWAKI
Cell culture dishes (100mm x 20mm)	TPP
Cell culture dishes (150mm x 20mm)	IWAKI
Cell culture dishes (60mm x 20mm)	IWAKI
Cell culture dishes (60mm x 20mm)	TPP
Cell cultures test plates (6 well plates)	TPP
Centrifuge 5418	Eppendorf
Centrifuge tubes 7 x 20mm	Beckmann
Confocal microscope LSM 510 Meta	Zeiss
Cooling centrifuge 1k15	Sigma
Dispenser	Eppendorf
Falcon tubes (15ml)	Sarstedt
Falcon tubes (50ml)	Sarstedt
Film cassette	Sigma
Filter paper	Whatman
Flow hood laminair HB 2448	Holten
Gel electrophoresis equipment	Bio Rad
Gel electrophoresis Mini PROTEAN Tetra Cell	Bio Rad
Gel electrophoresis power supply Power Pac 300	Bio Rad
Gel dryer Slab SGD 4050	Savant
Heating block thermomixer 5436	Eppendorf
Hybod-C extra membranes	Amersham
Incubator	Binder

Luer solo (10ml)	B Braun
Microscope (inverted) ID03 binocular	Zeiss
Microscope cover glasses (13mm)	Christine Gröpl
Microscope ID03	Zeiss
Microscope LSM Meta 510	Zeiss
pH – meter	Mettler Toledo
Saran wrap	Dow Chemical
Scale E5500S-D1	Sortorius
Stirrer MR 2000	Heidolph
Ultracentrifuge OPTIMA – TLX rotor (TLA 100)	Beckmann
Ultracentrifuge OPTIMA – TLX	Beckmann
Vacuum pump DIVAC 2,4L	Leybold
Wax plates	Anutex
X-ray film Amersham Hyperfilm MP (8x10 in.)	GE Healthcare
X-ray film X-Omat Blue XB (5x7 in.)	Kodak
X-ray film X-Omat Blue XB (8x10 in.)	Kodak

3. Methods

3.1. Cell culture

3.1.1. Preparation of cell culture media

A number of different cell culture media were prepared, depending on the cell line and the approach. For experiments with hamster cells, RPMI 1640 medium was used, whereas for experiments with HeLa cells the MEM medium was used. All media were stored at 4°C.

3.1.1.1. Growth RPMI medium (complete)

The following components were added to a new flask (500ml) of RPMI 1640 (without glutamine) medium: 220mg of geneticin was weighted into a tissue plate. Geneticin was resuspended in 10ml of the prepared medium, and the geneticin solution was sterile filtered into the medium flask. Further, 50ml fetal calf serum (FCS), 5ml glutamine, 5ml Pen/Strp and 1,2ml zeocin were added. The medium flask was closed and mixed. If the medium was not used up in two weeks, 1% of fresh glutamine was added to the medium, due to the instability of glutamine.

3.1.1.2. Starvation RPMI medium

To the RPMI 1640 starvation medium (without glutamine, methionine, cysteine and cystine) only 1% glutamine was added. However, glutamine was always freshly added to the aliquots which were used for the given experiment.

The antibiotics were not added, due to the fact that cells were only incubated up to one hour in the starvation medium.

3.1.1.3. High & low glucose RPMI media

The high and low glucose media were prepared out of the RPMI 1640 (without galactose and glucose) medium. First, glucose and galactose stock solutions (1M) were prepared: the appropriate amounts of glucose and galactose were dissolved in ddH2O. The stock solutions were sterile filtered into falcon tubes.

For the high glucose RPMI medium, the glucose stock solution was added to the RPMI 1640 (with glutamine, without glucose) medium to obtain a 6mM solution. For the high galactose RPMI medium (with glutamine, without glucose), the glucose and galactose stock solutions were added to the RPMI medium to obtain a 1mM glucose

and 5mM galactose solution. Additionally, non essential amino acids were added to the medium, since it was already out of date.

3.1.1.4. Growth MEM medium

The growth media for the HeLa cells was prepared as the growth media for hamster cells *(see 3.1.1.1)*. However, instead of the RPMI 1640 media, the MEM (low glucose, without glutamine) media was used. Additionally, 7% FCS was added, instead of 10%.

3.1.2. Thawing of cells

The frozen cells (cryo tubes) which were stored at -80°C or in liquid nitrogen tanks were taken out and left on ice. Only one cryo tube at a time was used in further steps, while the other cells were still on ice. One cryo tube was thawed in the hand till only a small piece of ice was left. At this point 0,5ml of fresh RPMI medium was taken out from a falcon tube containing 10ml pre-warmed RPMI medium, and transferred to the cryo tube. Further, the same volume was transferred from the cryo tube to the falcon. This was repeated for several times, and in the end the whole cryo tube content was transferred to the falcon tube.

The falcon tubes containing 11ml cell suspension (10ml RPMI medium and 1ml cryo tube content) were centrifuged at 4°C and 1300 rounds per minute (rpm) for 7 minutes. The supernatant was discarded and the cell pellets were resuspended with 4ml pre-warmed RPMI medium. Following to this step, the cells were seeded to a 60mm tissue plate and incubated at 37° and 5% CO2 over night (o/n).

On the following day, the cells were examined in the ID03 light microscope (Zeiss). Cells which reached a density >50% were split to 100mm plates *(see 3.1.3 Cultivation of cells)*. Cells which have grown slowly were left for several days in the 60mm plates, but the medium was replaced after two days to remove dead cells and to provide the living cells with fresh medium.

3.1.3. Cultivation of cells

The cells were cultivated on 100mm tissue plates, and they were split after reaching a density of approximately 80%. For splitting, the growth medium was removed and the cells were washed with pre-warmed 1x PBS. 10ml of pre-warmed PBS was carefully pipetted to the edge of the tissue plate, to avoid rinsing off the cells. This washing step was necessary to remove dead cells and the rests of the growth medium which could inhibit the activity of trypsin, which was used in the next steps.

After the washing step, the PBS was removed and 1ml of pre-warmed trypsin was added (trypsin was warmed at room temperature; otherwise it would become active at 37°C in the water bath). Trypsin was added to detach the cells from the tissue plate surface. The cells were incubated for approximately 4 minutes at 37°C with the trypsin solution. During incubation, the efficiency of trypsinisation was examined in the light microscope. If the cells were detached, growth medium was added to the cells to stop the trypsin activity. Otherwise, the trypsinisation was extended. Further, the required volume of cell suspension was transferred into a new tissue plate containing 10ml of fresh medium. The splitting ratio depended on the cell density; a ratio was chosen which allows the seeding of cells with a density of approximately 10% in the new plate.

Finally, the cells were evenly distributed by gentle stirring of the tissue plate. The cells were incubated at the standard conditions: 37°C and 5% CO_2.

Alternatively, if the cells were incubated for up to four days and in this time didn't reach the density of at least 50%, the growth medium was changed. The old medium was removed and fresh pre-warmed medium was added.

3.1.4. Freezing of cells (preparation of cryocultures)

Before freezing of the cells, they were expanded on three 150mm tissue plates (alternatively on eight 100mm plates). After the cells reached a density of at least 80%, they were harvested. The medium was removed and the cells were washed with pre – warmed 1x PBS *(see 3.1.3. Cultivation of cells)*. Afterwards, 2ml of trypsin was added and the cells were incubated at 37°C for four minutes. The trypsinisation was stopped by addition of growth medium and the cell suspension was partitioned into falcon tubes. Then the cells were centrifuged at 1300rpm for 7 minutes. The supernatant was removed and the cell pellets were resuspended in ice cold FCS - 10% DMSO: for each 150mm plate 5ml of this solution were used. The resuspended cells were aliquoted to cryotubes: 1ml/cryotube. Finally, the cryotubes were set into a freezing box which was stored for 24 hours at -80°C. The freezing box allowed a stepwise temperature decrease of 1°C per minute. After this period, the cells were transferred to storage boxes which were kept in liquid nitrogen tanks.

3.2. Screening for stable ERAD substrate expression

Screening for the ERAD substrate (RI-332 and RI-332-6HA) expression was done by pulse chase experiments, followed by immunoprecipitation and SDS-PAGE.

3.2.1. Pulse – chase analysis

3.2.1.1. Seeding of cells

Before the pulse – chase analysis, the cells were seeded and incubated for 48 hours in 6 – well plates. Seven chase time points were done for each experiment, and therefore seven 6 – well plates were used; every 6 – well plate for one chase time point. Each cell clone was seeded into one well with a density of 40 – 50% confluence. For the splitting ratio the effective growth surface was considered, and therefore following formula was used:

$$\frac{initial\ cell\ density\ (\%)}{desired\ cell\ density\ (\%)} \times 8$$

The effective growth surface in each well of the 6 – well plate is 8x smaller as in the 100mm tissue plate, therefore the factor "8" was used. The splitting procedure is described in *3.1.3 Cultivation of cells*.

3.2.1.2. Starvation phase

After the incubation period of 48 hours, the cell density was estimated under the microscope. Cells with a density of at least 80% confluence were used in further steps. Otherwise, the growth medium was changed and the cells were incubated for another 24 hours.

The growth medium was aspirated and the cells were briefly washed with pre-warmed PBS. After the PBS was removed, 1ml of pre-warmed starvation medium was added to each well. The cells were incubated for 30 minutes at 37°C and 5% CO2.

3.2.1.3. Pulse phase

Following to the starvation phase, the medium was aspirated and 0,8ml of pulse medium was added to each well. The cells were incubated at 37°C and 5% CO2 for exactly 15 minutes in order to label all proteins with [^{35}S] methionine and [^{35}S] cysteine, which were synthesized during this period.

3.2.1.4. Chase phase

Subsequent to the pulse phase, the medium was removed separately, and to each well 1ml of chase medium was added. Then the cells were incubated under the conditions described previously for several time periods; 5', 15', 30', 45', 60', 75' and 90'. Each incubation period was terminated by transferring the appropriate 6 – well plate to ice and keeping it in the cold room for at least 10 minutes. All further steps were performed on ice.

3.2.2. Cell lysis

After a short incubation period on ice, the cells were used for cell lysis. For this purpose, the medium from each well was removed with an adjustable, air-displacement pipette, and 1ml ice cold 1x PBS was added to each well. Then the 6 – well plate was gently pivoted and the PBS was again removed with a displacement pipette. 150μl of SDS lysis buffer was added to each well, while the plate was still on ice. Next, the cells were scraped using a rubber policeman and collected to labeled Eppendorf tubes which were also kept on ice. Afterwards, another 150μl SDS lysis buffer was added to the wells, and the same procedure was repeated to finally obtain a total volume of 300μl in each Eppendorf tube.

Once the lysates of all 6 – well plates were collected to the Eppendorf tubes, they were sonicated (maximum power and constant) for few seconds. Then the cell lysates were heated for 3' at 90° in a heating block.

After the boiling period, 1ml of ice cold SDS wash buffer was added to each Eppendorf tube and after gentle mixing the cell lysates were left on ice for few minutes to cool down. Then the cell lysates were centrifuged at 4°C and 14.000rpm for 12 minutes. Finally, 1.2ml of the supernatants was transferred to new Eppendorf tubes and the cell lysates were further used for immunoprecipitation.

3.2.3. Immunoprecipitation

Following to cell lysis, the lysates were used for immunoprecipitation. For this purpose, the lysates were incubated with the RI antibody and protein A sepharose beads.

3.2.3.1. Protein A sepharose beads preparation

The appropriate amount of protein A sepharose beads was weighed and distributed to two Eppendorf tubes. The beads were allowed to swell by addition of 1ml SDS

wash buffer to each tube, followed by 30' incubation at 4°C while turning on a rotating wheel. Afterwards, the beads were washed: they were centrifuged at 8000 rpm for 3', and the supernatant was discarded. The pellets were resuspended with 1ml SDS wash buffer followed by 10' incubation at the same conditions as before. This washing step was repeated two times, and finally the beads were resuspended in the appropriate amount of SDS wash buffer: 12,5µl wash buffer per 1mg previously weighed beads. The beads were kept at 4°C before use.

3.2.3.2. Antibody preparation

For immunoprecipitation αRI polyclonal antibodies (RI lum) were used. They were prepared by 1/10 dilution with SDS wash buffer. The diluted antiserum was also kept at 4°C till use.

3.2.3.3. Immunoprecipitation

35µl of the prepared beads *(see 3.2.3.1. Protein A sepharose beads preparation)* and 30µl of diluted αRI antiserum *(see 3.2.3.2. Antibody preparation)* were added to the cell lysates *(see 3.2.2. Cell lysis)*. The cell lysates were incubated together with the beads and antibodies for at least 14h (alternatively over weekend) at 4°C while gentle turning on a rotating wheel.

After the incubation period, the beads were precipitated. To this, the cell lysates were centrifuged for 3' at 13.000 rpm and the supernatant was discarded. Following to this, the beads were washed three times with 1ml SDS washing buffer each, and two times with 1ml PBS each in the same way. By discarding the supernatant in the last PBS washing step, the precipitates were ready to be processed for SDS – PAGE.

3.2.4. SDS PAGE

After processing of the precipitates with sample buffer (*see 3.2.4.2. Sample preparation and loading)*, they were loaded on a 10% polyacrylamide gel and finally visualized on X-ray films. The procedure is described below.

3.2.4.1. Preparation of polyacrylamide gels

First the separation gel solution was prepared. To this, the components *(see 2.2. Buffers and solutions)* were pipetted to a 50ml falcon tube. After every pipetting step, the solution was gently mixed while avoiding foaming. Then, 10% APS (10% APS was stored at -20°C: once used, it was stored at 4°C for max. two weeks) and TEMED were added to the gel solution, and again the solution was gently mixed. Finally, this

solution was pipetted to the assembled and cleaned Mini PROTEAN 3® System (total height of the separation solution was 5.5cm). After it was ensured that the system was tight and that the solution was not leaking out, the separation gel solution was covered by iso-butanol.

The polymerization of the separation gel typically lasted about 20 minutes (if fresh APS was used) and the end of polymerization was noticed by the formation of a third, aqueous phase between the gel solution and iso-butanol. After polymerization, the iso-butanol was replaced by water in order to remove any iso-butanol residue. This washing step was done twice. Finally, the remaining water was absorbed by filter paper.

The stacking gel solution was prepared analogously to the separation gel and pipetted on the polymerized separation gel. The comb was inserted into the stacking gel and the gel was left to polymerize.

3.2.4.2. Sample preparation and loading

The sample buffer *(see 2.2. Buffers and solutions)* was completed by addition of 2 – mercaptoethanol just before use (because 2 – mercaptoethanol is instabile). 20µl of the completed sample buffer was added to each sample *(see 3.2.3.3. Precipitation)*. Then the samples were incubated for 3' at 95°C followed by short centrifugation. At this point the samples were ready for loading to the gel, and they were not kept on ice anymore.

The outermost slots of each gel were loaded with sample buffer. One slot of each gel was loaded with the NEC-811 protein MW marker and the remaining slots were loaded with 17µl samples from each chase time-point.

3.2.4.3. Gel electrophoresis

Once loaded with samples, the gels were connected to the power supply. The electrophoresis was performed at constant 90V for approximately 2 hours, i.e. till the sample buffer reached the end of the gel.

3.2.4.4. Gel fixation and enhancing

After electrophoresis, the Mini PROTEAN 3® System was dismounted and the stacking gel was removed. The separation gel was carefully transferred to a container, containing the fixation solution. After 30 minutes of fixation while shaking, the

fixation solution was exchanged by the EN3HANCE solution and the gels were incubated for another 30 minutes while shaking. Then the EN3HANCE solution was discarded separately and the gels were gently washed with tap water. Afterwards, the tanks containing the gels were filled with water and incubated for another 20 minutes while shaking.

3.2.4.5. Gel drying

The washed gels were transferred to wet filter papers, and the filter papers were positioned on the gel dryer and covered by saran wrap. Then the dryer was assembled and the gels were dried for approximately 40 minutes at 80°C. After a cool down for 10 minutes, the gels were ready for fluorography.

3.2.5. Fluorography

The gels which were attached to the filter papers after drying were adjusted to appropriate film cassettes together with X – ray films in the dark room. The assembled and closed cassettes were incubated at -80°C for at least 12 hours. After this exposure time, the cassettes were left for about one hour at room temperature in order to warm up. Then the cassettes were opened in the dark room and the X – ray films were developed.

3.3. Half life determination of the ERAD substrates RI332 and RI332-6HA

In order to determinate the half life times of RI332 and RI332-6HA, a similar procedure was applied as described in *3.2. Screening for stable ERAD substrate expression*. The deviations from the procedure are described below.

3.3.1. Pulse chase analysis

In order to prepare cells for the pulse chase analysis, the QC clones were seeded to the 6 – well plates at a density of 40%. The G3 clones were seeded at a density of 50%. This was done due to the fact that the QC cells had a faster growth rate. After an incubation period of two days at 37°C and 5% CO2, the cells typically reached a density of approximately 90% which was optimal for further experiments.

Unlike the pulse chase analysis for screening studies described in *3.2.1. Pulse – chase analysis*, in the half life determination studies the cells were additionally incubated in the presence of drugs/inhibitors *(see 2.6. Inhibitors)*. In these cases, a pre-incubation of the cells was done with the appropriate inhibitor, prior to the starvation phase.

Also the starvation, pulse and chase phases were done in presence of the appropriate inhibitor.

3.3.1.1. Pulse chase with drugs

Deoxymannojirimycin (dMJ) was supplied in 10mg packages. To obtain a 50mM stock [=25x], the powder content was dissolved in sterile ddH2O. This was done under sterile conditions. The dMJ stock was stored at -20°C. For the half life determination of the ERAD substrates, a final concentration of 2mM was used.

For pulse chase with dMJ, five chase time points were done: 5', 30', 60', 75' and 90'. Therefore, the following volumes of media were prepared in falcon tubes:

- **Pre-incubation medium (1ml/well):** 20,5ml complete medium + 820µl of dMJ stock
- **Starvation medium (0,8ml/well):** 16,5ml starvation medium + 660µl of dMJ stock
- **Pulse medium (0,8ml/well):** 16,5ml starvation medium + 660µl of dMJ stock + 440µl NEG-072 Expre^{35}s^{35}s protein labeling mix
- **Chase medium (1ml/well):** 20,5ml complete medium + 820µl stock of dMJ stock + 205µl Met + 205µl Cys

The total amount of inhibitor was approximately 3ml (of the stock solution) for each set of experiments.

Kifunensine (KIF) was supplied in 1mg packages. The powder was dissolved in warm, sterile ddH2O to obtain a 500x stock [1mg/ml]. The stock solution was kept at -20°C. For the pulse chase analysis, a final concentration of 2µg/ml was used. In case of KIF, seven chase time points were done as with controls (in the absence of the drugs): 5' – 90'. The media were prepared as follows:

- **Pre-incubation medium (1ml/well):** 29ml complete medium + 58µl KIF stock
- **Starvation medium (1ml/well):** 29ml starvation medium + 58µl KIF stock
- **Pulse medium (0,8ml/well):** 23,5ml starvation medium + 47µl KIF stock + 600µl NEG-072 Expre^{35}s^{35}s protein labeling mix

- **Chase medium (1ml/well):** 29ml complete medium + 58µl KIF stock + 290µl Met + 290µl Cys

Total amount of used KIF stock was 221µl for each set of experiments.

5mg of **Carbobenzoxy-L-leucyl-L-leucyl-L-leucinal (ZLLL)** was dissolved in 1,05ml DMSO to obtain a 10mM ZLLL stock [=200x]. The ZLLL stock was stored at -20°C. For the pulse chase analysis, a final concentration of 50µM was diluted out of the stock solution.

As for dMJ, only five chase time points were done with ZLLL: 5', 30', 60', 75' and 90'. Therefore, the media were prepared as follows:

- **Pre-incubation medium (1ml/well):** 20,5ml complete medium + 102,5µl of ZLLL stock
- **Starvation medium (1ml/well):** 20,5ml starvation medium + 102,5µl of ZLLL stock
- **Pulse medium (0,8ml/well):** 16,5ml starvation medium + 82,5µl of ZLLL stock + 440µl NEG-072 Expre^{35}s^{35}s protein labeling mix
- **Chase medium (1ml/well):** 20,5ml complete medium + 102,5µl stock of ZLLL stock + 205µl Met + 205µl Cys

For each pulse chase analysis, 390µl of the ZLLL stock was used.

Castanospermine (CST) was delivered in 10mg packages. The content was dissolved in 1ml sterile ddH2O to obtain a 52,9mM stock solution [=52,9x]. Like all other drugs, the CST stock solution was kept at -20°C. For the pulse chase analysis, all chase time points were done as with controls. The media were prepared as follows:

- **Pre-incubation medium (1ml/well):** 29ml complete medium + 549µl CST stock
- **Starvation medium (0,8ml/well):** 23ml starvation medium + 435µl CST stock
- **Pulse medium (0,8ml/well):** 23ml starvation medium + 435µl CST stock + 600µl ^{35}S NEG-072 Expre^{35}s^{35}s protein labeling mix

- **Chase medium (1ml/well):** 29ml complete medium + 549µl CST stock + 290µl Met + 290µl Cys

All further steps including cell lysis, immunoprecipitation, and SDS-PAGE were done in the same way as described in *3.2. Screening for stable ERAD substrate expression*. The developed X-ray films were analyzed with a densitometer to allow precise half life determination of the ERAD substrates.

3.3.2. Densitometry

The Fusion-FX7 imager was used for scanning of the developed X – ray films. To this, the films were placed into the imager which was operated with the Fusion-CAPT-Software.

After the films were set in the imager, the film was focused by the "autofocus" option in the software. Then the films were exposed for 0.4 seconds to UV light and then the images were captured. The images (with .tiff extensions) were further analyzed with the ChemiImager 4400 software.

The figures were analyzed by the "Spot denso" option which is found in "Analysis tools". Because the bands were dark, the option "invert" was used. Each band was circumscribed by the rectangle tool. Afterwards, for each lane, i.e. for each chase time point slot, a background was defined by the background rectangle tool. Then the two rectangles in each lane (one defining the endogenous ribophorin I and the second defining the soluble truncated ribophorin I) were linked to the appropriate background rectangle tool.

The raw data were copied to Microsoft Excel 2007 in which the analysis was continued. The coefficients were calculated of each soluble truncated ribophorin I and its corresponding endogenous ribophorin I (both in the same chase time point lane). With other words, each soluble ribophorin was normalized with its corresponding endogenous ribophorin I. The coefficient of the soluble ribophorin at time point 5' was set as 100%. The soluble ribophorins of the different time points were related to the first one (5').

For each clone an exponential regression (first order kinetics) was calculated on the results of each pulse chase experiment. This regression generated two formulas with y being the relative amount of soluble ribophorin after a certain chase time x (e.g.):

$$y = 118{,}36286e^{-0{,}01472x}$$

$$R^2 = 0{,}97970$$

The first formula was used for the calculation of the half life. To this, the positive exponent (in this case: 0,01472) was applied to following formula:

$$t_{1/2} = \frac{\ln(2)}{positive\ exponent}$$

So in the given example:

$$t_{1/2} = \frac{\ln(2)}{0{,}01472} = \mathbf{47{,}09\ minutes}$$

The second formula gave information about the curve progression. The progression was better the closer the value was to 1. In the case of the sample, the progression was almost ideal.

3.3.3. Restoring of the wild type phenotype in QC cells

In order to restore the G3 wild type phenotype in the QC cell lines, the cells were cultivated in high galactose medium. Subsequent to the high galactose cultivation, pulse chase analysis and all further steps described earlier were done to estimate the half life of the soluble truncated ribophorins. The preparation of high glucose and high galactose media is described in *3.1.1.3. High & low glucose RPMI media.*

3.3.3.1. Pulse chase analysis

Different from the earlier described pulse chase analysis, the cells were seeded and cultivated for 48 hours in the high galactose and high glucose media in parallel. After this period, the cell density was estimated in the light microscope. If the minimal cell density of 80% was reached, the experiment was continued. The starvation phase (30') was performed in methionine free RPMI medium with and without galactose (5mM), respectively. The same was true for the pulse phase (15') except that the labeled methionine was added to both media. Apart from these deviations, the pulse chase analysis and all following steps (i.e. cell lysis, immunoprecipitation, SDS PAGE

and densitometry) were performed as described in *3.2. Screening for stable ERAD substrate expression* and *3.3.2. Densitometry*.

3.3.3.2. Cell visualization

QC cells were cultivated in 100mm tissue plates with the high galactose medium for seven days in order to restore the wild type morphology. During the cultivation, the cells were split every time they had reached a density of more than 90%. On the 7th day images of the cells were taken in the microscope.

3.4. Analysis of ERAD substrate – calnexin association

In order to analyze the interaction between calnexin and the ERAD substrates (RI332 and RI332 – 6HA), the pulse chase protocol was modified. Accordingly, co – immunoprecipitation was done. Finally, SDS PAGE was performed and the gels were analyzed by densitometry.

3.4.1. Pulse chase analysis

For the purpose of the calnexin – ERAD substrates interaction analysis, only two chase time points were chosen: 5' and 60'. For both chase points three wells of the 6 – well plates were seeded with each of the four clones. After an incubation period of 48 hours, the cell density was estimated. Cells with a minimal density of 80% were further processed. After a standard starvation phase for 30', the pulse phase was done for 60' (instead of 15'). Finally, the cells were incubated in the chase phase for 5' and 60' minutes, respectively.

3.4.2. Cell lysis

One well of each clone was used for the SDS lysis already described previously (*stringent* lysis), while the two remaining wells were used for a more gentle lysis method (*non – stringent* lysis; *see 3.4.2.1. Non stringent lysis (CHAPS)*). In order to perform the stringent lysis, the procedure described in *3.2.2. Cell lysis* was followed, whereas the non – stringent lysis was different.

3.4.2.1. Non stringent lysis (CHAPS)

Two wells of each clone were washed with ice cold PBS. Next, 300µl of the CHAPS lysis buffer *(see 2.2. Buffers and solutions)* was added to each well. The cells were scraped and collected in labeled Eppendorf tubes which were kept on ice. Afterwards, additional 300µl of the CHAPS lysis buffer was added to the same wells, and again the cells were scraped and collected in the appropriate Eppendorf tubes. The collected

cells (600µl in total) were kept on ice for 30'. After the incubation period, the cell lysates were centrifuged for 10' at 4°C and maximum speed. Subsequent to the centrifugation step, a pre-cleaning was performed by transferring 570µl of the cell suspensions to new Eppendorf tubes and adding of 30µl protein A sepharose beads (the beads were prepared as described in *3.2.3.1. Protein A sepharose beads preparation*, but with CHAPS wash buffer instead of SDS wash buffer) to each tube. In order to finish the pre-washing step, the eppendorf tubes were incubated for 30' at 4°C and while rotating, followed by 5' centrifugation at maximum speed. The supernatant was used for the co – immunoprecipitation.

3.4.2.2. Co – immunoprecipitation

The supernatants of each clone were collected to obtain a total volume of 1140µl. Afterwards, the lysates were aliquoted to four Eppendorf tubes: 200µl to two tubes (=400µl) and 350µl to the other two tubes (=700µl). The two Eppendorf tubes of each clone containing 200µl solution were used for only one immunoprecipitation, while the other two tubes were used for two consecutive immunoprecipitations. However, 30µl of protein A sepharose beads was added to each tube. Then 30µl of αRI polyclonal antibody (RI lum; 1:10 dilution) was added to one 200µl and one 350µl tube, while 30µl of αcalnexin polyclonal antibody (1:10 dilution) was added to the other two tubes (200µl and 350µl). All samples were incubated o/n at 4°C while rotating.

Following to the o/n incubation, the samples were washed with CHAPS wash buffer. This was done in the following manner: the samples were centrifuged for 3' at RT and 8000 rpm. Afterwards, the supernatant was discarded and the pellets were resuspended in 1ml chaps wash buffer. Then the samples were rotated for 10' at 4°C. The same procedure was repeated two more times, and a third time with HBS instead of the CHAPS wash buffer.

After the washing steps, the samples which were used for only one immunoprecipitation were resuspended in fresh sample buffer, and afterwards they were frozen at -20°C where they were kept o/n. The samples which were intended for a co – immunoprecipitation were processed as follows: the samples were centrifuged and the supernatant (mainly HBS) was discarded. The pellets were resuspended in 150µl SDS lysis buffer and were incubated for 5' at 95°C. After the

samples were boiled up, they were centrifuged at 8000rpm for 3'. Subsequently, the supernatant was transferred to new Eppendorf tubes. Another 150μl SDS lysis buffer was added to the old samples in order to repeat the boiling step. Again the samples were centrifuged and the supernatants were collected in the appropriate tubes. Then 1ml of SDS wash buffer was added to 300μl of each sample. Afterwards, 30μl of protein A sepharose beads (prepared in SDS wash buffer) was added to each sample. Finally, 30μl of αRI polyclonal or αcalnexin polyclonal antibodies (both diluted 1:10) were added to the samples as follows: the αRI antibody was added to the samples which were previously immunoprecipitated with αcalnexin antibodies, and the αcalnexin antibodies were added to the samples which were previously immunoprecipitated with αRI antibodies. All samples were incubated over night while rotating at 4°C.

After the incubation period, the samples were washed with SDS wash buffer and PBS as already described. Then 20μl fresh sample buffer was added and all samples (including the stringent and non – stringent samples from the day before) were boiled at 95°C for 3'. Finally, the samples were ready for loading on the polyacrylamid gels.

3.4.2.3. SDS PAGE and densitometry

SDS PAGE was performed as described earlier. However, two different exposure times were performed for each gel. A short exposure time of 12-24 hours, and a long exposure time of 3-4 weeks. The films were analyzed with the ChemiImager 4400 software as already described.

3.5. Intracellular localization of RI332 and RI332-6HA

The two ERAD substrates were localized with immunofluorescence using antibodies for three different compartments: ER, ERGIC and Golgi. For this purpose, the cells were grown on cover slips (CS) and stained with the appropriate antibodies.

3.5.1. Seeding of cells

The cells were seeded on sterile CSs. In order to do so, sterile CSs were supplied in 100mm tissue culture plates. Afterwards, 10ml of pre-warmed medium was added to the plates paying attention that the CSs stay on the ground of the plates, i.e. that they do not swim in top of medium. Then, cells were split into the plates containing CSs

Combinations with αRI antibodies		
RI polyclonal (1:200) (RI, RI332 and RI332-6HA marker)	with	CALNEXIN monoclonal (1:50) (ER marker)
RI polyclonal (1:200) (RI, RI332 and RI332-6HA marker)	with	ERGIC53 monoclonal (1:1000) (ERGIC marker)
RI polyclonal (1:200) (RI, RI332 and RI332-6HA marker)	with	CTR433 monoclonal (1:40) (Golgi marker)
Combinations with αHA antibodies		
HA.11 monoclonal (1:50) (RI332-6HA marker)	with	CALNEXIN polyclonal (1:200) (ER marker)
HA.11 monoclonal (1:50) (RI332-6HA marker)	with	ERGIC53 polyclonal (1:50) (ERGIC marker)
HA.11 monoclonal (1:50) (RI332-6HA marker)	with	GIANTIN polyclonal (1:2000) (Golgi marker)

Table 8. Antibody combinations used for the localization experiments

with a total density of about 10 - 20%. The cells were incubated for 48 hours at 37°C and 5% CO2.

3.5.1.1. Incubation with drugs

Additionally, the cells were also incubated with drugs in some experiments. For this, the cells were seeded just as described in *3.5.1. Seeding of cells*, but after 34 hours incubation, the growth medium was removed and new medium containing the appropriate inhibitor was added *(see 2.6. Inhibitors)*. Then the cells were incubated for additional 14 hours at 37°C and 5% CO2.

3.5.2. Fixation of the cells

After incubation, the growth medium was discarded and the cells were washed with 1x PBS. During washing, it was paid attention that the CSs stay on the bottom of the dish. PBS was removed and cold methanol (-20°C) was added to the dishes (enough methanol to cover all CSs). The cells were incubated for 3' at -20°C. Then the methanol was removed and the cells were briefly washed three times with PBS, and additionally incubated for 10' in PBS while shaking.

3.5.3. Immunolabeling

After washing, blocking solution was added to the dishes containing the CSs. The cells were incubated with blocking solution for one hour while shaking at RT. Meanwhile, the primary antibodies were diluted and kept on ice. Typically, two different antibodies were used (one monoclonal and one polyclonal) for staining. However, for the analysis of co-localizations, single stainings were done as well. (see table 8 for antibody combinations).

After the incubation in PBS, 20µl of the diluted antibodies were pipetted on wax plates. Then the CSs were put on the drops with the cells facing down. Before

applying, the CSs were dripped off by leaning the CS's edge to a paper towel. The wax plate was put into a wet chamber and incubated for one hour at 37°C.

Afterwards, the CSs were transferred to 6 well plates in order to remove unbound antibodies. For the washing steps, blocking solution was pipetted to each well containing CSs and the 6 – well plates were incubated for 10' while shaking. Then the blocking solution was discarded and fresh blocking solution was added. Washing was repeated three times. After washing, the cells were incubated with the 2nd antibodies. Both 2nd antibodies *(see 2.5. Antibodies)* were prepared in blocking solution at a concentration of 1:200. Then the 2nd antibody dilution was portioned per 20μl on the wax plate, and the CSs were put on the drops with the cells facing down. The wax plate was incubated in the wet chamber for one hour at 37°C. All working steps with 2nd antibodies were performed under dimmed conditions.

After this incubation, the CSs were transferred to 6 – well plates in order to be washed. Washing was performed as described earlier but with two additional washing cycles with PBS instead of blocking solution. Finally, the CS's were mounted on glass slides. Small drops of mounting solution were placed to the glass plates and they were covered with the CSs, with the cells facing down. The excess of mounting medium was soaked up and the CSs were sealed with nail varnish which was applied to the edges of the CSs. The glass slides were stored at 4°C.

3.5.4. Visualization

Cells were visualized with the LSM 510 META microscope (Zeiss), and with the help of the ZEN 2009 software. Before imaging, adjustment of the microscope was done as follows.

3.5.4.1. Microscope adjustment

All parameters were adjusted using the ZEN 2009 software. The optic parameters were adjusted as follows: the Plan-Apochromat 63x objective was chosen and the transmitted light filter was set to 100%. Then the transmitted light fieldstop was set to 82.07%. Two different reflectors were used: FSet20 for the red channel and FSet10 for the green channel.

Two lasers were turned on: Argon/2 (laser lines [nm]: 458, 477, 488 and 514) and HeNe1 (laser line [nm]: 561).

In the imaging setup, the “Channel mode” was used and the track was switched after every frame. The scan mode was set to “Frame” and the frame size was 512 x 512. The scanning speed was set to 8. The pinhole for both channels was set to 1.35.

Above parameters were used for all samples. However, it was not necessary to adjust the parameters each time: the “reuse” option in the ZEN 2009 software was used in order to reset all parameters automatically once they were configured for one picture.

3.5.4.2. Imaging

The microscopic slides prepared were applied on the microscope. Segregated cells were searched directly in the microscope. Once found, they were visualized in the ZEN 2009 software. The “Snap” option was chosen in order to have a first look at the staining. The “Range indicator” was used for each channel separately in order to adjust the offset and overexposure. For this, “Continuous scan” was started and the “Master gain” was increased (or decreased) just before red signals appear on the cells. The “Digital offset” was also adjusted in order to remove the blue background. Finally, both lasers were selected and the “Start experiment” option was chosen. The pictures were saved and used for further processing.

3.5.4.3. Threshold setup

In order to perform colocalization studies, first of all, single stainings were used to adjust the thresholds for each staining. For this, a single staining of the ERAD substrate (either a staining with RI lum, or with the HA.11, respectively) was opened in the ZEN 2009 software. The part “Colocalization” was selected, and in the case of HA.11 staining the vertical threshold was set up in a way that all dots (signals) remain limited to the 2nd scatter region. For RI lum staining, the signals were limited to the 1st scatter region. The same was done with single stainings of all antibodies.

3.5.4.4. Raw colocalization data

Once the thresholds were adjusted for all antibody combinations, double stainings were opened and the raw data located in the “Colocalization” part were copied to the clipboard, and further to a Microsoft Excel 2007 file.

3.5.4.5. Statistical evaluation

Statistical evaluation of the colocalization data was done with the statistics software SPSS 19.0 (IBM). First, variables were defined in the *variable view* folder for the

statistical evaluation of the influence of the inhibitors used on the ERAD substrate colocalization. The variables for each antibody combination (HA.11 vs. CALNEXIN, HA.11 vs. GIANTIN, RI lum vs. ERGIC53 and RI lum vs. CTR433) were defined in separate SPSS files as shown in table 9.

In order to evaluate the ERAD substrate distribution in the different cellular compartments, SPSS files for each antibody and cell line combination were created with the variables shown in table 10.

Name	Type	Column format	Decimal number	Value labels	Missing values	No. of columns	Scale level
Cells	Number	8	0	1=G3_RI332 2=G3_RI332-6HA 3=QC_RI332 4=QC_RI332-6HA	999	8	Nominal
Condition	Number	8	0	1=Control 2=CST 3=KIF 4=ZLLL	999	8	Nominal
CH3T2	Number	8	3	-	999	8	Scale
CH3T2W	Number	8	3	-	999	8	Scale

Table 9. Variables used for statistical evaluation of the influence of the inhibitors on the ERAD substrate location.

Name	Type	Column format	Decimal number	Value labels	Missing values	No. of columns	Scale level
Cells	Number	8	0	1=G3_RI332 2=G3_RI332-6HA 3=QC_RI332 4=QC_RI332-6HA	999	8	Nominal
Combination of antibodies	Number	8	0	1=HA_GIANTIN 2=HA_CALNEXIN 3=RI_CTR433 4=RI_ERGIC53	999	8	Nominal
CH3T2 / CH2T1	Number	8	3	-	999	8	Scale
CH3T2W / CH2T1W	Number	8	3	-	999	8	Scale

Table 10. Variables used for statistical evaluation of ERAD substrate colocalization with different cellular compartments.

After defining all variables, raw data were copied from Microsoft Excel to the Dataview map in SSPS. In case of the 6HA tagged substrates, raw data from the CH3T2 and CH3T2W were used. The CH3T2 colocalization coefficient is the number of red pixels (RI332-6HA signals) colocalized with green signals (Golgi apparatus or calnexin signals) with no respect on the signals intensity, whereas the CH3T2W colocalization coefficient takes the signal intensity into account. Raw data from the CH2T1 and CH2T1W channels were used for colocalization evaluation of the non-tagged substrates. The CH2T1 colocalization coefficient is the number of green signals (RI and RI332 signals) colocalized with red signals (Golgi apparatus or ERGIC signals) with no respect on the signals intensity, whereas the CH2T1W colocalization coefficient taks the signal intensity into account. Finally, a 2-sided t-test of independent samples was performed. The results of every t-test were collected in form of two tables which will be explained in the part *4. Results*.

4. Results

4.1. Half life determination of the ERAD substrates RI332 and RI332-6HA

In the first part of this section (4.1.1. to 4.1.20; Figs. 15 to 34) a typical experiment (fluorogram and quantitation of densitometric scanning using a first order kinetics) for each cell line and condition is shown. Each experiment was performed at least in duplicate (mostly in triplicate), and the mean values were used for drawing the charts shown in figures 15 to 34. For the determination of the degradation kinetics, the first chase time point was the 15 minutes time point, since for most of the experiments there was still an increase of the RI332 (and RI332-6HA, respectively) amount observed between 5' and 15' minutes, most likely due to a lag phase.

In the second part (4.1.21; Figs. 35 to 36) an overview over all half life determinations by pulse chase experiments is given. This includes a statistical analysis for all sets of experiments. Table 11 gives an overview of the mean half life times, number of experiments and standard deviations for each experiment.

4.1.1. Half life of RI-332 in the G3 cell line (clone 13) in absence of drugs

Three pulse chase experiments were performed in order to determine the half life of RI332 in the G3 cell line (G3-RI332; clone 13). As seen in figure 15 (lower panel), the endogenous ribophorin I is stable during the whole chase period, while the relative amount of the ERAD substrate RI332 becomes less during chase time. The quantitation of the relative amounts of RI332 during the chase time determined by densitometric scanning is shown in upper panel of figure 15. The estimated mean half life of RI332 is *47,19 ± 4,06 minutes*.

4.1.2. Half life of RI-332-6HA in the G3 cell line (clone 10) in absence of drugs

Three pulse chase experiments were performed in order to determine the half life of RI332-6HA in the G3 cell line (G3-RI332-6HA; clone 10). The quantitation of the relative amounts of RI332-6HA during the chase time determined by densitometric scanning is shown in upper panel of figure 16. The tagged ERAD substrate RI332-6HA seems to be slightly more stable than the non-tagged variant (RI332 in G3-RI332; clone 13): *57,19 ± 13,73 minutes*

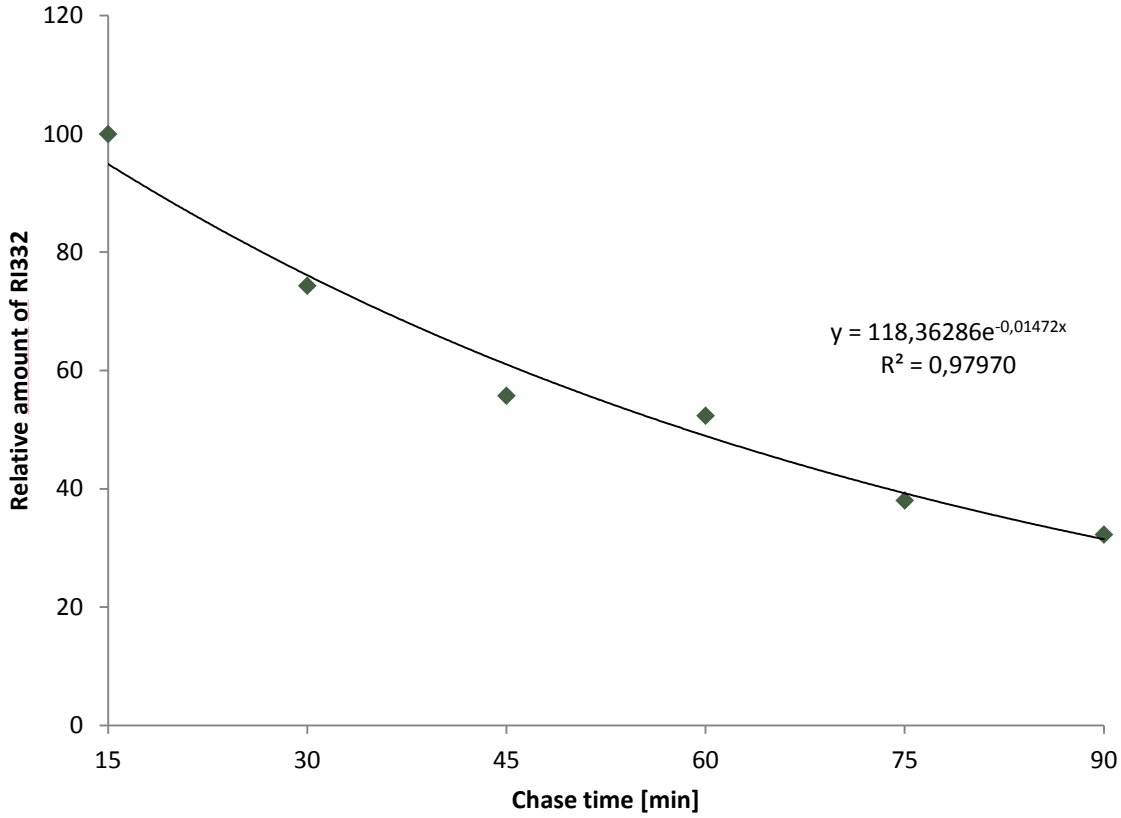

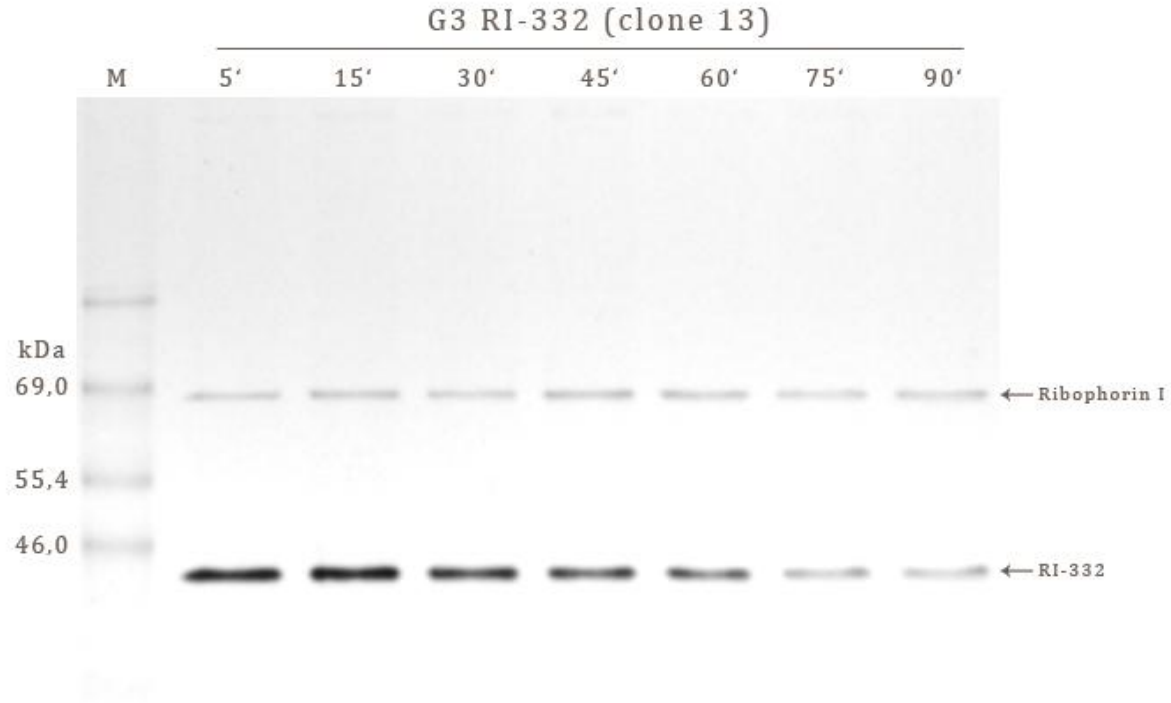

Figure 15. Above: relative amount of RI332 in G3 cells (clone 13) grown in the absence of inhibitors. Chase time points 15 – 90 minutes. Below: fluorography of G3 RI-332 (clone 13)

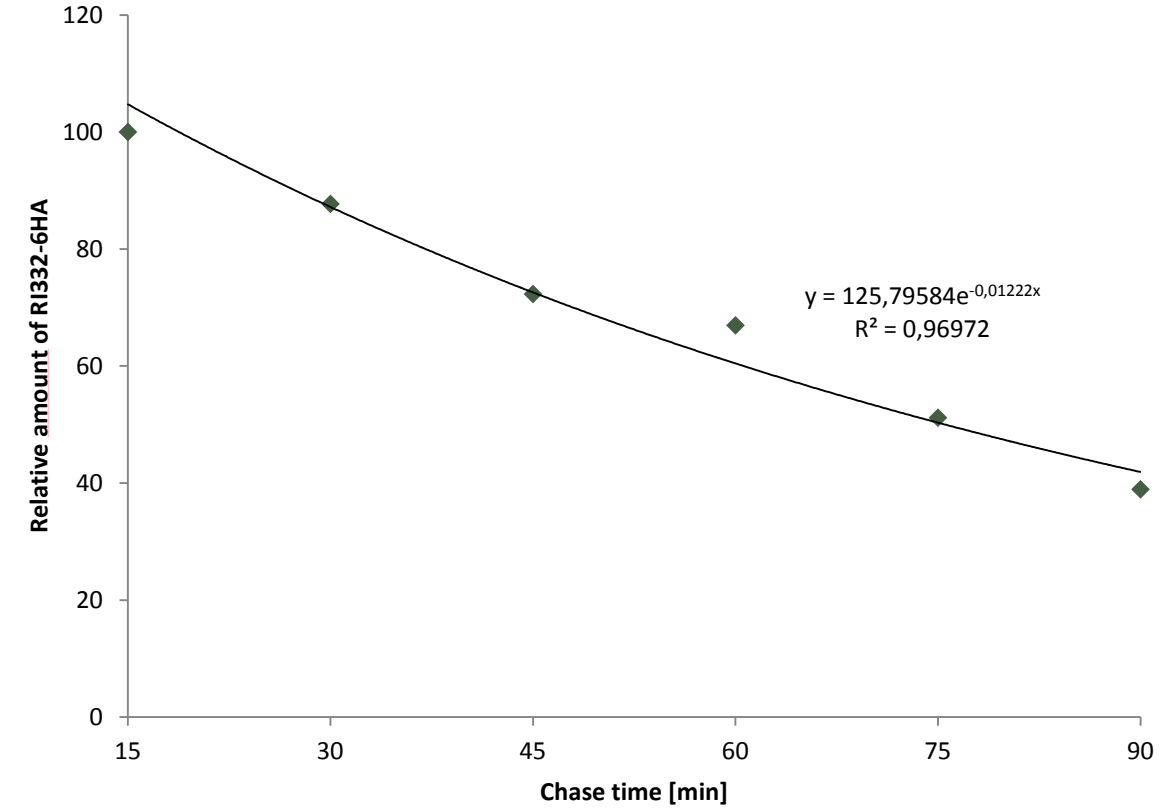

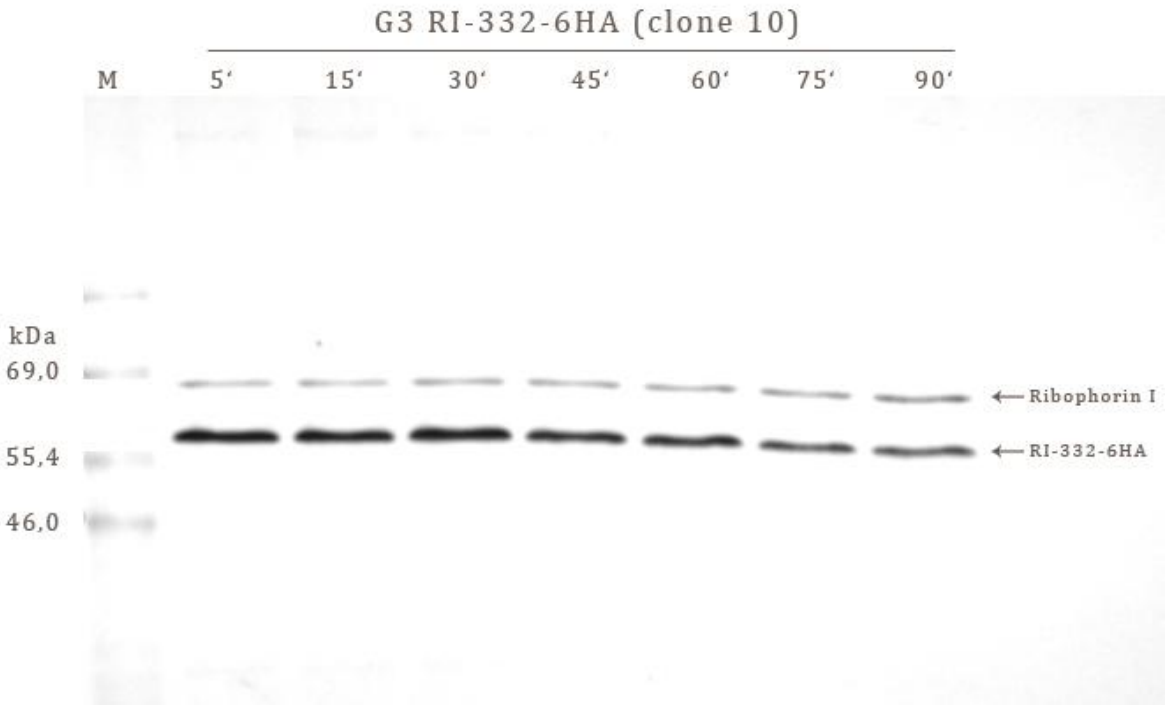

Figure 16. Above: relative amount of RI332-6HA in G3 cells (clone 10) grown in the absence of inhibitors. Chase time points 15 – 90 minutes. Below: fluorography of G3 RI-332-6HA (clone 10)

4.1.3. Half life of RI-332 in the QC cell line (clone GG) in absence of drugs

Three pulse chase experiments were performed in order to determine the half life of RI332 in the QC cell line (QC-RI332; clone GG). From figure 17 it becomes obvious that the ERAD substrate RI332 is considerably less stable than in the G3 cell line. The mean half life determined in this cell line is *21,33 ± 4,64 minutes*.

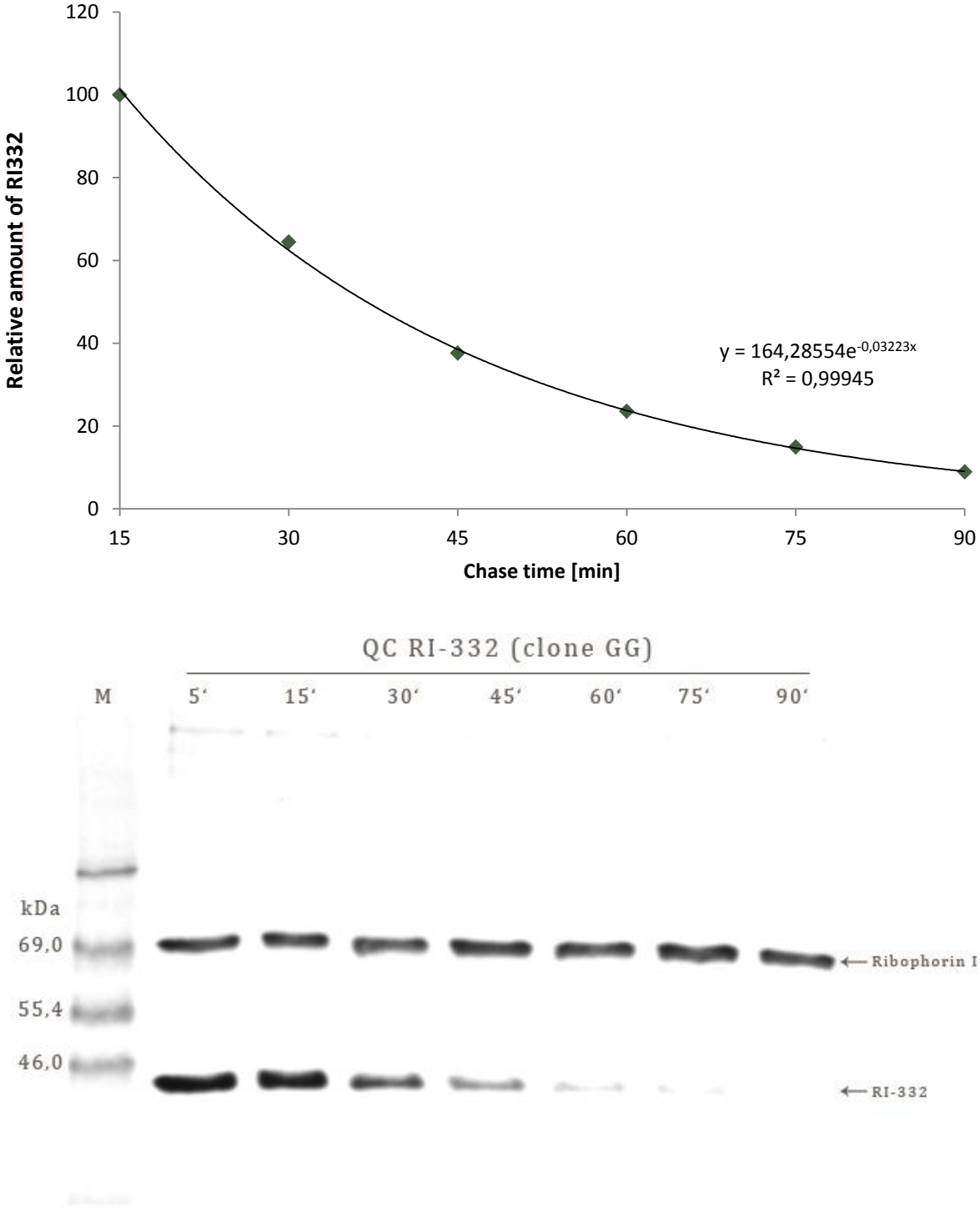

Figure 17. Above: relative amount of RI332 in QC cells (clone GG) grown in the absence of inhibitors. Chase time points 15 – 90 minutes. Below: fluorography of QC RI-332 (clone GG)

4.1.4. Half life of RI-332-6HA in the QC cell line (clone 5) in absence of drugs

Three pulse chase experiments were performed in order to determine the half life of RI332-6HA in the QC cell line (QC-RI332-6HA; clone 5). Similar to the non tagged form, RI332-6HA is significantly less stable than the tagged ERAD substrate in the G3 cell line. The mean half life determined is *17,84 ± 6,86 minutes*.

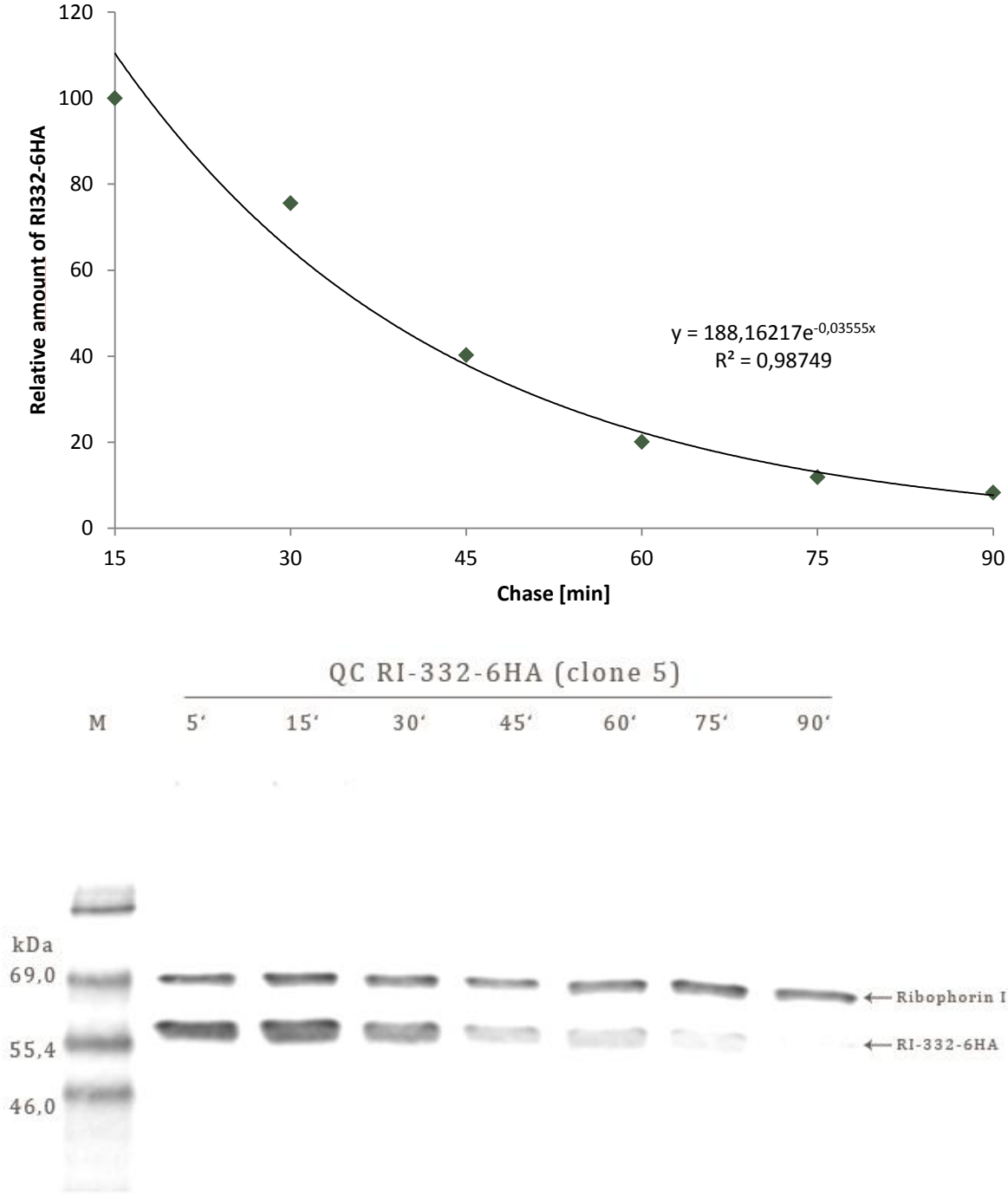

Figure 18. Above: relative amount of RI332-6HA in QC cells (clone 5) grown in the absence of inhibitors. Chase time points 15 – 90 minutes. Below: fluorography of QC RI-332-6HA (clone 5)

4.1.5. Half life of RI-332 in the G3 cell line (clone 13) in presence of CST

As shown in figure 19, the presence of CST slightly enhances the degradation of RI332 in the G3 cell line. The inconsistent ribophorin I signal on the gel is most likely due to faulty pipetting. However, this is not distorting the results, because every signal for the ERAD substrate is normalized with the appropriate amount of ribophorin I. The half life time of RI332 in the G3 cell line, and in presence of CST, is *31,69 ± 3,46 min*.

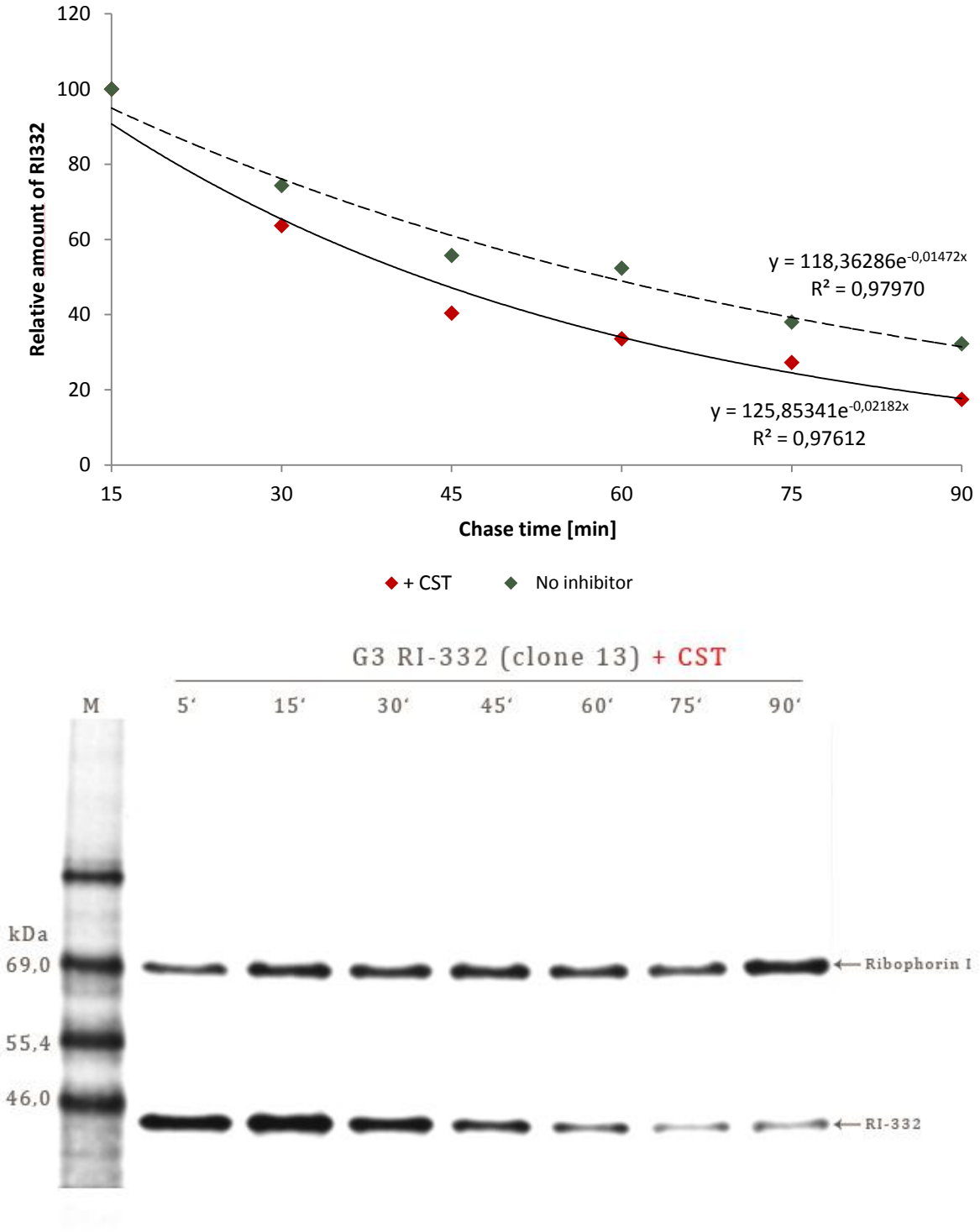

Figure 19. Above: relative amount of RI332 in G3 cells (clone 13) grown in the presence of CST (inhibitor of glucosidases I & II). Chase time points 15 – 90 minutes. Below: fluorography of G3 RI-332 (clone 13)

4.1.6. Half life of RI-332-6HA in the G3 cell line (clone 10) in presence of CST

As shown in figure 20, CST enhances the degradation of RI332-6HA. This indicates that the two ERAD substrates (RI332 and RI332-6HA) seem to avoid the CNX cycle in the G3 cell lines. However, the degradation of RI332-6HA is negligible in contrast to the non tagged version in presence of CST (see figure 19 upper panel). The mean half life time of RI332-6HA in the presence of CST is 49,48 ± 2,96 minutes.

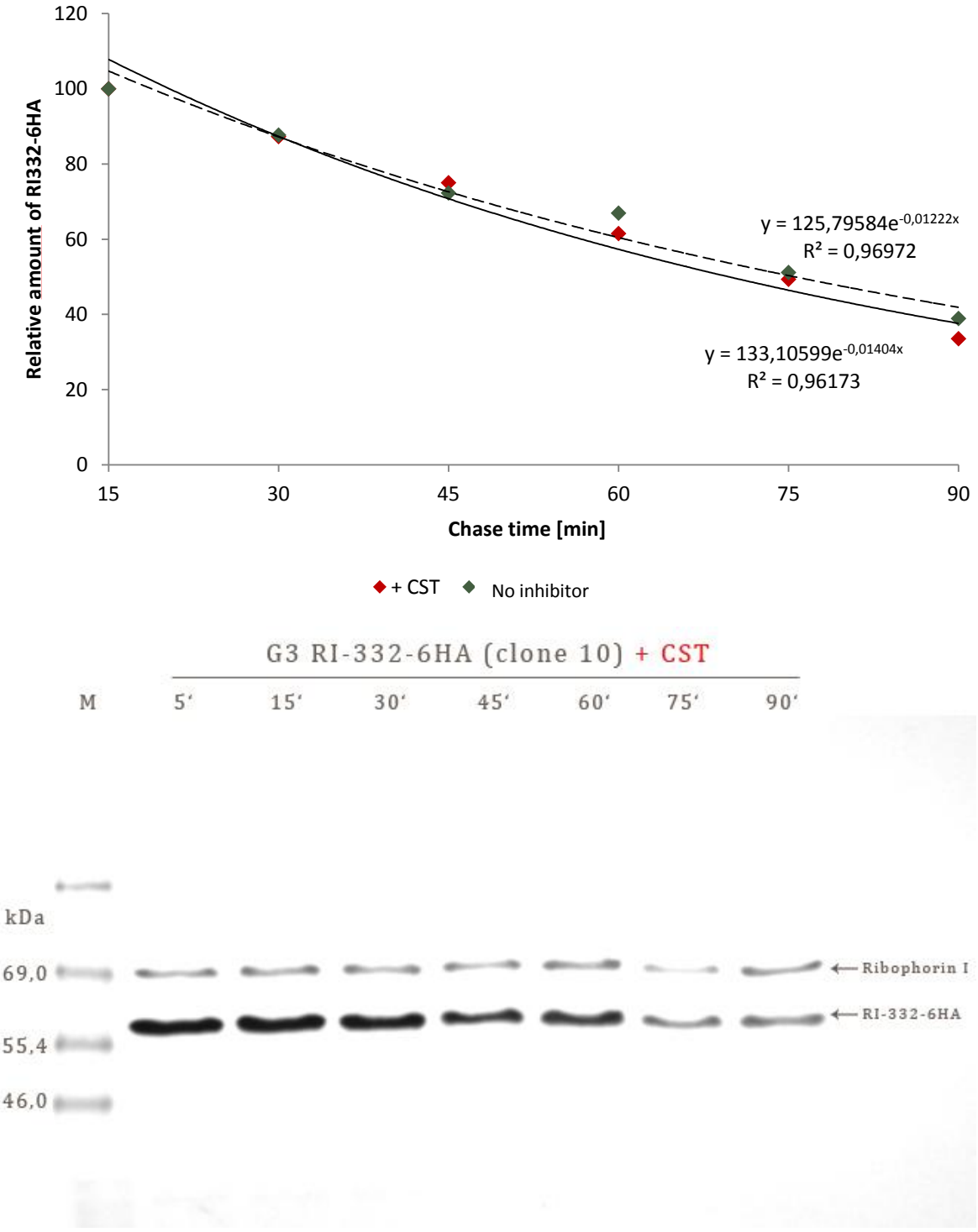

Figure 20. Above: relative amount of RI332-6HA in G3 cells (clone 10) grown in the presence of CST (inhibitor of glucosidases I & II). Chase time points 15 – 90 minutes. Below: fluorography of G3 RI-332-6HA (clone 10)

4.1.7. Half life of RI-332 in the QC cell line (clone GG) in presence of CST

In contrast to the G3 cell line, the degradation of RI332 surprisingly is not enhanced in the QC cells in presence of CST. Actually, the RI332 is stabilized in the presence of CST. The half life time determined for the ERAD substrate in presence of CST is 68,15 ± 22,00 minutes.

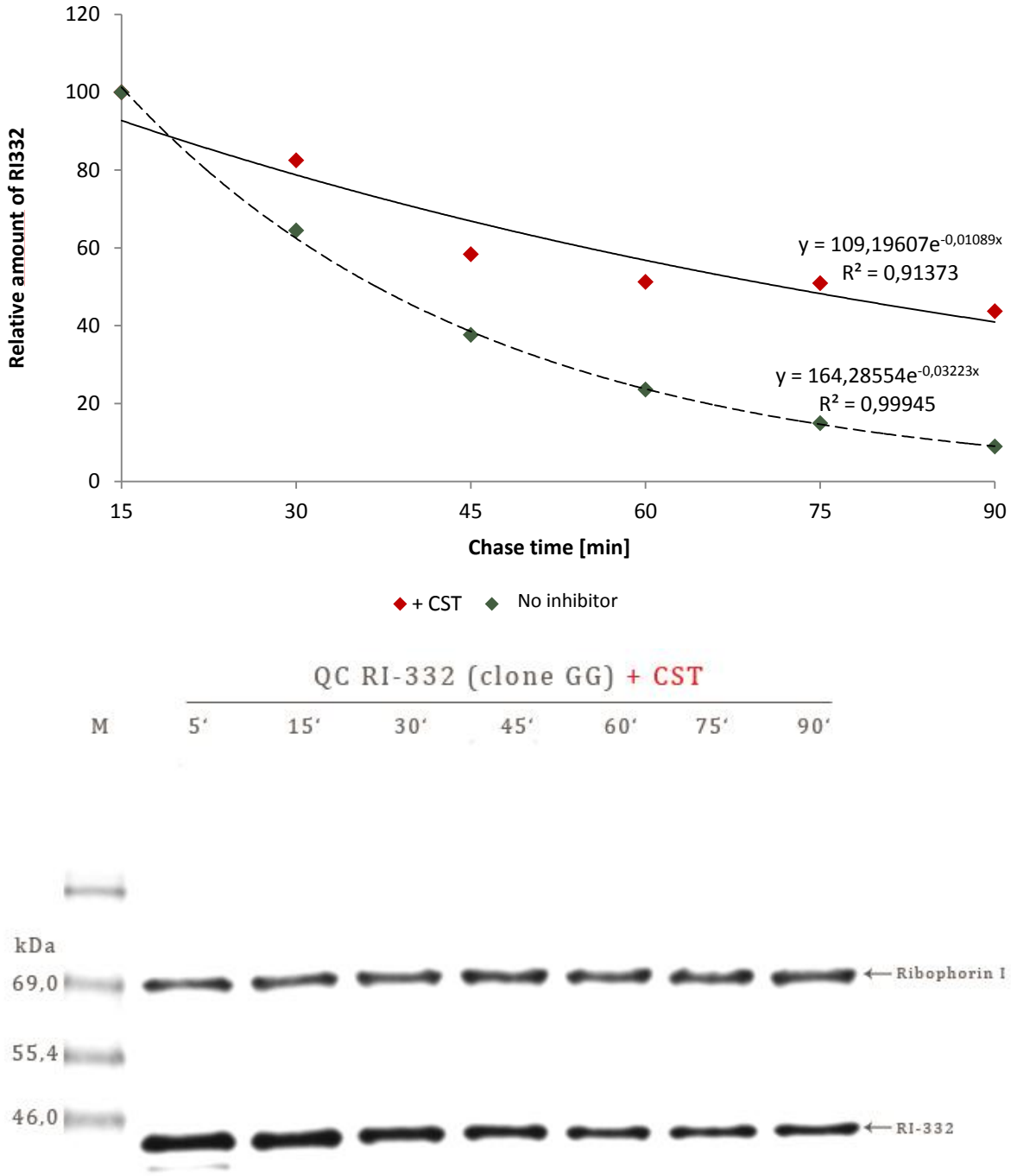

Figure 21. Above: relative amount of RI332 in QC cells (clone GG) grown in the presence of CST (inhibitor of glucosidases I & II). Chase time points 15 – 90 minutes. Below: fluorography of QC RI-332 (clone GG)

4.1.8. Half life of RI-332-6HA in the QC cell line (clone 5) in presence of CST

As for RI332, the tagged ERAD substrate is also stabilized in the presence of CST in the QC cells. The estimated mean half life of RI332-6HA is 47,97 ± 9,50 minutes.

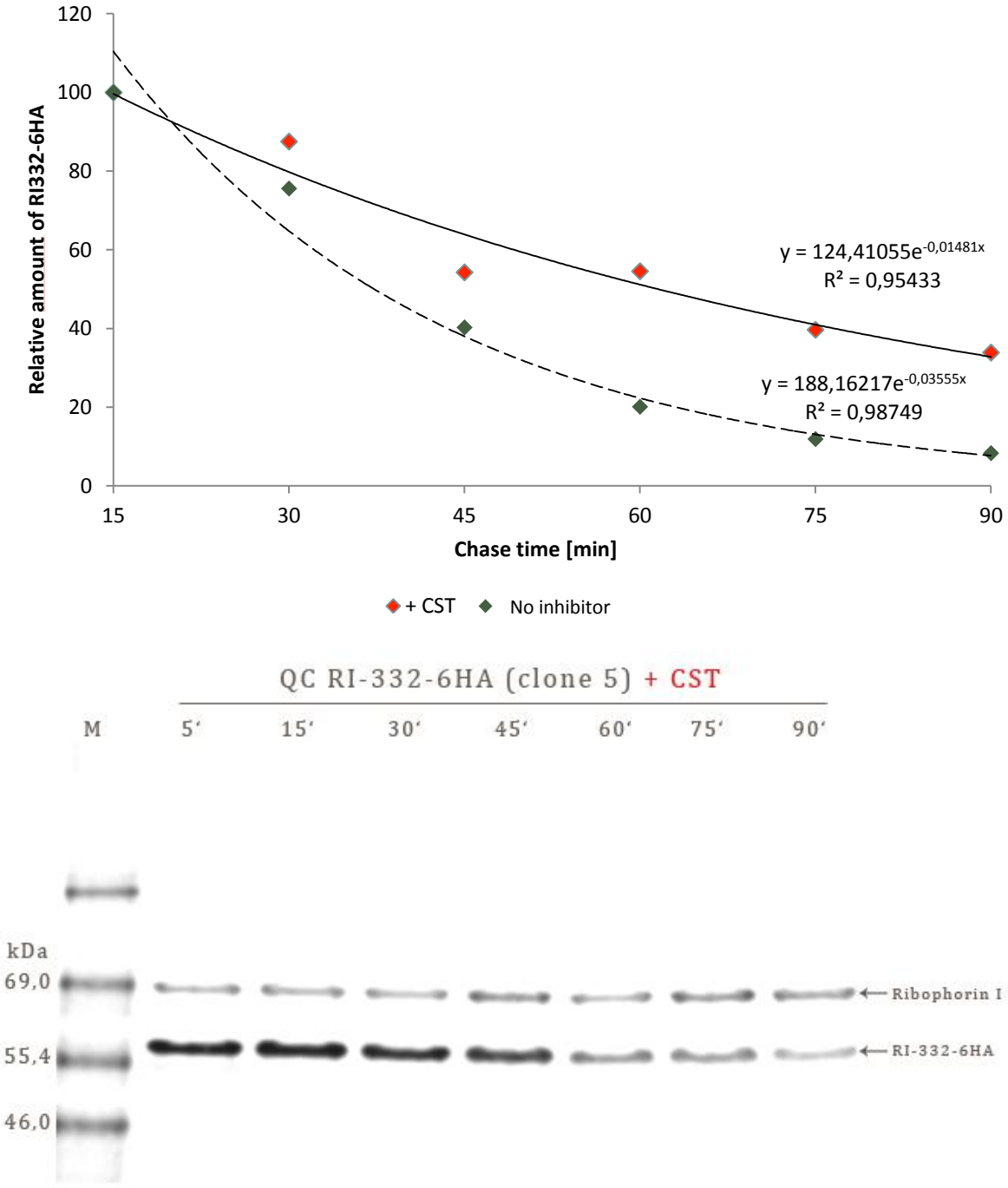

Figure 22. Above: relative amount of RI332-6HA in QC cells (clone 5) grown in the presence of CST (inhibitor of glucosidases I & II). Chase time points 15 – 90 minutes. Below: fluorography of QC RI-332-6HA (clone 5)

4.1.9. Half life of RI-332 in the G3 cell line (clone 13) in presence of DMJ

In order to estimate the half life of RI332 in G3 cells in presence of DMJ, three pulse chase experiments were performed. As seen in figure 23, DMJ dramatically influences the RI332 half life. The stabilized ERAD substrate has a mean half life time of 319,69 ± 95,37 minutes.

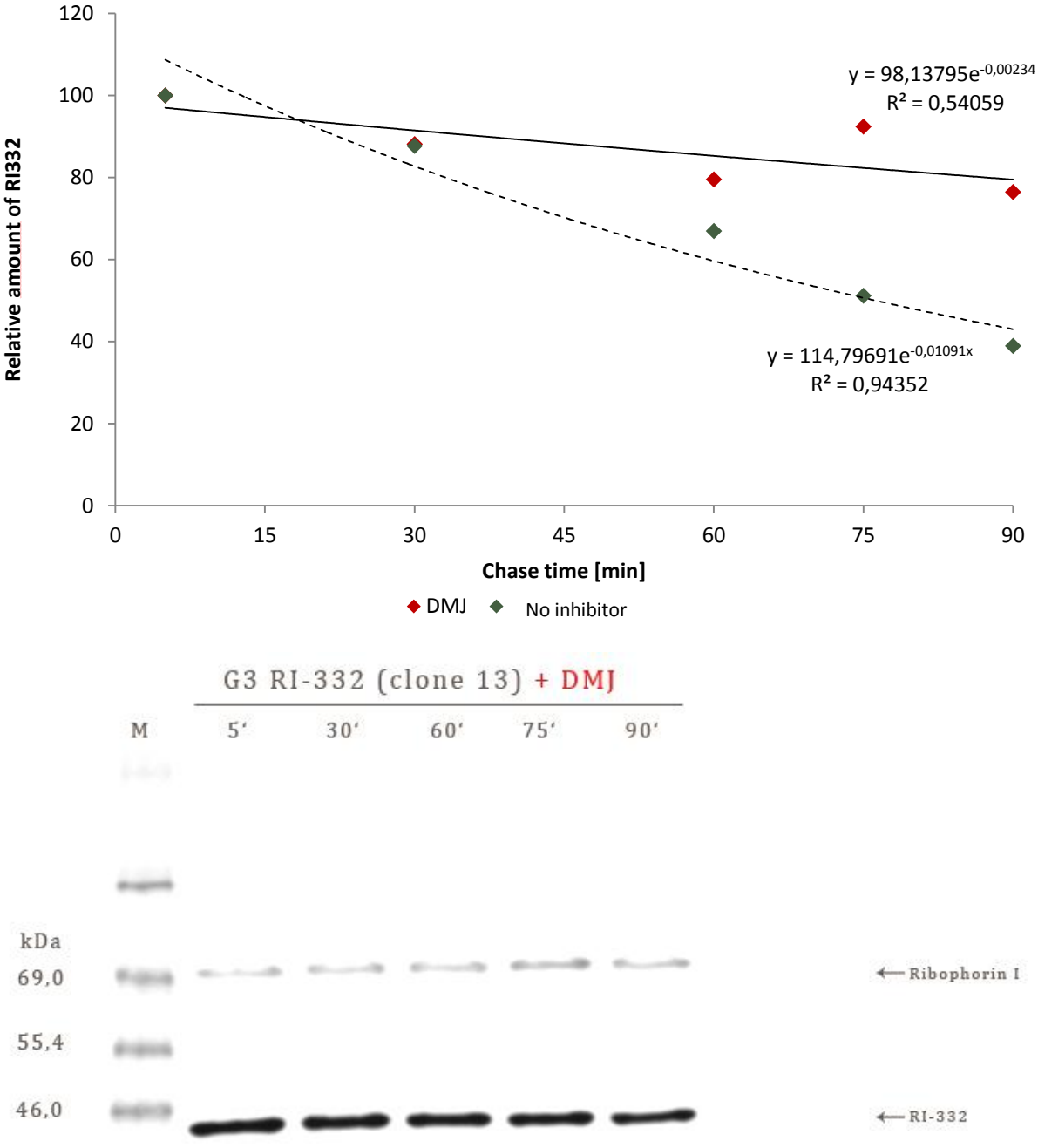

Figure 23. Above: relative amount of RI332 in G3 cells (clone 13) grown in the presence of DMJ (inhibitor of ER manosidases I & II). Chase time points 5 – 90 minutes. Below: fluorography of G3 RI-332 (clone 13)

4.1.10. Half life of RI-332-6HA in the G3 cell line (clone 10) in presence of DMJ

The presence of DMJ stabilizes also the tagged ERAD substrate in G3 cells. The mean half life time of RI332-6HA is 535,96 ± 108,86 minutes.

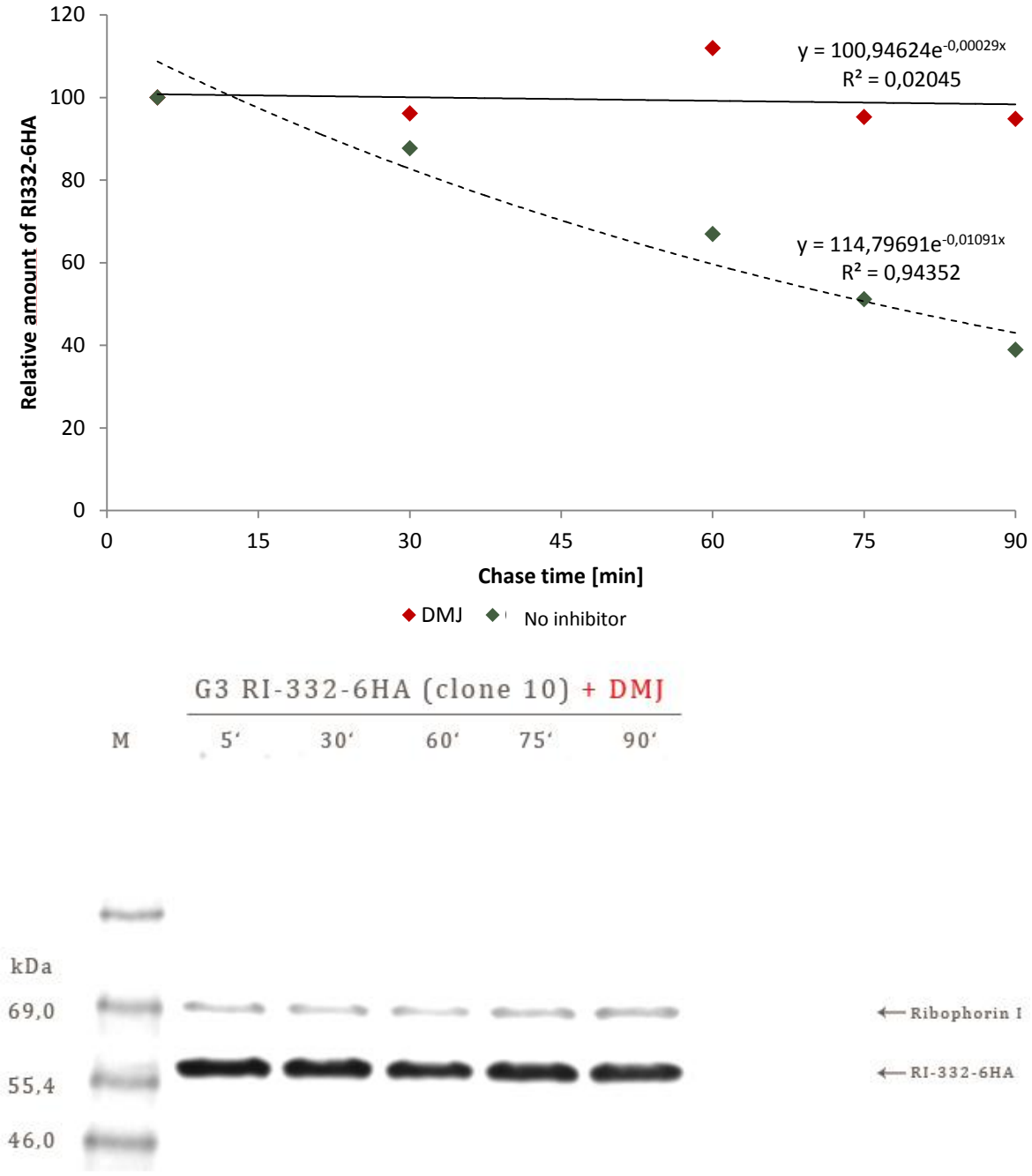

Figure 24. Above: relative amount of RI332-6HA in G3 cells (clone 10) grown in the presence of DMJ (inhibitor of ER manosidases I & II). Chase time points 5 – 90 minutes. Below: fluorography of G3 RI-332-6HA (clone 10)

4.1.11. Half life of RI-332 in the QC cell line (clone GG) in presence of DMJ

In contrast to the G3 cells, DMJ seems to have no effect on the stability of RI332 in the QC cells. As seen in figure 25, the half life time of RI332 in presence of DMJ is hardly influenced: 28,54 ± 6,92 minutes.

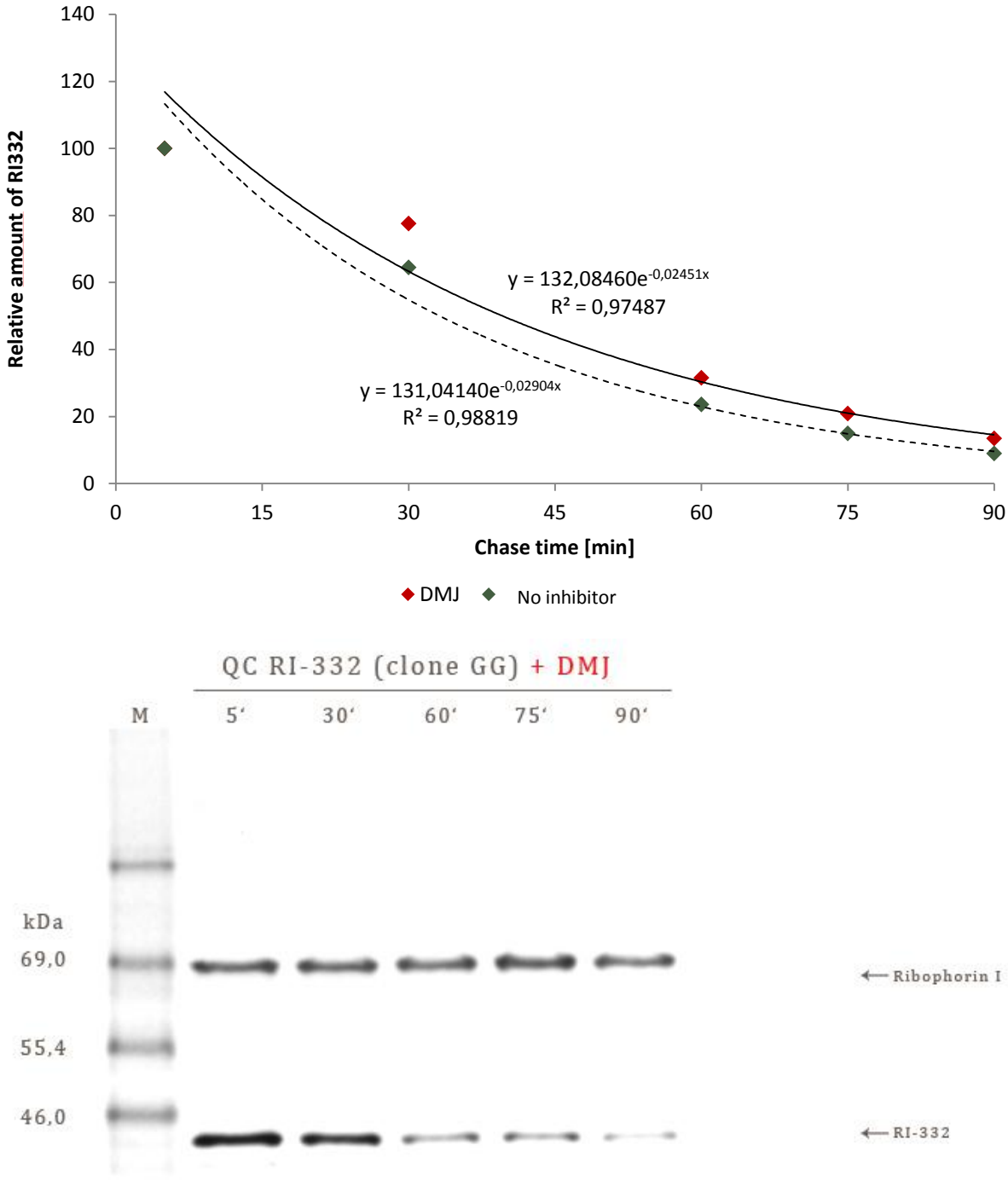

Figure 25. Above: relative amount of RI332 in QC cells (clone GG) grown in the presence of DMJ (inhibitor of ER manosidases I & II). Chase time points 5 – 90 minutes. Below: fluorography of QC RI-332 (clone GG)

4.1.12. Half life of RI-332-6HA in the QC cell line (clone 5) in presence of DMJ

Unexpectedly, DMJ seems to influence the RI332-6HA stability in the QC cell line. The three pulse chase experiments indicate the consistency of the data. The mean half life time of the tagged ERAD substrate in presence of DMJ is 110,77 ± 3,80 minutes.

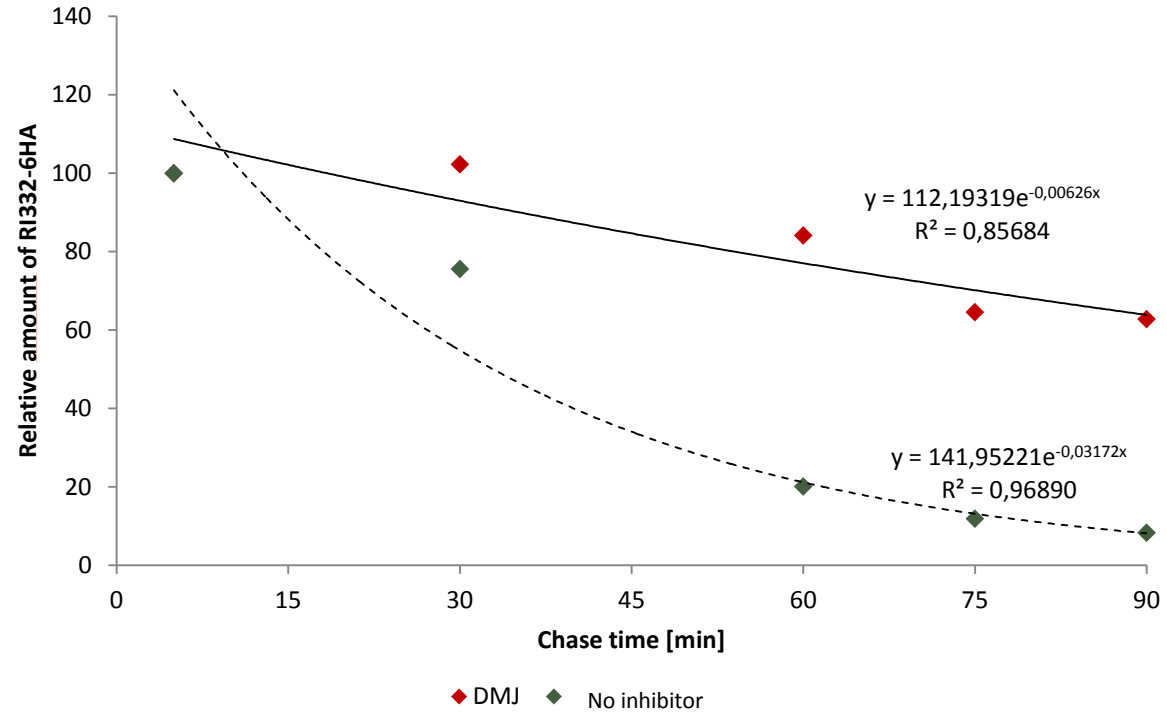

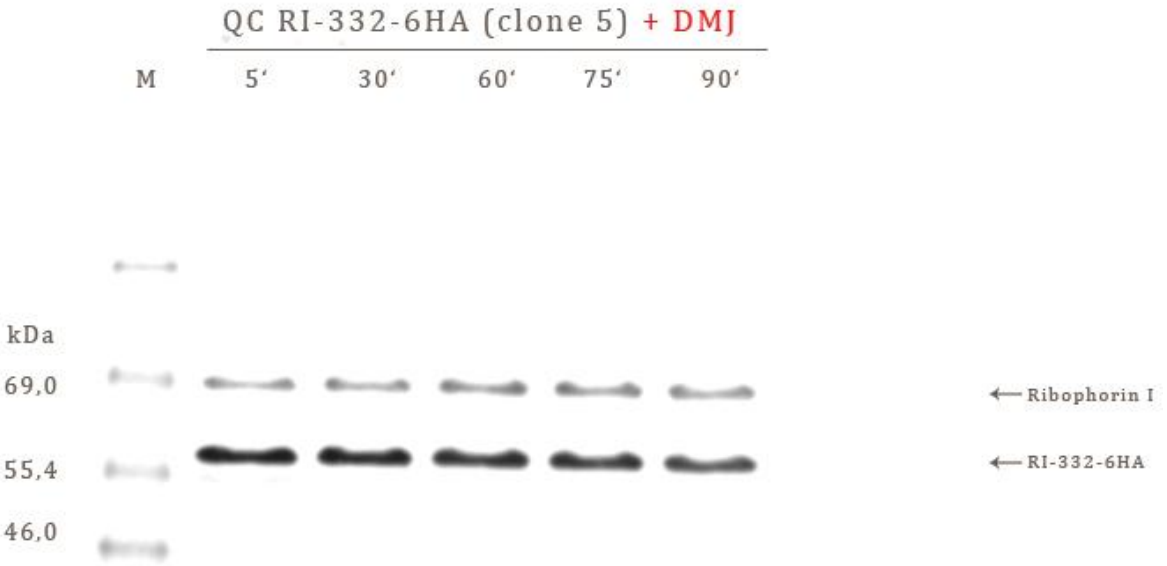

Figure 26. Above: relative amount of RI332-6HA in QC cells (clone 5) grown in the presence of DMJ (inhibitor of ER manosidases I & II). Chase time points 5 – 90 minutes. Below: fluorography of QC RI-332-6HA (clone 5)

4.1.13. Half life of RI-332 in the G3 cell line (clone 13) in presence of KIF

As KIF is also an inhibitor of the ER mannosidases, the effect of KIF on the ERAD substrates is similar as in presence of DMJ. RI332 is stabilized by KIF in the G3 cell line. At time point 45', less of ribophorin I and RI332 is present, which is most likely attributed to faulty pipetting. The estimated mean half life time of RI332 is 272,83 ± 65,30 minutes.

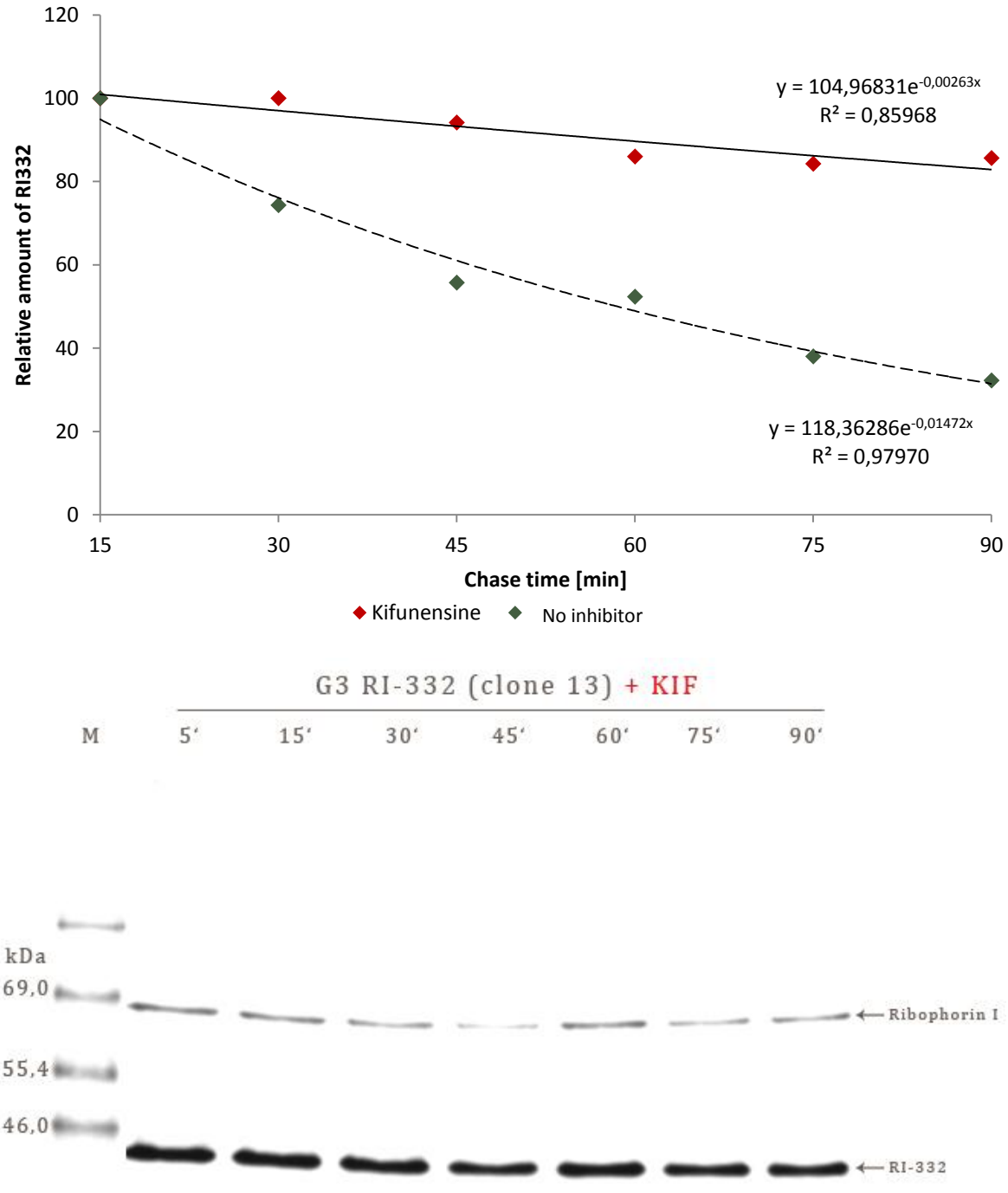

Figure 27. Above: relative amount of RI332 in G3 cells (clone 13) grown in the presence of KIF (inhibitor of ER manosidases I & II). Chase time points 15 – 90 minutes. Below: fluorography of G3 RI-332 (clone 13)

4.1.14. Half life of RI-332-6HA in the G3 cell line (clone 10) in presence of KIF

As expected, RI332-6HA is stabilized by KIF in the G3 cell line. The mean half life time determined is 605,14 ± 67,82 minutes.

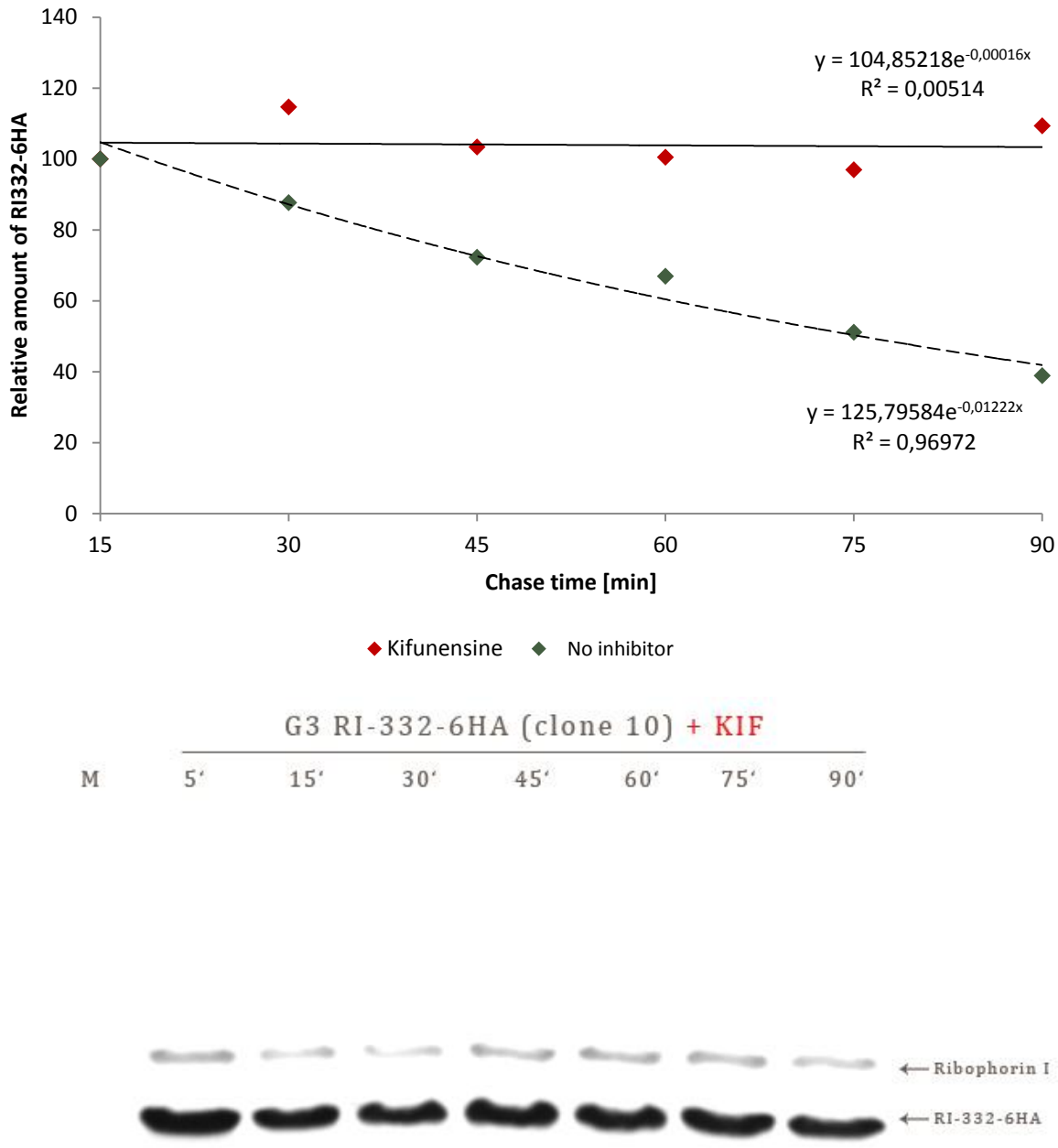

Figure 28. Above: relative amount of RI332-6HA in G3 cells (clone 10) grown in the presence of KIF (inhibitor of ER manosidases I & II). Chase time points 15 – 90 minutes. Below: fluorography of G3 RI-332-6HA (clone 10)

4.1.15. Half life of RI-332 in the QC cell line (clone GG) in presence of KIF

Similar to DMJ, KIF seems to have hardly an influence on the stability of RI332 in the QC cell line. The estimated mean half life time of RI332 is 31,73 ± 0,43 minutes.

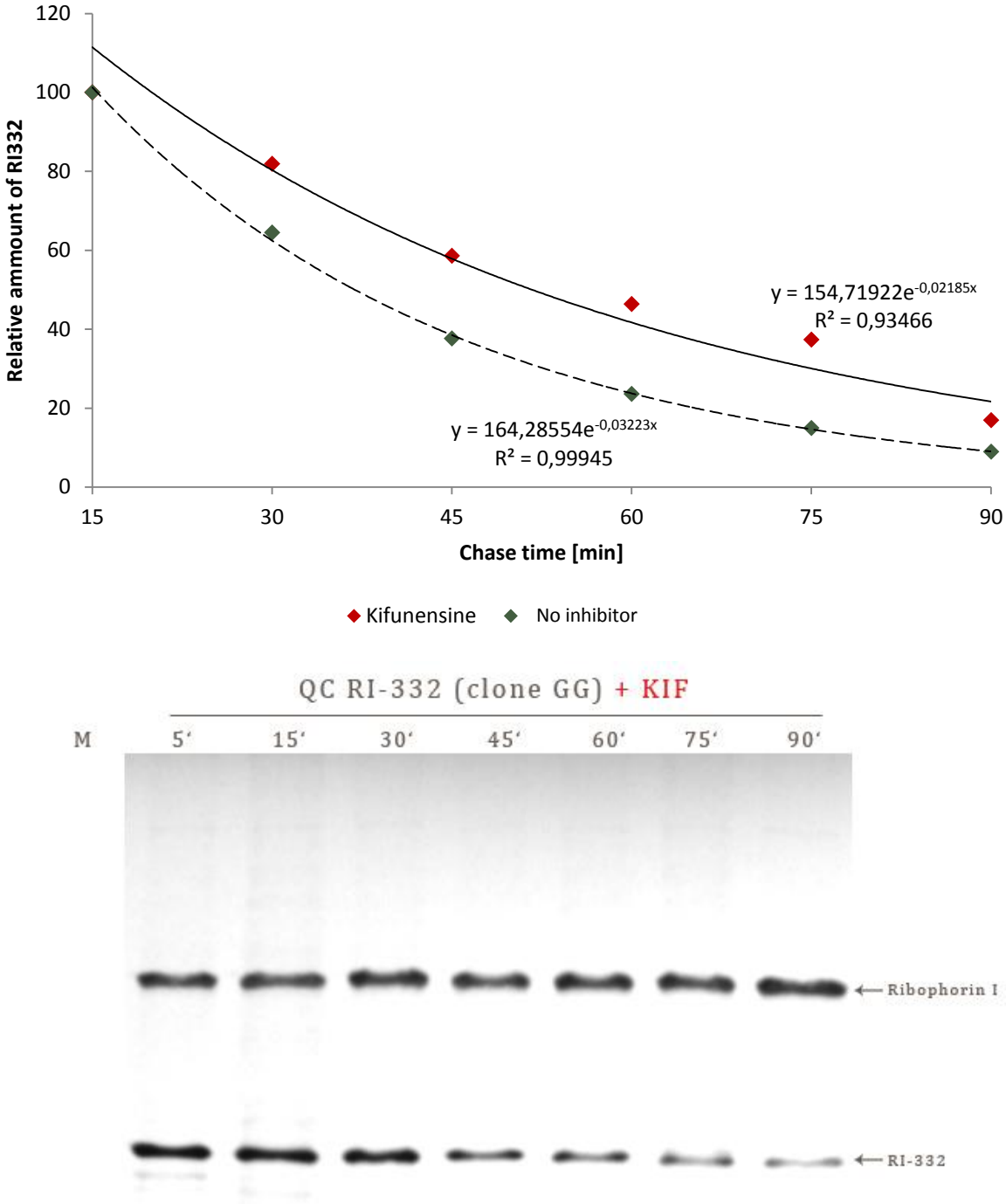

Figure 29. Above: relative amount of RI332 in QC cells (clone GG) grown in the presence of KIF (inhibitor of ER manosidases I & II). Chase time points 15 – 90 minutes. Below: fluorography of QC RI-332 (clone GG)

4.1.16. Half life of RI-332-6HA in the QC cell line (clone 5) in presence of KIF

Due to inhibition of ER mannosidase I by KIF (and DMJ), RI332-6HA is stabilized even in the QC cells. This unexpected fact is indicated by consistent data derived from three pulse chase experiments. The half life time of RI332-6HA is 272,54 ± 56,13 minutes.

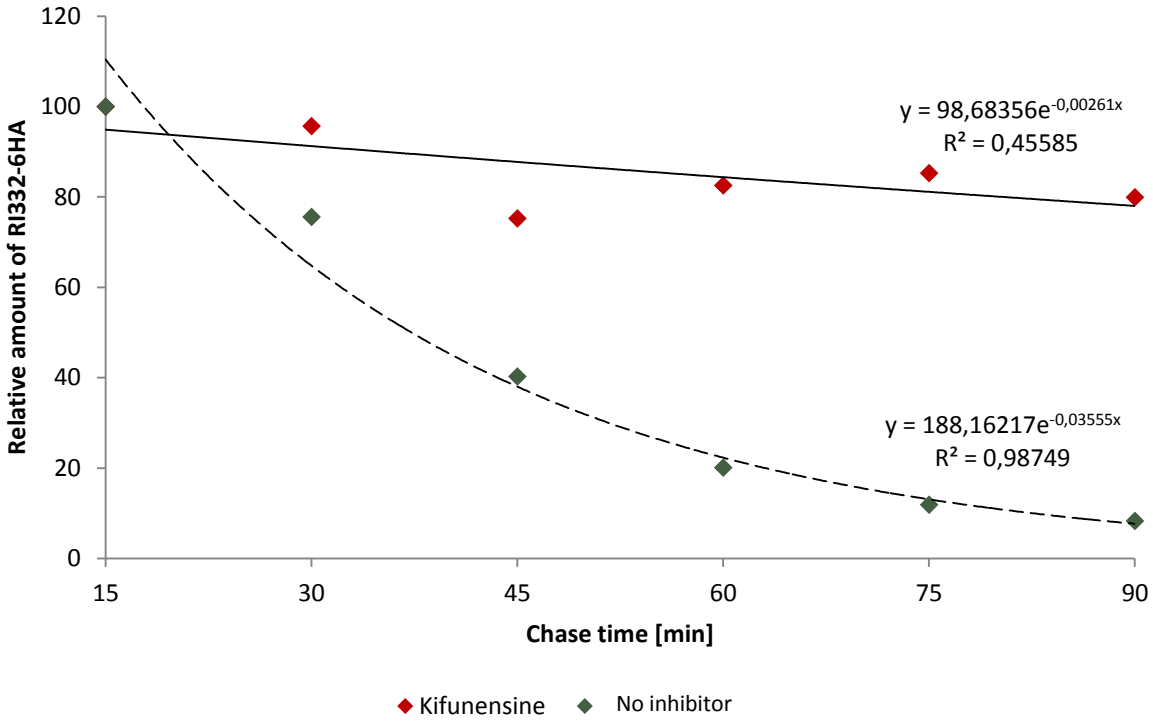

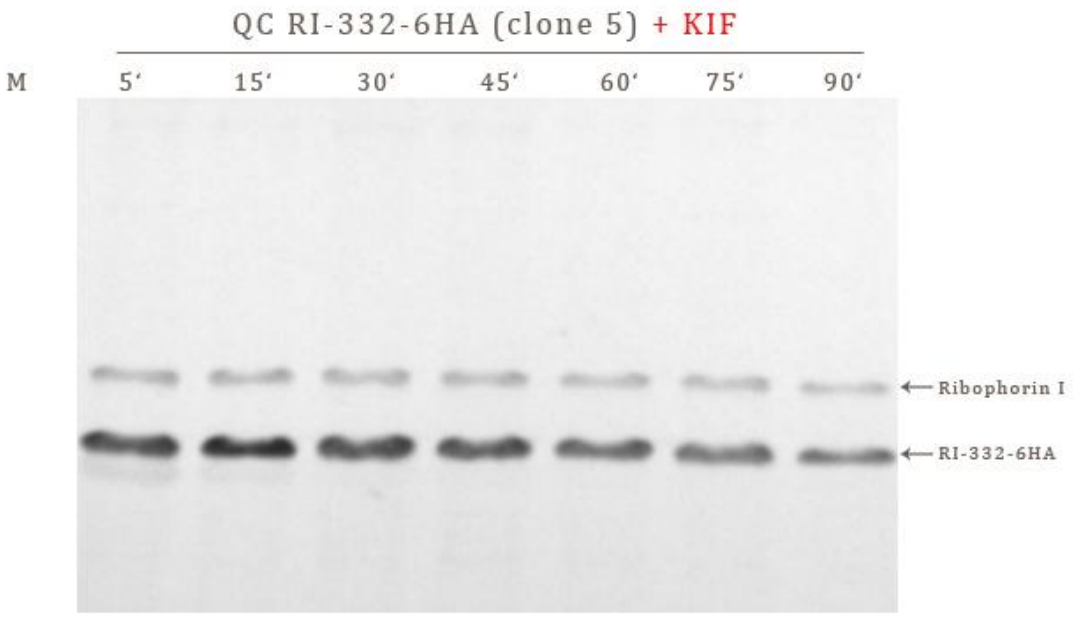

Figure 30. Above: relative amount of RI332-6HA in QC cells (clone 5) grown in the presence of KIF (inhibitor of ER manosidases I & II). Chase time points 15 – 90 minutes. Below: fluorography of QC RI-332-6HA (clone 5)

4.1.17. Half life of RI-332 in the G3 cell line (clone 13) in presence of ZLLL

Not surprisingly, the ERAD substrates are stabilized by the inhibition of the proteasome. In case of ZLLL, additional bands are seen in the later chase time points. This is due to the fact that only the degradation itself is inhibited, but not the trimming reactions. Therefore, the additional bands seen in figure 31 represent RI332 proteins with different sugar trees. The estimated mean half life time of RI332 is: 266,97 ± 53,04 minutes.

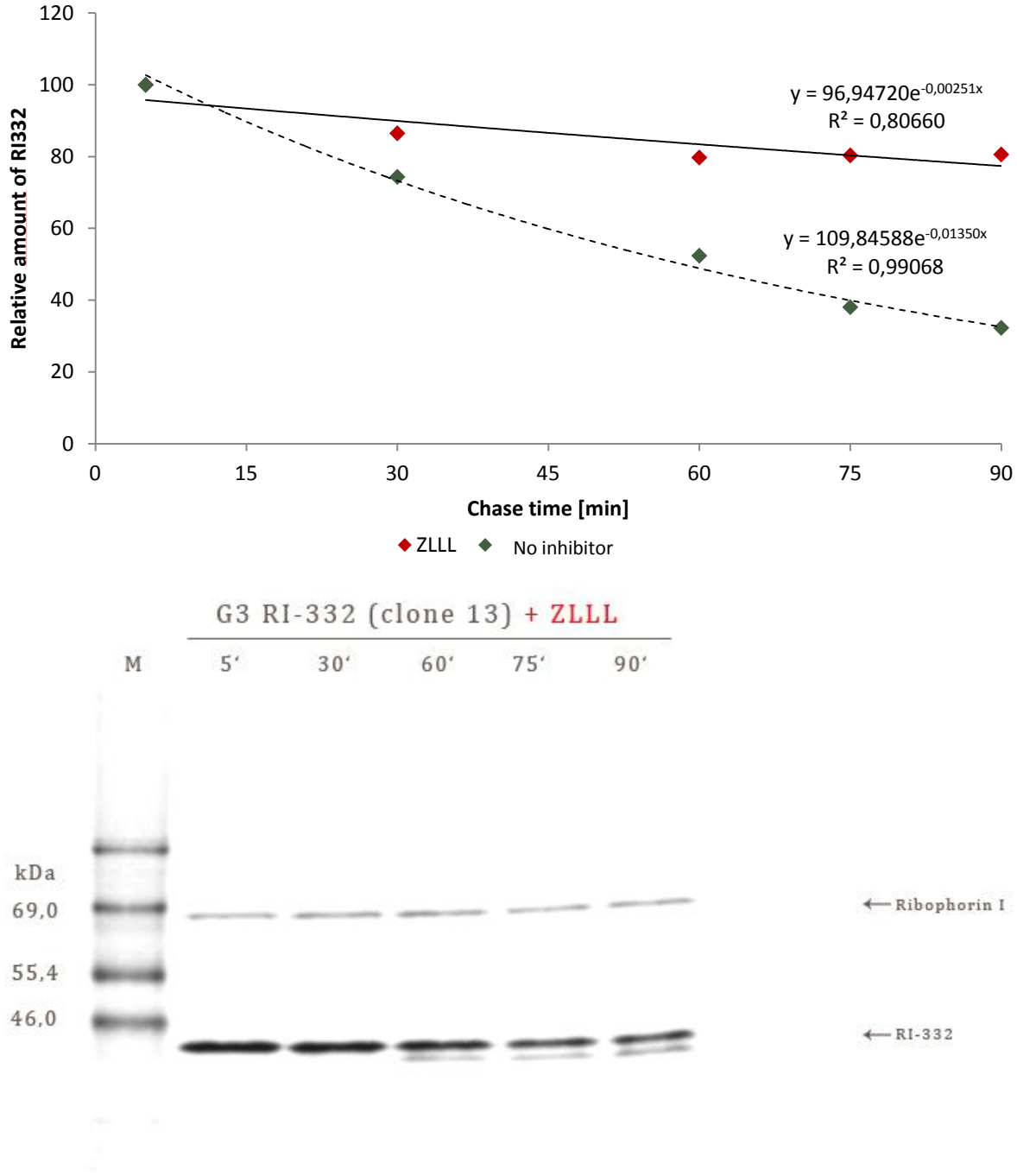

Figure 31. Above: relative amount of RI332 in G3 cells (clone 13) grown in the presence of ZLLL (inhibitor of the proteasome). Chase time points 5 – 90 minutes. Below: fluorography of G3 RI-332 (clone 13)

4.1.18. Half life of RI-332-6HA in the G3 cell line (clone 10) in presence of ZLLL

Analogous to the RI332 substrate, RI332-6HA is also stabilized by ZLLL in the G3 cell line. The different RI332 variants (with different sugar trees) are not that evident as in case of RI332, but they still can be seen in figure 32. The estimated half life time of RI332-6HA is 188,84 ± 25,87 minutes.

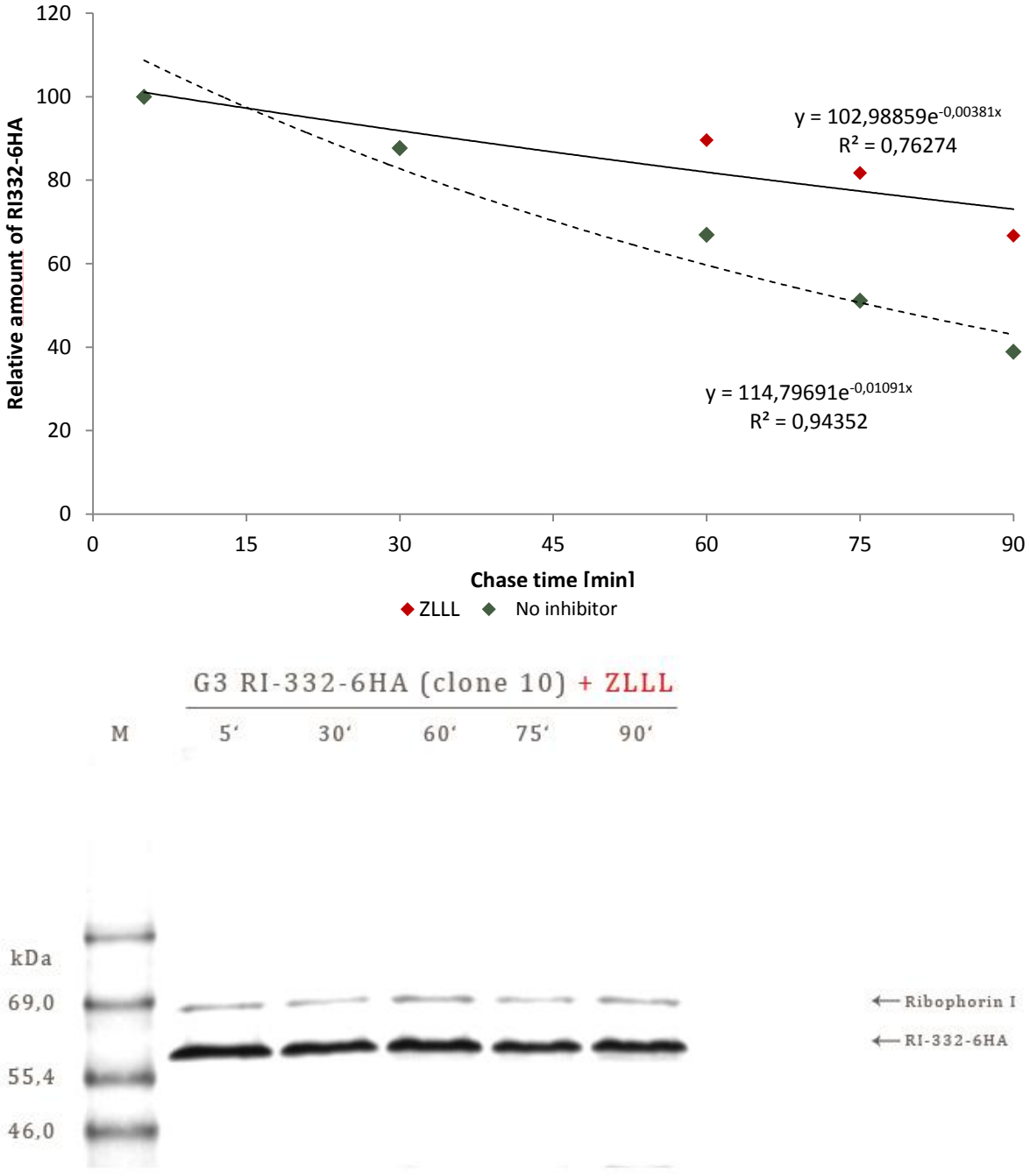

Figure 32. Above: relative amount of RI332-6HA in G3 cells (clone 10) grown in the presence of ZLLL (inhibitor of the proteasome). Chase time points 5 – 90 minutes. Below: fluorography of G3 RI-332-6HA (clone 10)

4.1.19. Half life of RI-332 in the QC cell line (clone GG) in presence of ZLLL

The inhibition of the proteasome has the same effect in all cell lines, including the QC cells. A dramatic stabilization of the RI332 substrate in presence of ZLLL is obvious. The different RI332 trimming variants are especially present in the QC cell line (see figure below). The estimated half life time of the ERAD substrate is 110,17 ± 5,94 minutes.

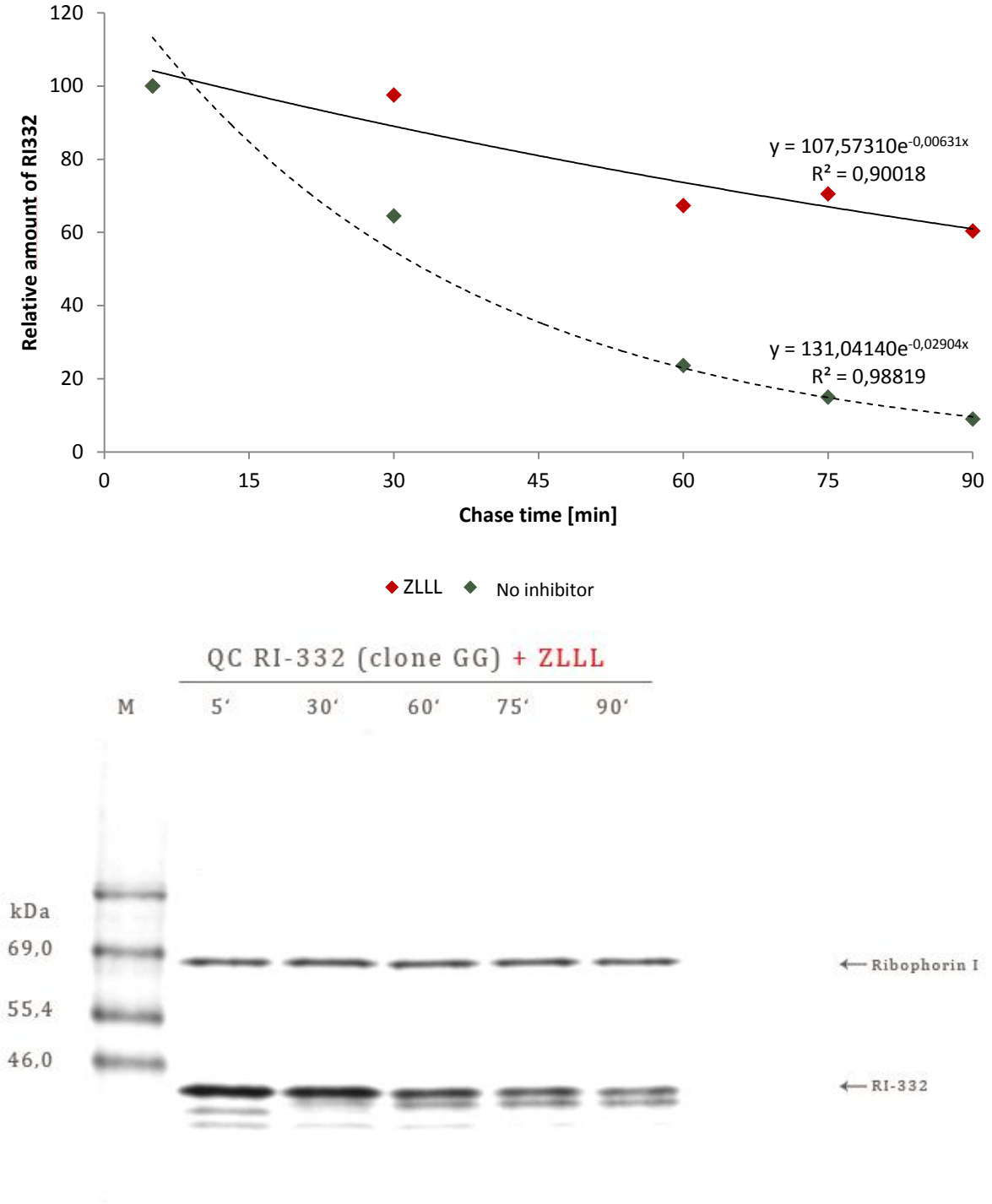

Figure 33. Above: relative amount of RI332 in QC cells (clone GG) grown in the presence of ZLLL (inhibitor of the proteasome). Chase time points 5 – 90 minutes. Below: fluorography of QC RI-332 (clone GG)

4.1.20. Half life of RI-332-6HA in the QC cell line (clone 5) in presence of ZLLL

As expected, RI332-6HA is stabilized in the QC cell line by the presence of ZLLL. The estimated half life time of RI332-6HA is 194,37 ± 44,66 minutes.

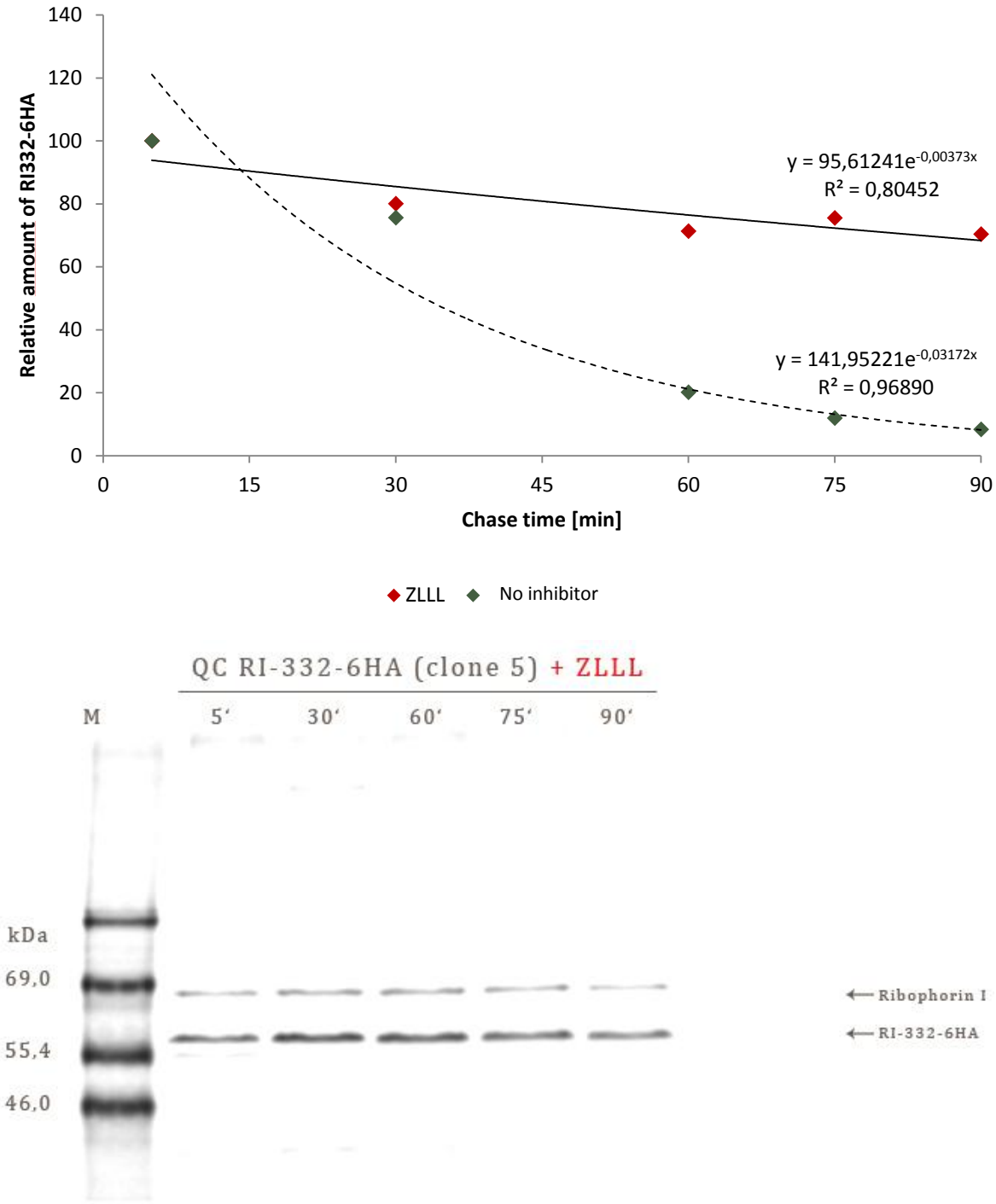

Figure 34. Above: relative amount of RI332-6HA in QC cells (clone 5) grown in the presence of ZLLL (inhibitor of the proteasome). Chase time points 5 – 90 minutes. Below: fluorography of QC RI-332-6HA (clone 5)

4.1.21. Overview of half lives of RI-332 and RI-332-6HA

In figure 35, the half lives of RI332 and RI332-6HA in the G3 cells are graphically depicted. The stabilization of the substrates by DMJ, KIF and ZLLL is obvious. The effect observed is not that dramatic for the QC cells (figure 36). All half lives and standard deviations are shown in table 11.

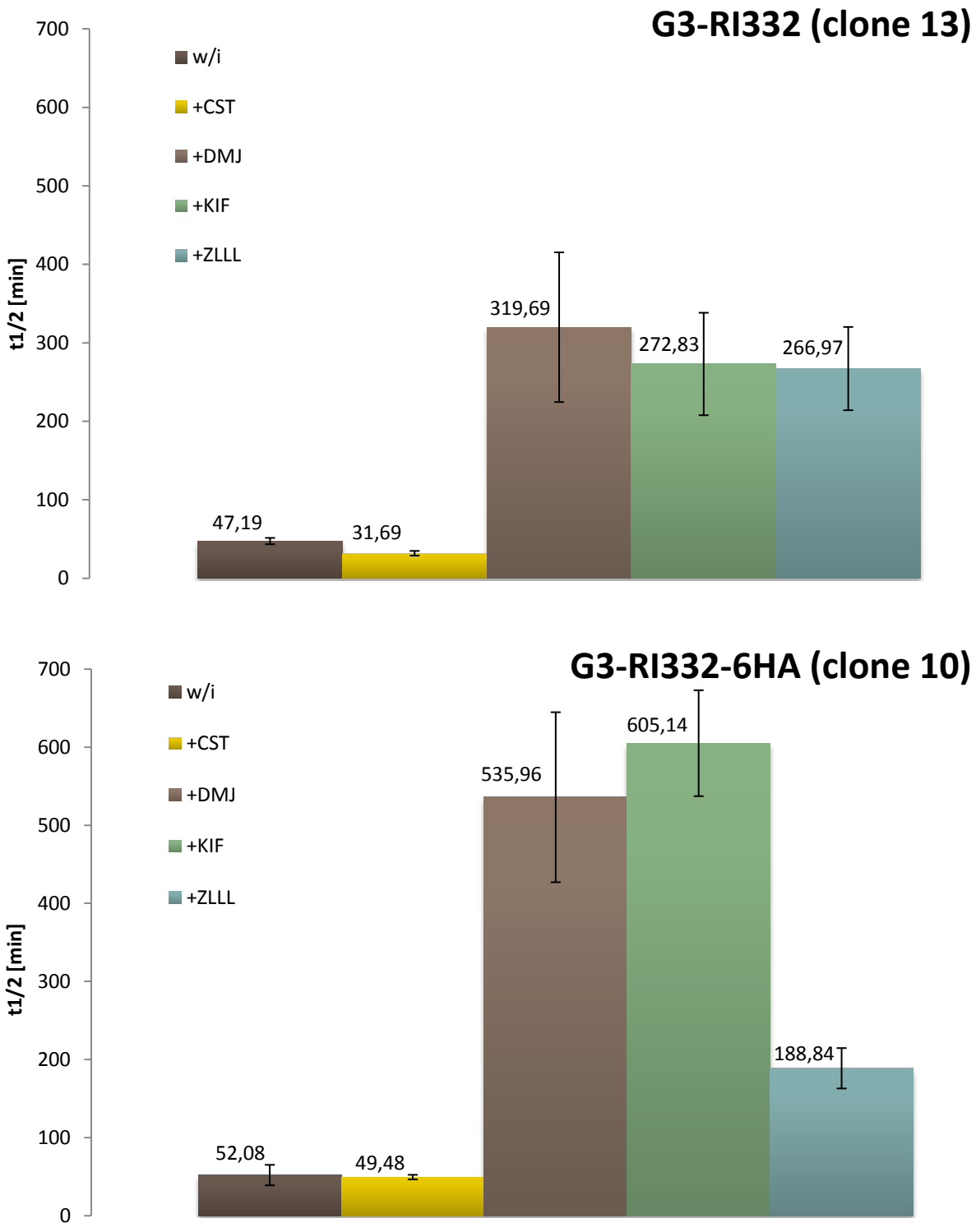

Figure 35. Above: half lives of RI332 in the absence and presence of inhibitors in G3 cells (clone 13). Below: half lives of RI332 – 6HA in the absence and presence of inhibitors in G3 cells (clone 10).

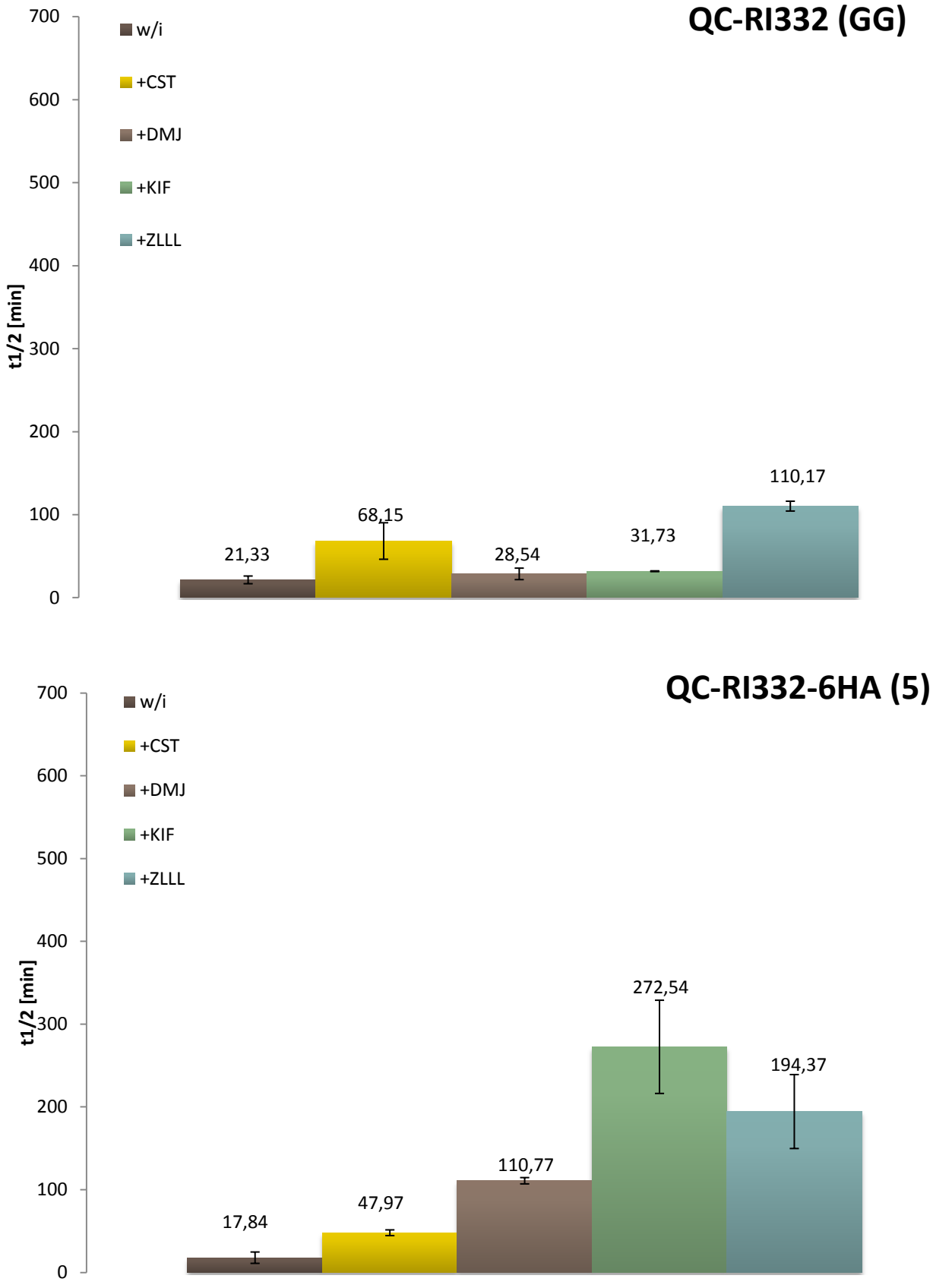

Figure 36. Above: half lives of RI332 in the absence and presence of inhibitors in QC cells (clone GG). Below: half lives of RI332 – 6HA in the absence and presence of inhibitors in QC cells (clone 5).

Cell line	ERAD substrate	Inhibitor	# of experiments	t1/2	Standard deviation
G3 RI332	RI332	None	3	**47,19**	*4,06*
G3 RI332	RI332	CST	3	**31,69**	*3,46*
G3 RI332	RI332	KIF	2	**272,83**	*65,30*
G3 RI332	RI332	DMJ	3	**319,69**	*95,37*
G3 RI332	RI332	ZLLL	3	**266,97**	*53,04*
QC RI332	RI332	None	3	**21,33**	*4,64*
QC RI332	RI332	CST	3	**68,15**	*22,00*
QC RI332	RI332	KIF	2	**31,73**	*0,43*
QC RI332	RI332	DMJ	3	**28,54**	*6,92*
QC RI332	RI332	ZLLL	3	**110,17**	*5,94*
G3 RI332-6HA	RI332-6HA	None	3	**57,19**	*13,73*
G3 RI332-6HA	RI332-6HA	CST	3	**49,48**	*2,96*
G3 RI332-6HA	RI332-6HA	KIF	2	**605,14**	*67,82*
G3 RI332-6HA	RI332-6HA	DMJ	3	**535,96**	*108,86*
G3 RI332-6HA	RI332-6HA	ZLLL	3	**188,84**	*25,87*
QC RI332-6HA	RI332-6HA	None	3	**17,84**	*6,86*
QC RI332-6HA	RI332-6HA	CST	3	**47,97**	*9,50*
QC RI332-6HA	RI332-6HA	KIF	2	**272,54**	*56,13*
QC RI332-6HA	RI332-6HA	DMJ	3	**110,77**	*3,80*
QC RI332-6HA	RI332-6HA	ZLLL	3	**194,37**	*44,66*

Table 11. Half live times of the ERAD substrates under different conditions in the four cell lines used

4.2. Restoring of the wild type phenotype in the QC cell lines

In this section (Figs. 37 to 40) a typical experiment (fluorogram and quantitation of densitometric scanning using a first order kinetics) for each cell line grown in the absence of inhibitors, but in presence or absence of galactose is shown.

Pulse chase experiments of cells grown in the absence of galactose were only performed with five different chase time points (see figures 37 and 38). Pulse chase experiments of cells grown in presence of galactose were performed with seven time points. The estimated relative amounts of RI332 and RI332-6HA are graphically shown in figures 39 and 40. The relative amounts of the ERAD substrates are compared between cells grown in the presence of 6mM glucose (without galactose), 5mM galactose and the standard RPMI 1640 growth medium (with glucose, without galactose).

An overview of all half life times is shown in figure 41 (no standard deviations are shown due to the fact that these experiments were performed only once).

Changes in morphology of QC cells grown in absence and presence of galactose are shown in figure 42. QC cells grown without galactose are more compact, whereas QC cells grown in the presence of galactose are more flat. The flat phenotype is characteristic to the wild type (G3) cells.

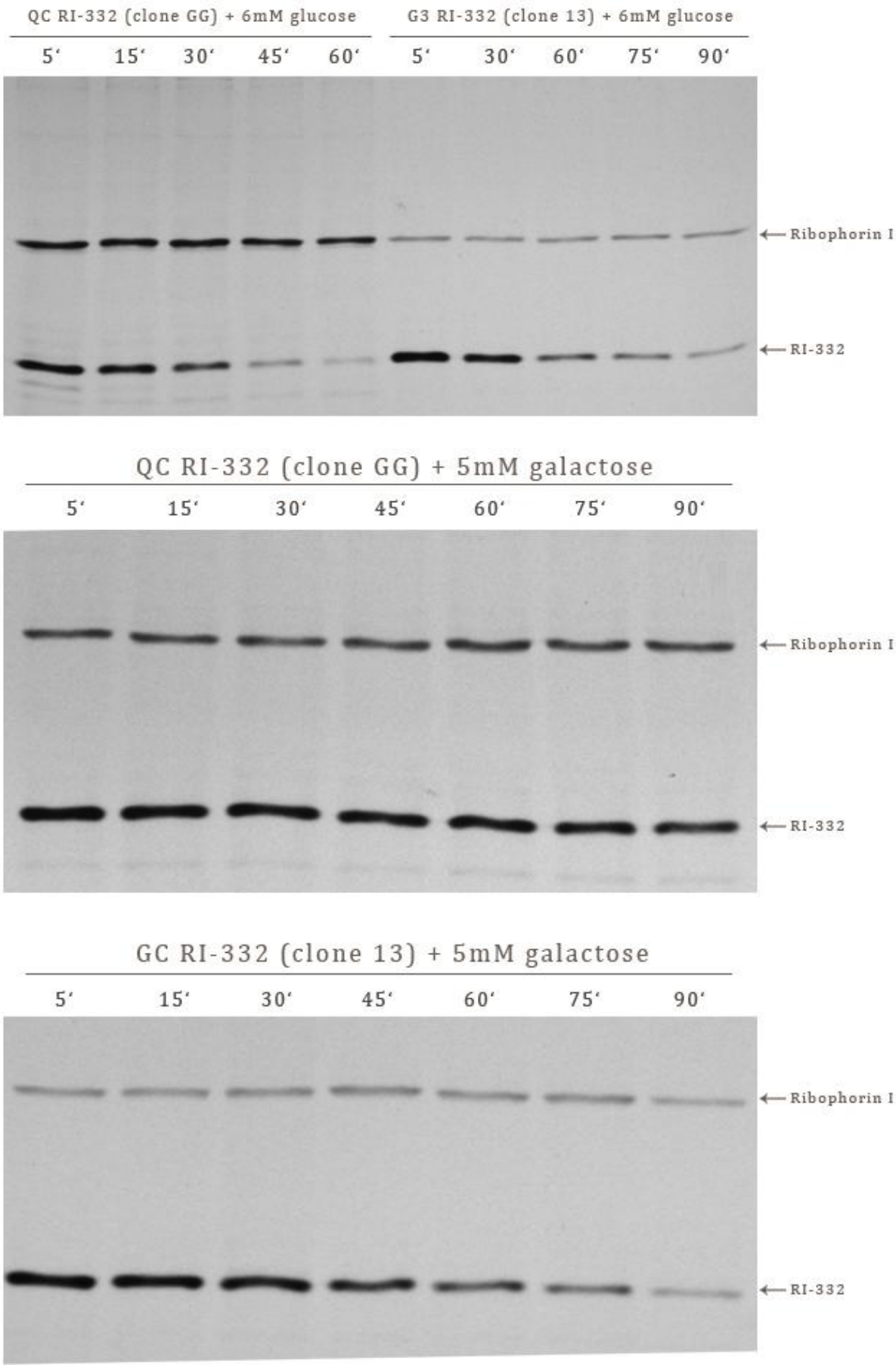

Figure 37. Fluorography of G3 RI332 and QC RI332 cells grown in the presence and absence of galactose

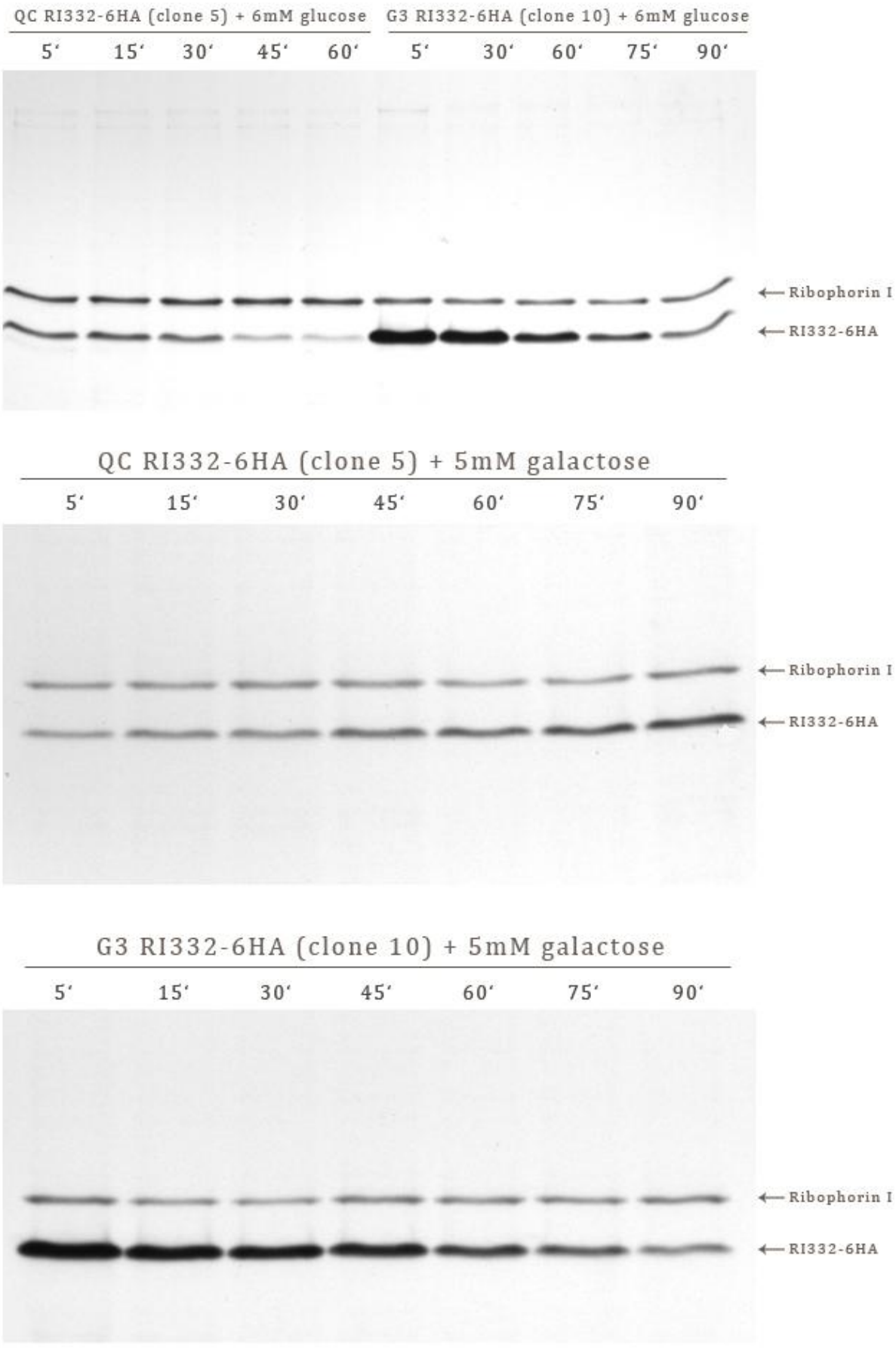

Figure 38. Fluorography of G3 RI332-6HA and QC RI332-6HA cells grown in the presence and absence of galactose

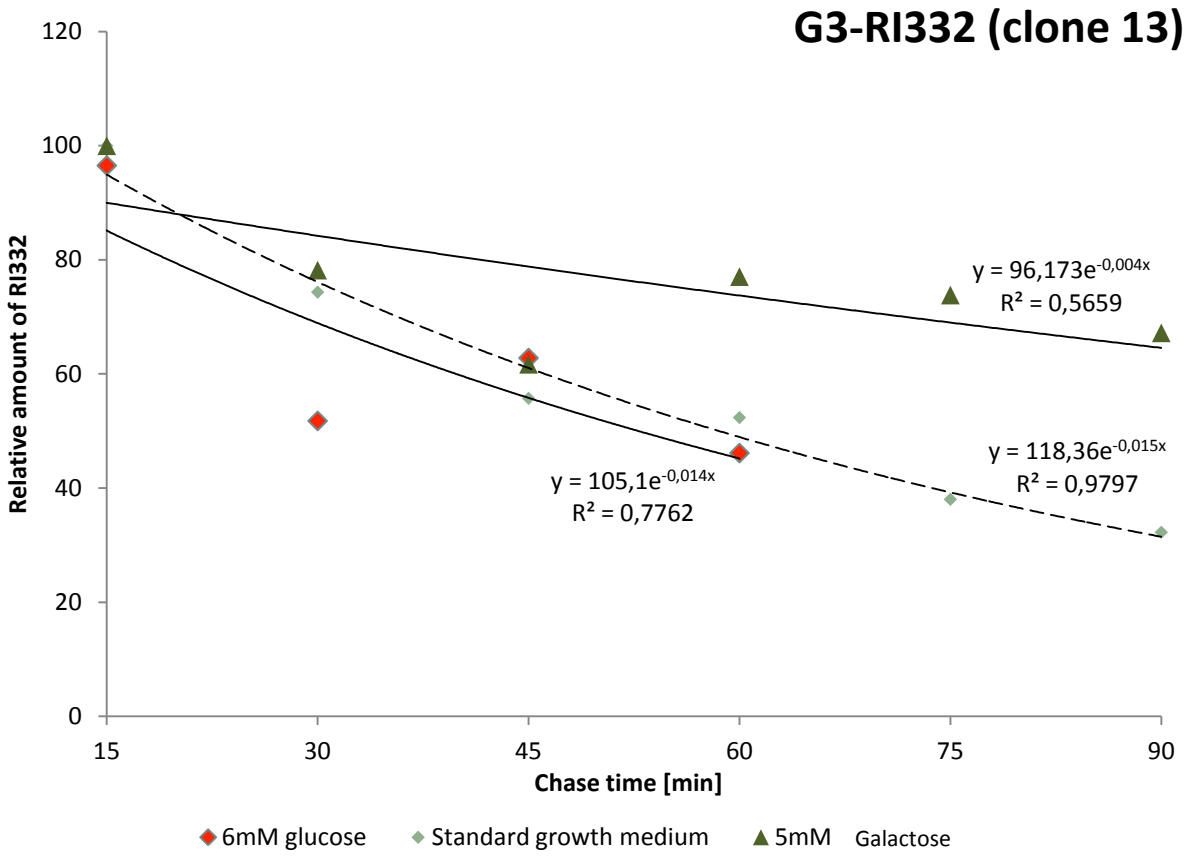

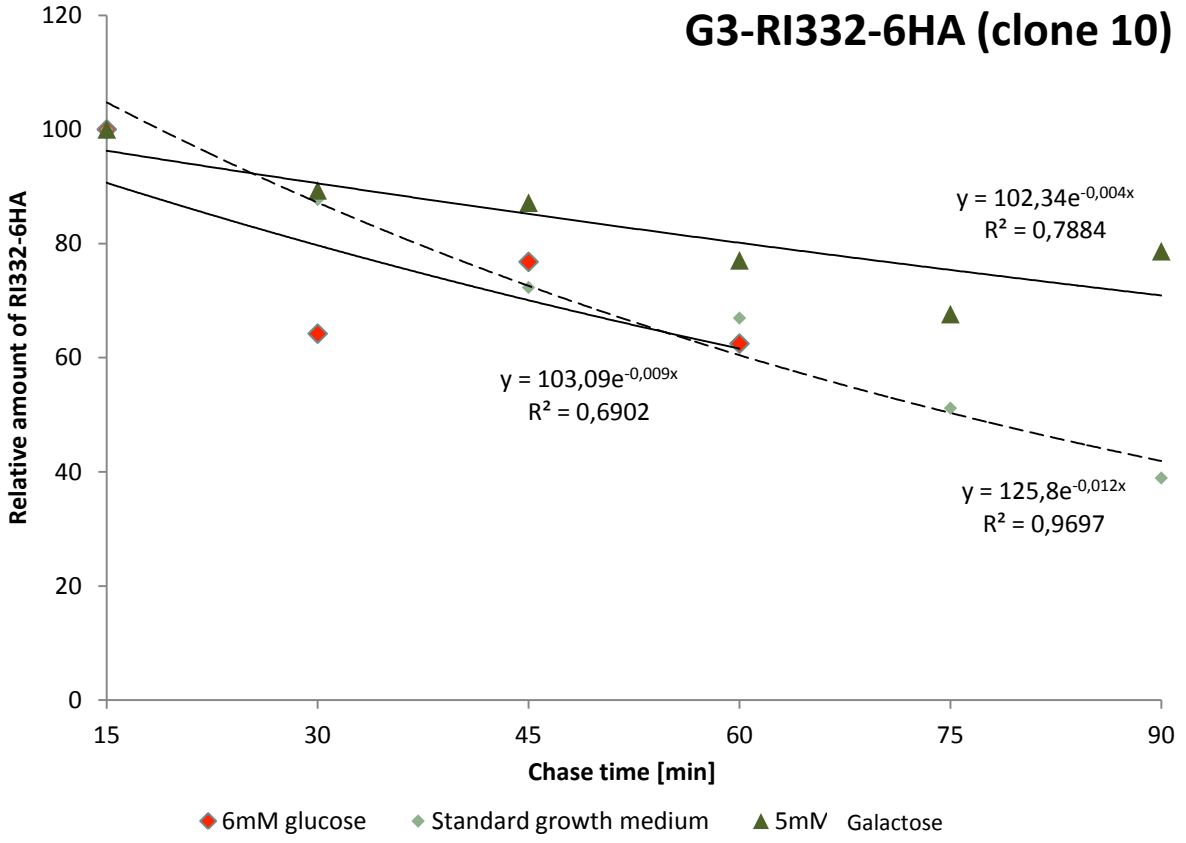

Figure 39. Above: relative amounts of RI332 in G3 RI-332 cells grown in i) the standard growth medium, ii) 6mM glucose growth medium and iii) 5mM galactose growth medium. Below: relative amounts of RI332-6HA in G3 RI332-6HA cells grown in i) the standard growth medium, ii) 6mM glucose growth medium and iii) 5mM galactose growth medium.

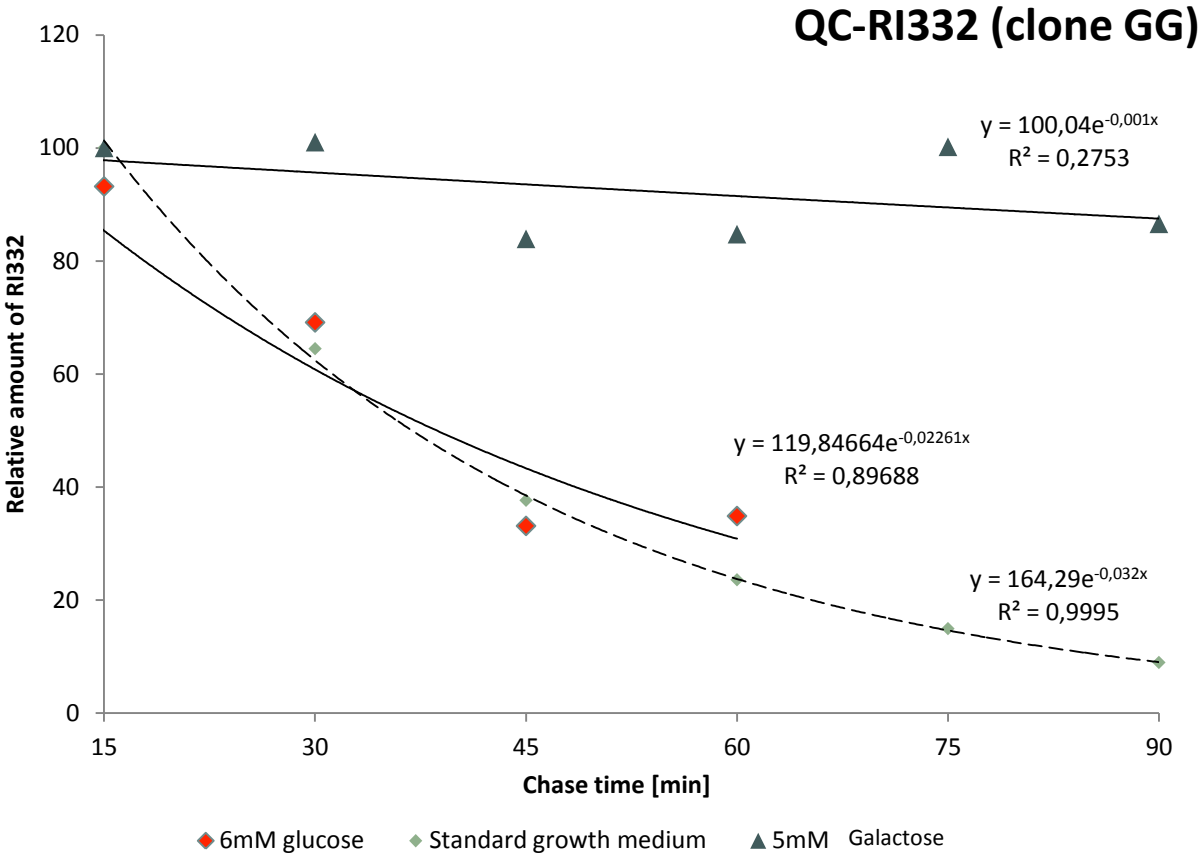

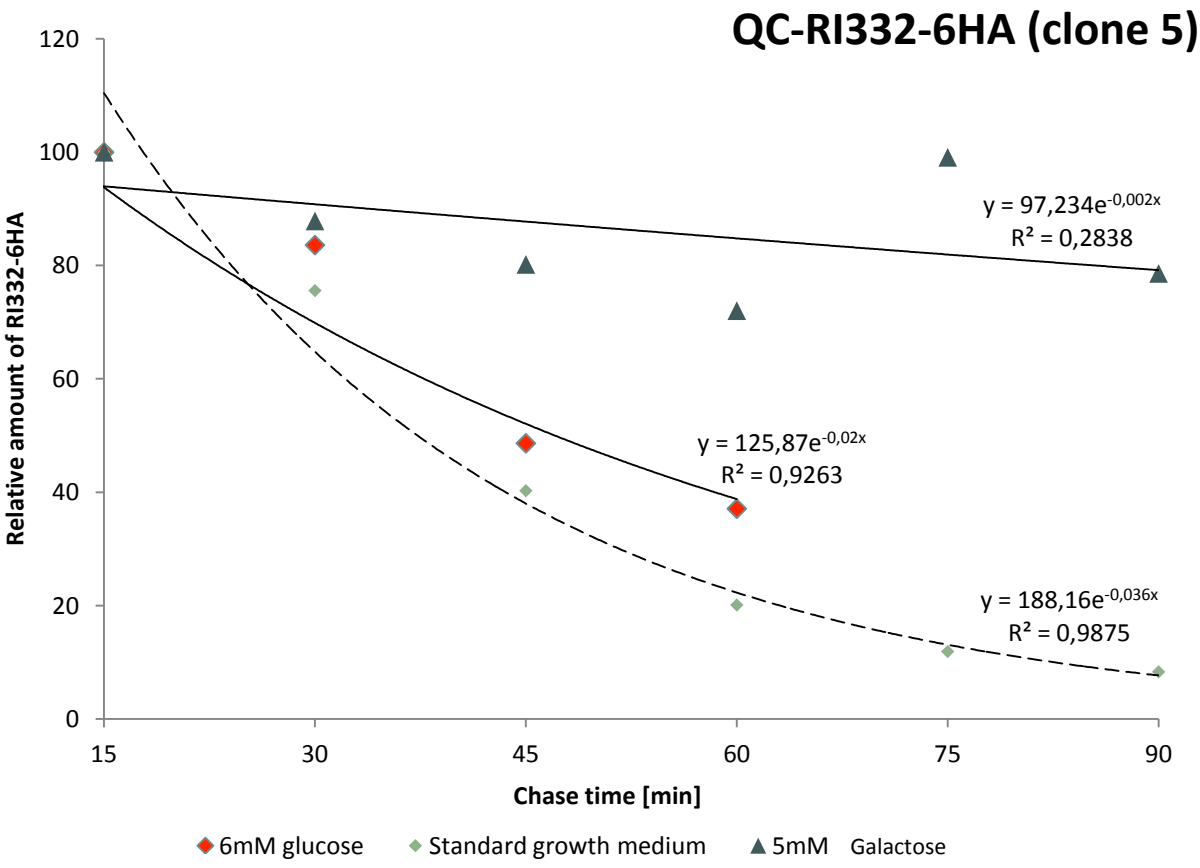

Figure 40. Above: relative amounts of RI332 in QC RI-332 cells grown in i) the standard growth medium, ii) 6mM glucose growth medium and iii) 5mM galactose growth medium. Below: relative amounts of RI332-6HA in QC RI332-6HA cells grown in i) the standard growth medium, ii) 6mM glucose growth medium and iii) 5mM galactose growth medium.

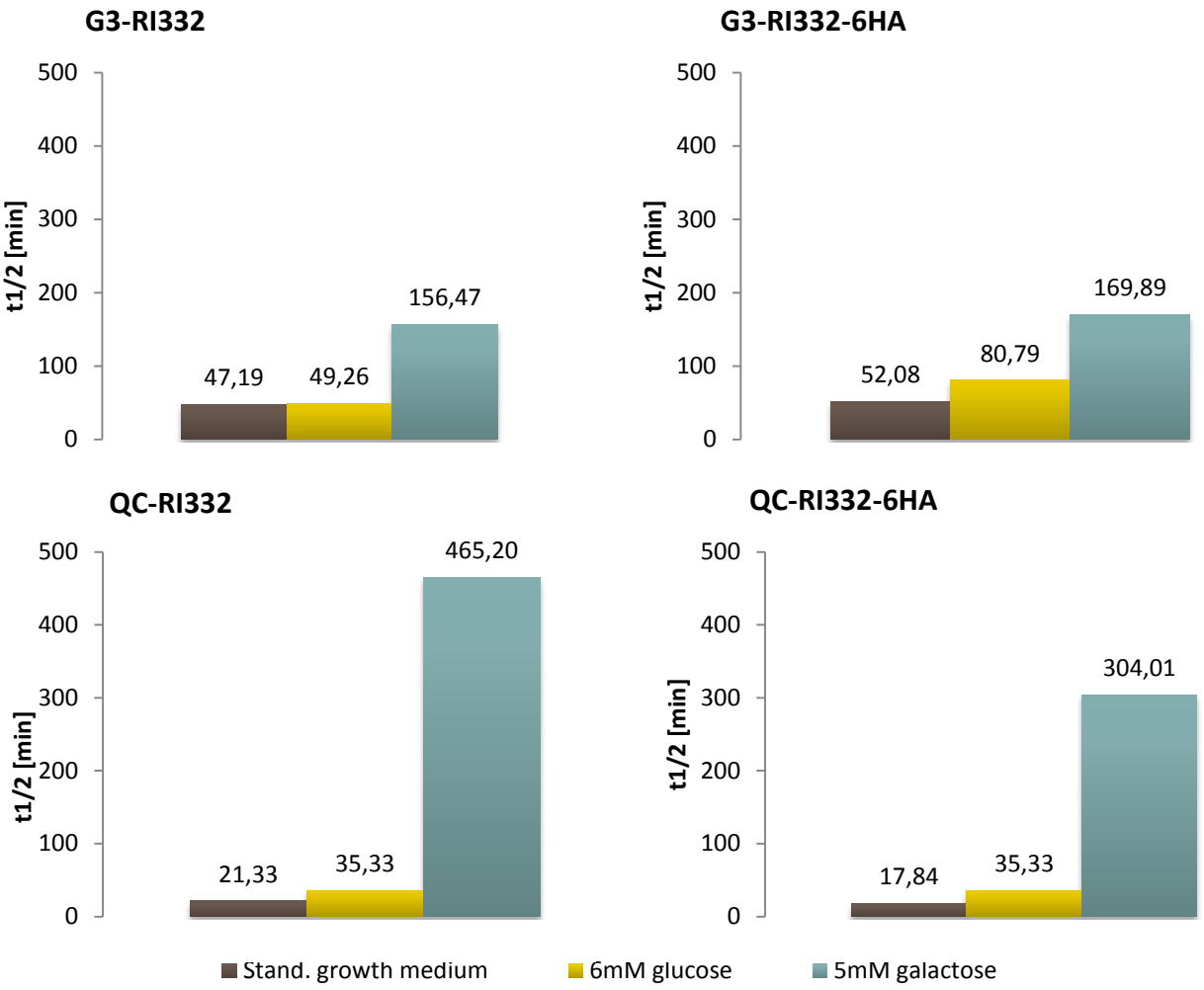

Figure 41. Comparison of RI332 and RI332-6HA half lives in cell lines grown in different growth media.

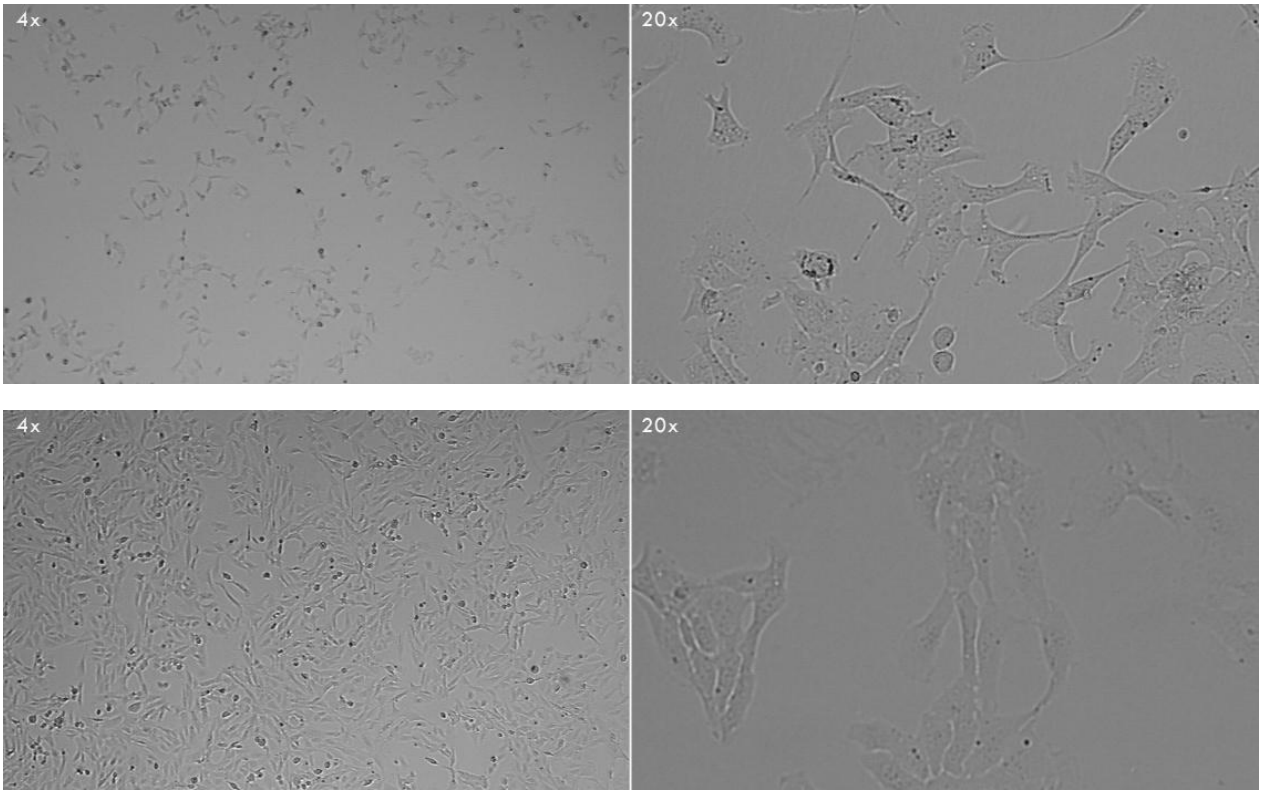

Figure 42. Restoring of the wt phenotype in QC RI332-6HA clone 5. Above: cells grown in absence of galactose (6mM glucose). Below: cells grown in presence of galactose (5mM)

4.3. ERAD substrate – calnexin association

In this section (Figs. 43 to 50) a typical co-immuno precipitation experiment for each cell line is shown. Each fluorogram corresponds to one chase time point (details see images below). Each gel was exposed for one day and also for six days. The short exposure period was necessary to avoid a smear in the Cal (ns) lane. However, this short exposure was not sufficient to depict bands in the Cal/RI and RI/Cal lanes.

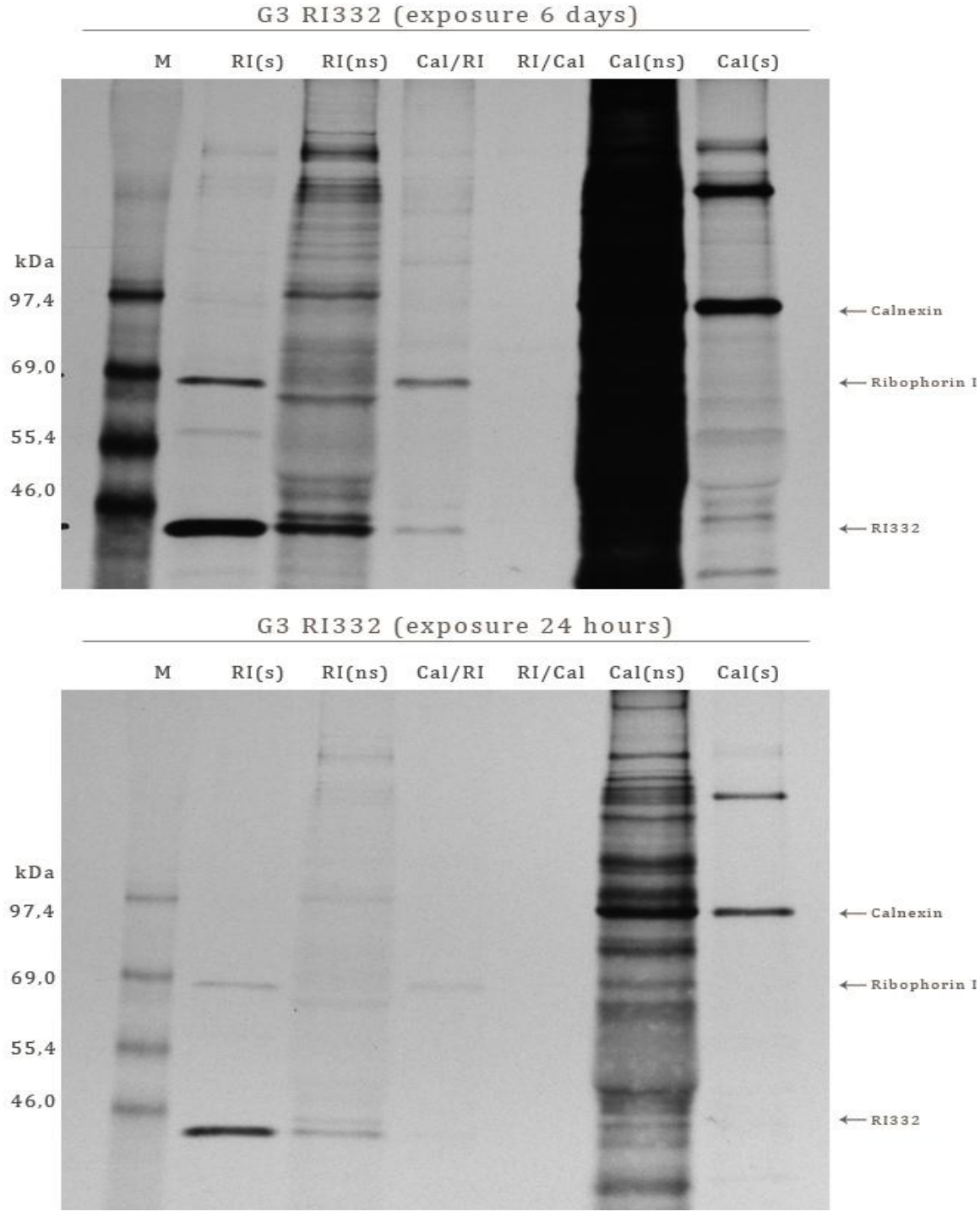

Figure 43. Fluorography of co-immunoprecipitation. G3 RI332 clone 13. Chase time: 5'. Exposure time: 6 days (above) and 24 hours (below). RI lum and calnexin antibodies were used for stringent cell lysis (s) and non stringent cell lysis (ns). Co-immunoprecipitation was performed sequentially with calnexin – RI lum (Cal/RI) and RI lum – calnexin (RI/calnexin) antibodies, respectively.

For unknown reasons the ERAD substrates in the non stringent lane are at a slightly different height and/or show double bands in contrast to the stringent lane.

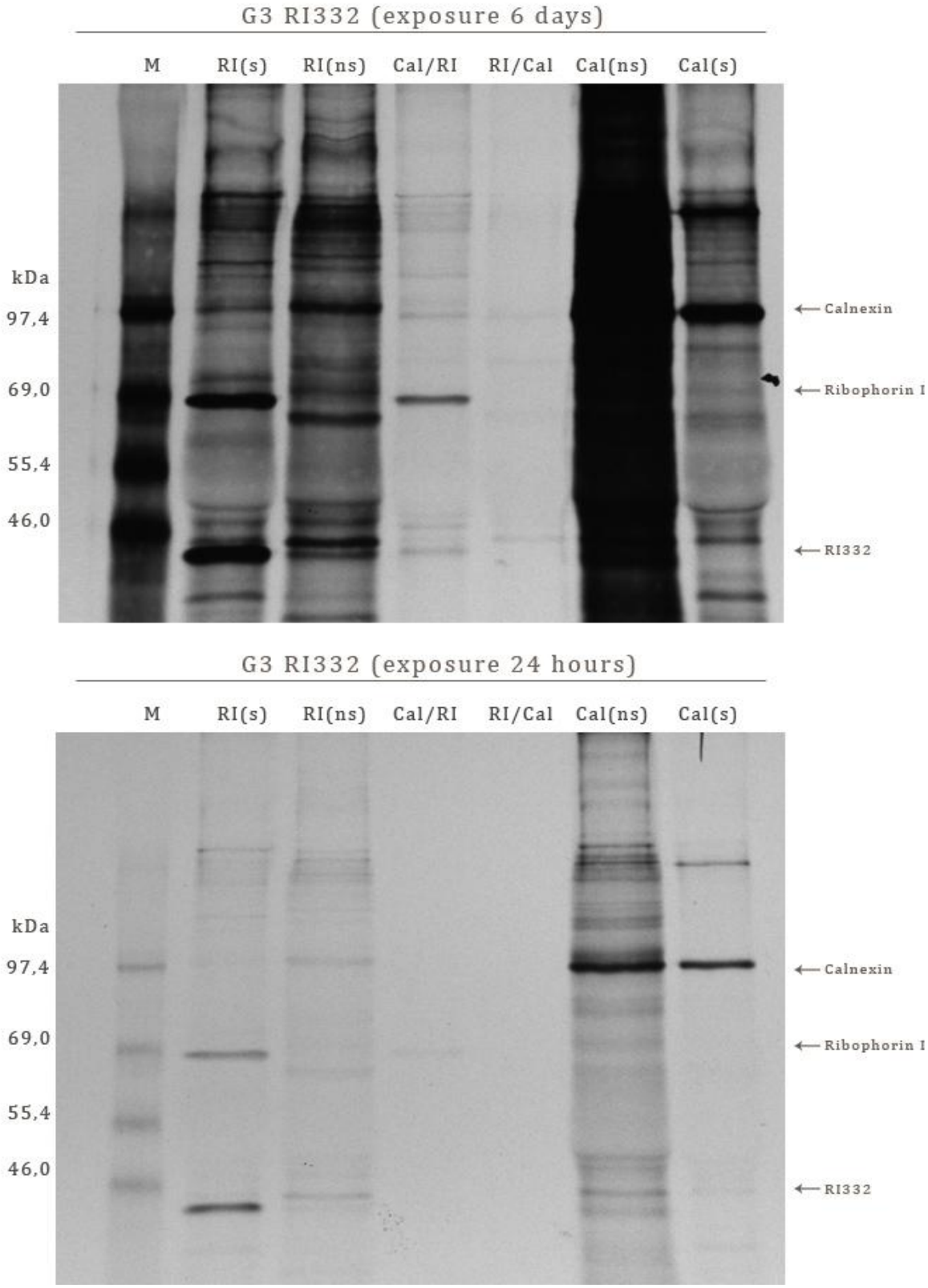

Figure 44. Fluorography of co-immunoprecipitation. G3 RI332 clone 13. Chase time: 60'. Exposure time: 6 days (above) and 24 hours (below). RI lum and calnexin antibodies were used for stringent cell lysis (s) and non stringent cell lysis (ns). Co-immunoprecipitation was performed sequentially with calnexin – RI lum (Cal/RI) and RI lum – calnexin (RI/calnexin) antibodies, respectively.

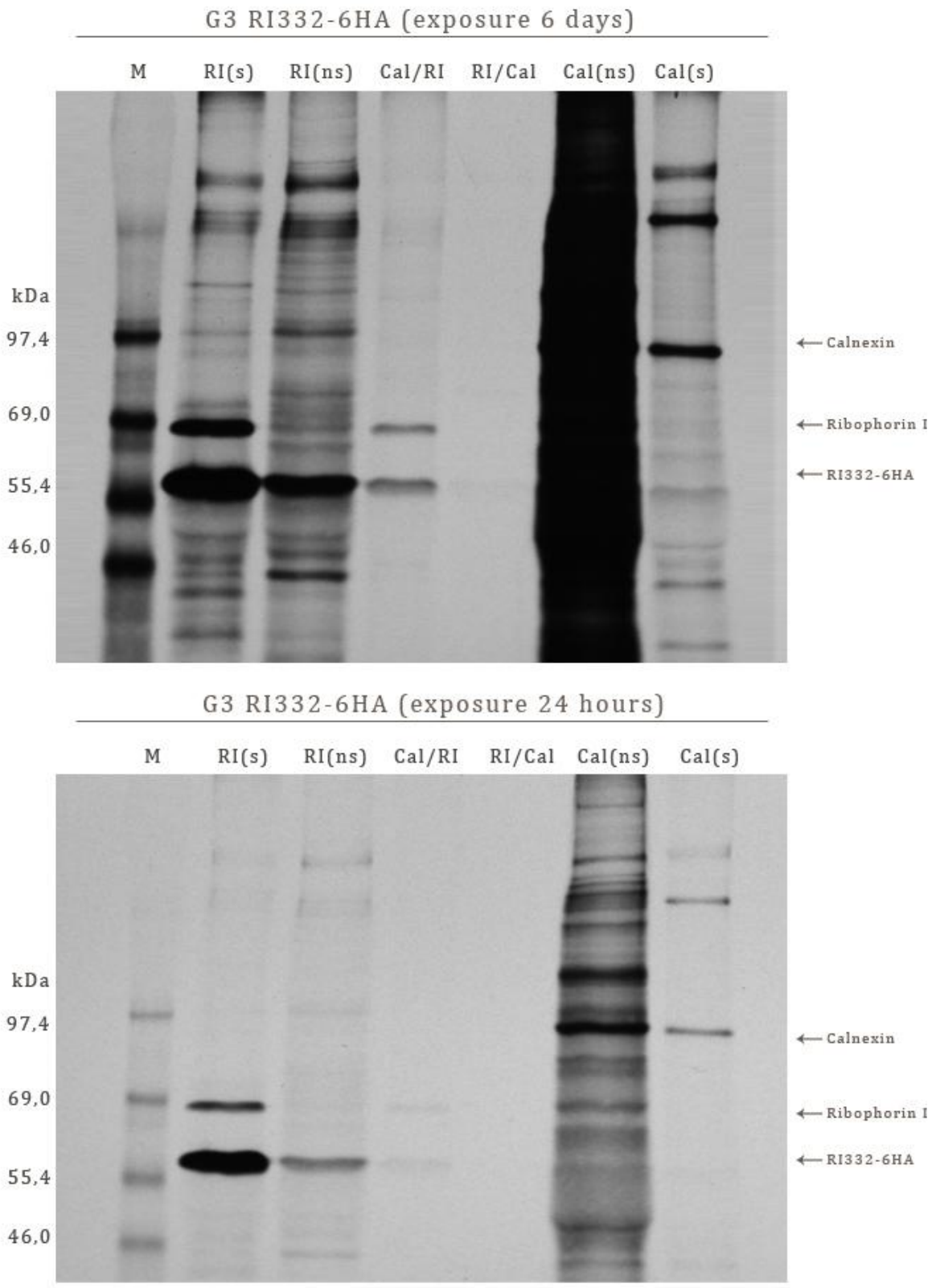

Figure 45 Fluorography of co-immunoprecipitation. G3 RI332-6HA clone 10. Chase time: 5'. Exposure time: 6 days (above) and 24 hours (Below). RI lum and calnexin antibodies were used for stringent cell lysis (s) and non stringent cell lysis (ns). Co-immunoprecipitation was performed sequentially with calnexin – RI lum (Cal/RI) and RI lum – calnexin (RI/calnexin) antibodies, respectively.

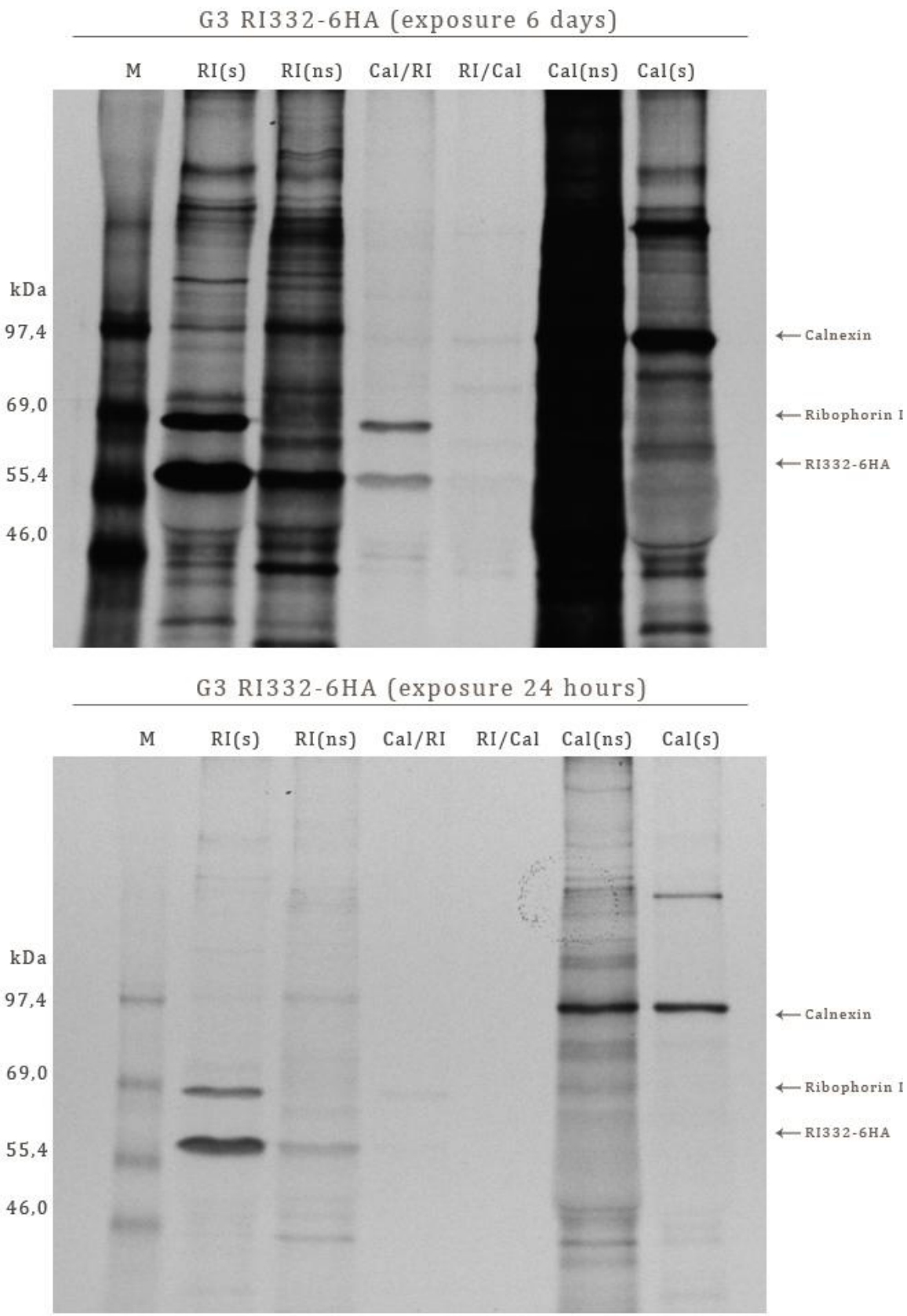

Figure 46. Fluorography of co-immunoprecipitation. G3 RI332-6HA clone 10. Chase time: 60'. Exposure time: 6 days (above) and 24 hours (Below). RI lum and calnexin antibodies were used for stringent cell lysis (s) and non stringent cell lysis (ns). Co-immunoprecipitation was performed sequentially with calnexin – RI lum (Cal/RI) and RI lum – calnexin (RI/calnexin) antibodies, respectively.

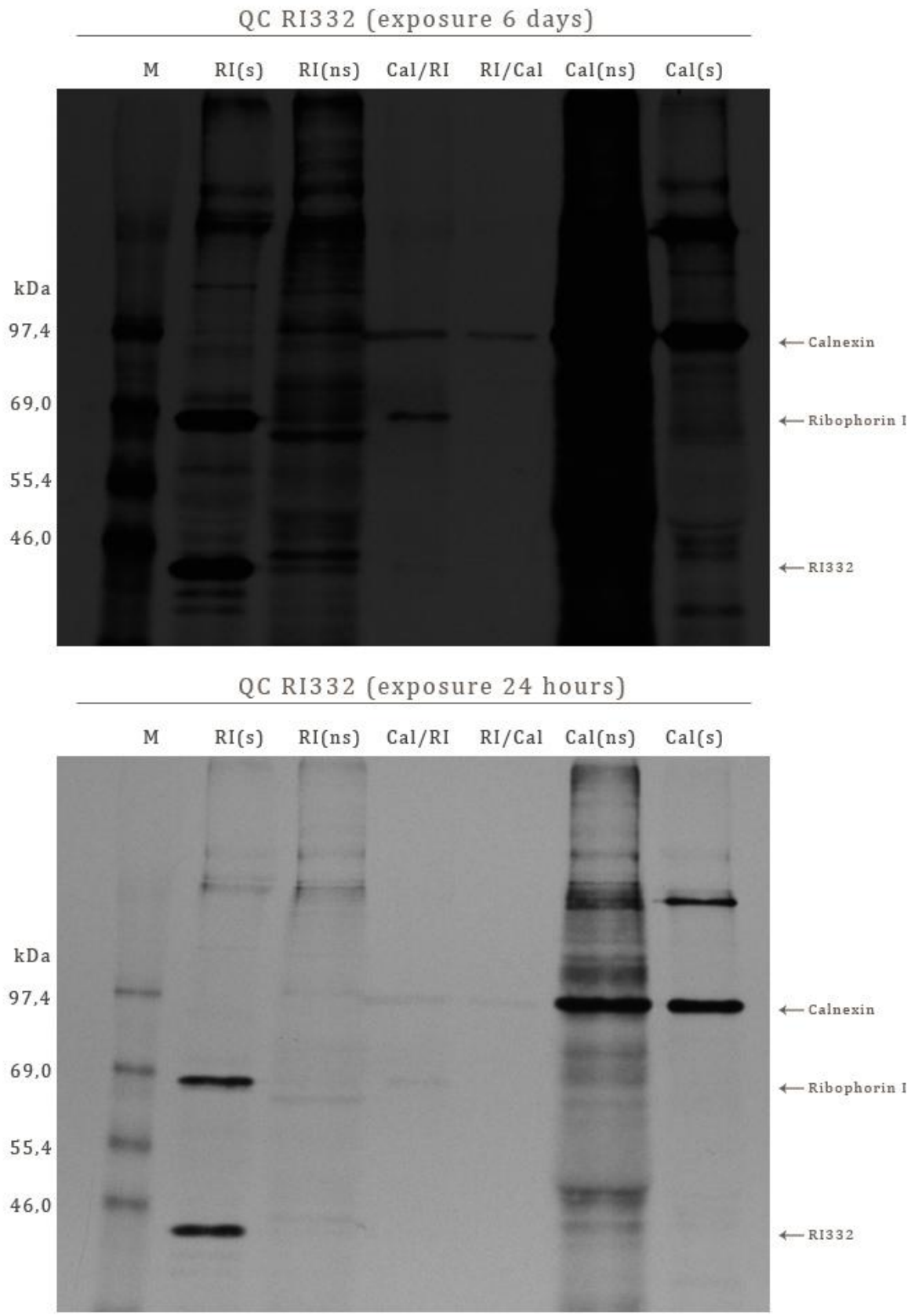

Figure 47. Fluorography of co-immunoprecipitation. QC RI332 clone GG. Chase time: 5'. Exposure time: 6 days (above) and 24 hours (Below). RI lum and calnexin antibodies were used for stringent cell lysis (s) and non stringent cell lysis (ns). Co-immunoprecipitation was performed sequentially with calnexin – RI lum (Cal/RI) and RI lum – calnexin (RI/calnexin) antibodies, respectively.

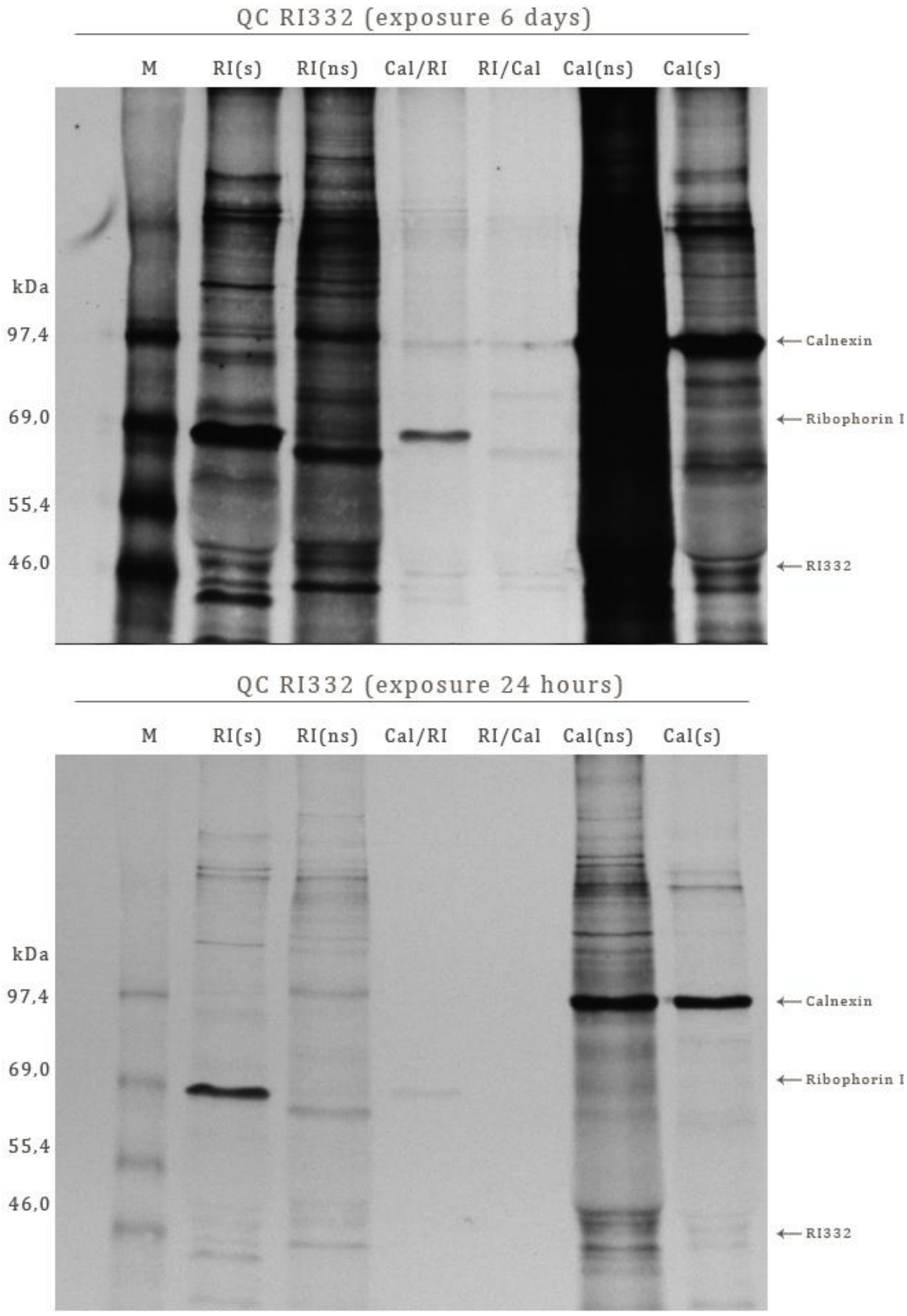

Figure 48. Fluorography of co-immunoprecipitation. QC RI332 clone GG. Chase time: 60'. Exposure time: 6 days (above) and 24 hours (Below). RI lum and calnexin antibodies were used for stringent cell lysis (s) and non stringent cell lysis (ns). Co-immunoprecipitation was performed sequentially with calnexin – RI lum (Cal/RI) and RI lum – calnexin (RI/calnexin) antibodies, respectively.

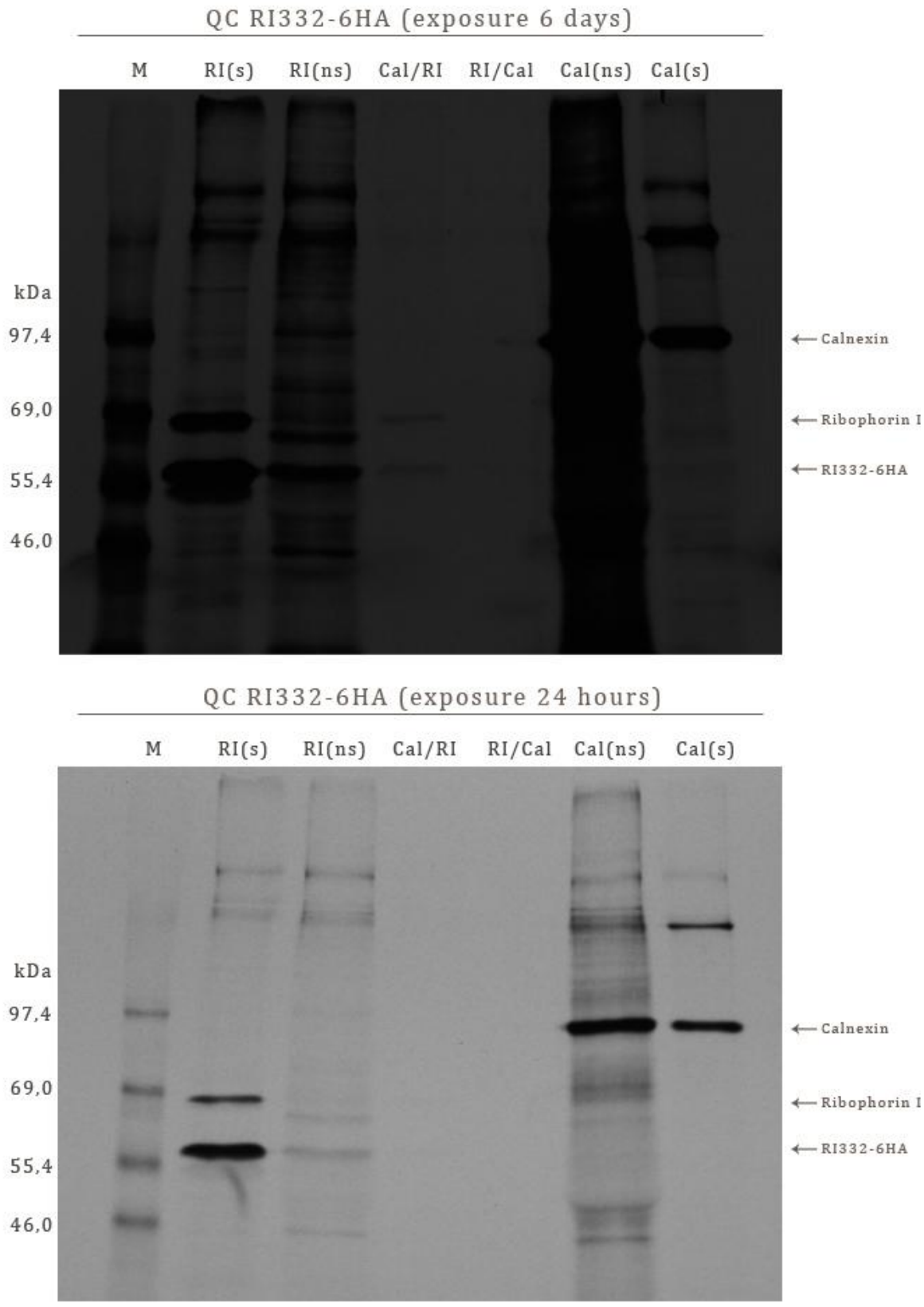

Figure 49. Fluorography of co-immunoprecipitation. QC RI332-6HA clone 5. Chase time: 5'. Exposure time: 6 days (above) and 24 hours (Below). RI lum and calnexin antibodies were used for stringent cell lysis (s) and non stringent cell lysis (ns). Co-immunoprecipitation was performed sequentially with calnexin – RI lum (Cal/RI) and RI lum – calnexin (RI/calnexin) antibodies, respectively.

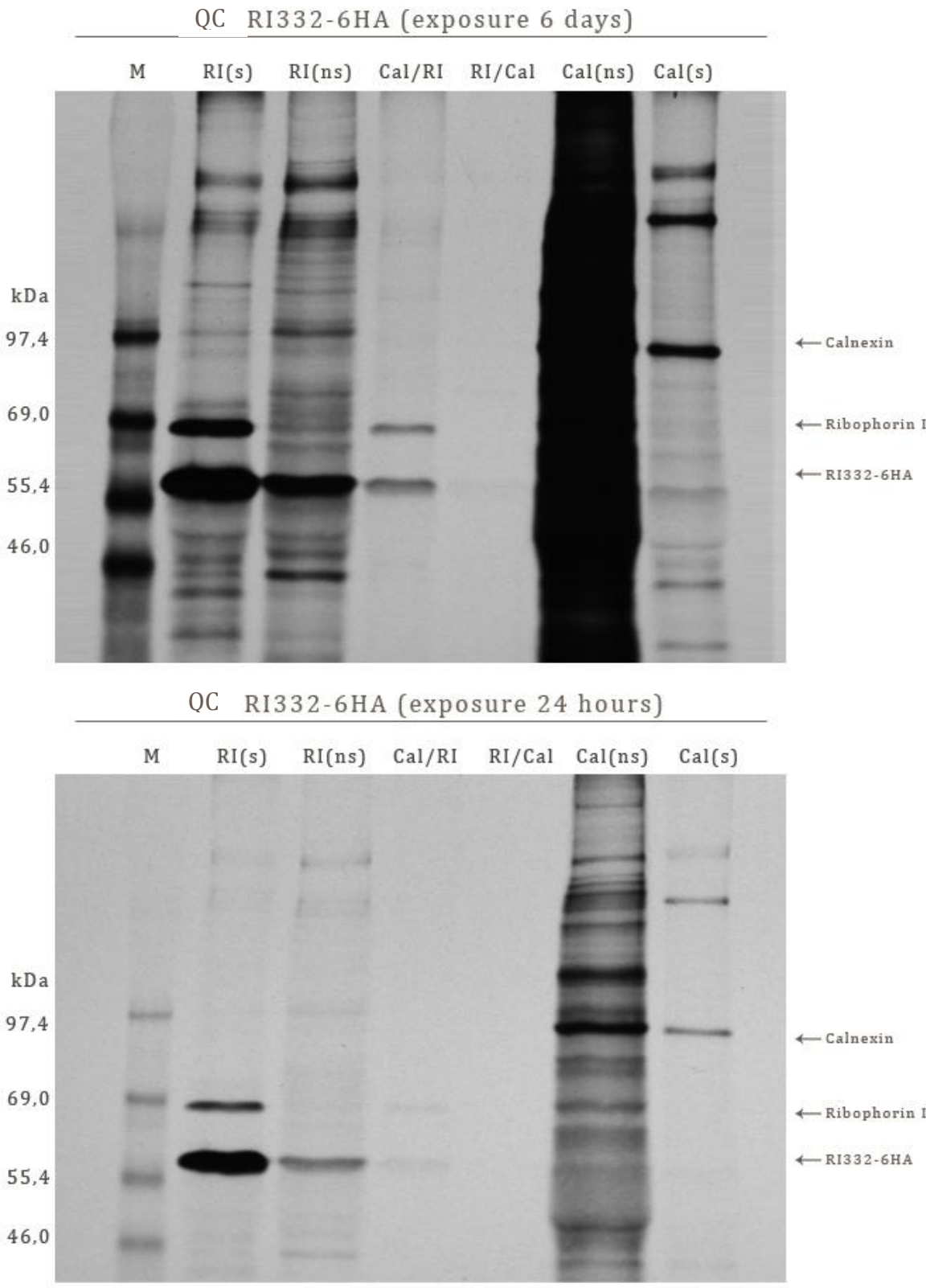

Figure 50. Fluorography of co-immunoprecipitation. QC RI332-6HA clone 5. Chase time: 60'. Exposure time: 6 days (above) and 24 hours (Below). RI lum and calnexin antibodies were used for stringent cell lysis (s) and non stringent cell lysis (ns). Co-immunoprecipitation was performed sequentially with calnexin – RI lum (Cal/RI) and RI lum – calnexin (RI/calnexin) antibodies, respectively.

In the figure below the relative interactions between the ERAD substrate and calnexin are shown. It is notable that the interaction is stronger in the G3 cell lines compared to the QC cell lines, especially at 5 minutes chase.

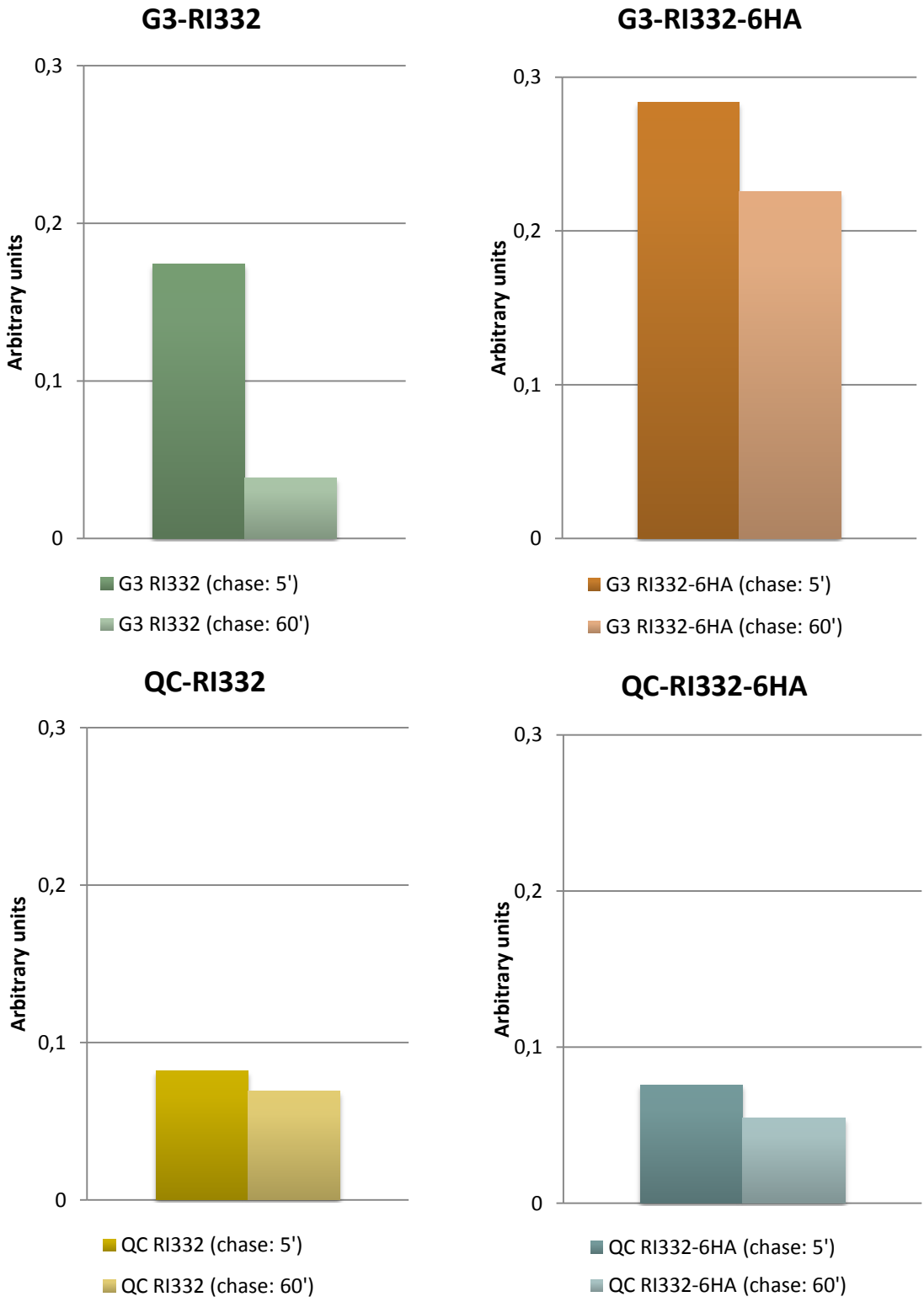

Figure 51. Relative interaction between the ERAD substrates (RI332 and RI332-6HA) and calnexin. The signals for the ERAD substrates, after co-immunoprecipitation with calnexin – RI lum, were normalized with those from the endogenous ribophorin I from the stringent cell lysis.

4.4. Localization of the ERAD substrate

In the first section (4.4.1. Fluorescence microscopy imaging), double stainings of the G3 and QC cells are presented. In the case of the non-tagged ERAD substrates (in G3 RI332 and QC RI332 cells), RI332 was localized with the RI lum antibody and compared to two other compartments (ERGIC and Golgi apparatus). An analysis of co-localization with the ER compartment was not possible, because no working monoclonal ER antibody was available. However, RI lum was also specific to the endogenous ribophorin I, although preferentially the tagged versions of the protein are stained (unpublished data).

The HA tagged ERAD substrates (in G3 RI332-6HA and QC RI332-6HA cells) were specifically visualized with the HA.11 antibody. The RI332-6HA location was compared to two other compartments: ER and Golgi apparatus. No comparison to the ERGIC compartment was possible, because no working polyclonal antibody for the ERGIC was available. Figures 52 to 59 depict all double stainings in cells grown in absence and presence of inhibitors. It is obvious that all stainings worked properly with no (or negligible) background.

In the second section (4.4.2. Statistical evaluation data of the colocalization assays) the appropriate estimated colocalization coefficients are presented. The results of the t-tests are given by SPSS in form of two tables. The first table gives information about the number of analyzed values (number of analyzed cells under given conditions), mean values of the colocalization coefficient and the standard deviations. In order to read the second table properly, the similarities of the variances should be checked. If the variances are similar (if the p value of the Levene test is greater than 0.05), the significance has to be read in the row “Variances are the same”. Otherwise, the significance has to be read in the row “Variances are not the same”. If the significance of the t-test is greater than 0.05, the null hypothesis will be retained. This means that no significant difference is present. If the significance of the t-test is smaller than 0.05, the alternative hypothesis will be applied (there is a significant difference between the two groups).

For a better overview, the two standard SPSS output tables are shown only for one t-test (tables 12 and 13). For all other t-tests, the data are filtered with respect to the variance of the Levene test. The filtered data are shown in tables 14 to 22.

4.4.1. Fluorescence microscopy imaging

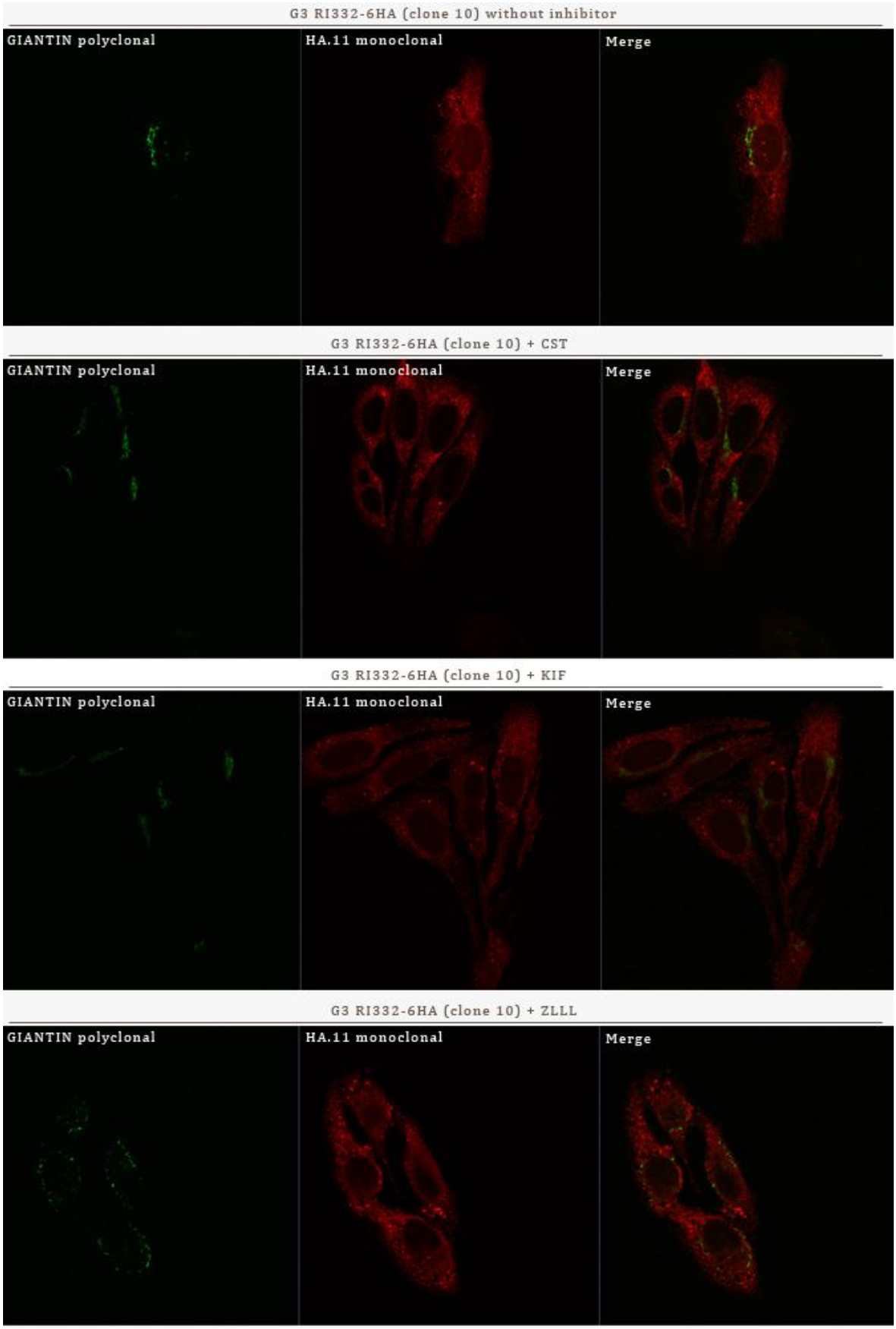

Figure 52. Double stainings of Golgi apparatus (GIANTIN polyclonal) and RI332-6HA (HA.11 monoclonal) in G3 cells (clone 10). Cells were grown in the absence of inhibitors, and in the presence of CST, KIF and ZLLL, respectively.

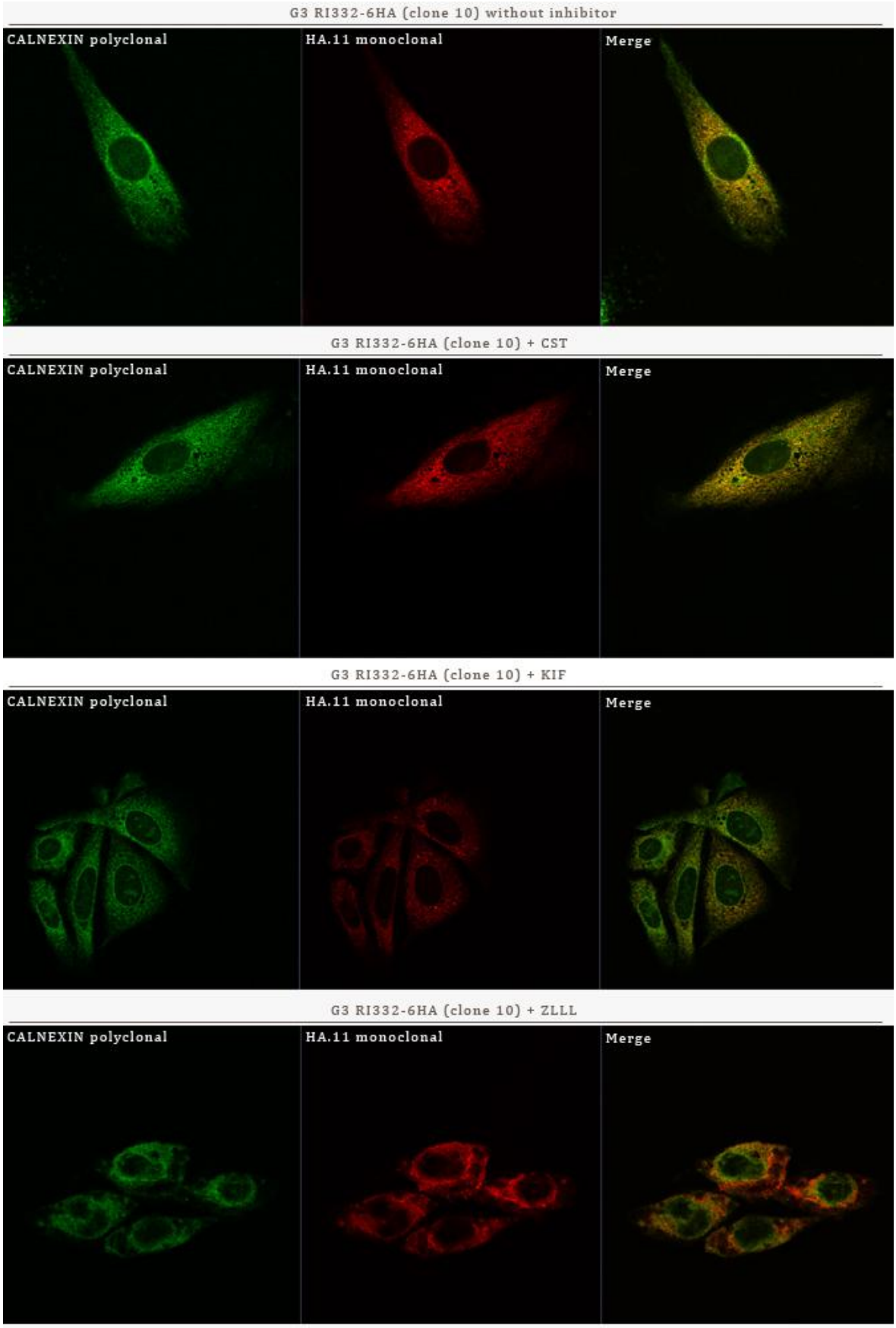

Figure 53. Double stainings of ER (CALNEXIN polyclonal) and RI332-6HA (HA.11 monoclonal) in G3 cells (clone 10). Cells were grown in the absence of inhibitors, and in the presence of CST, KIF and ZLLL, respectively.

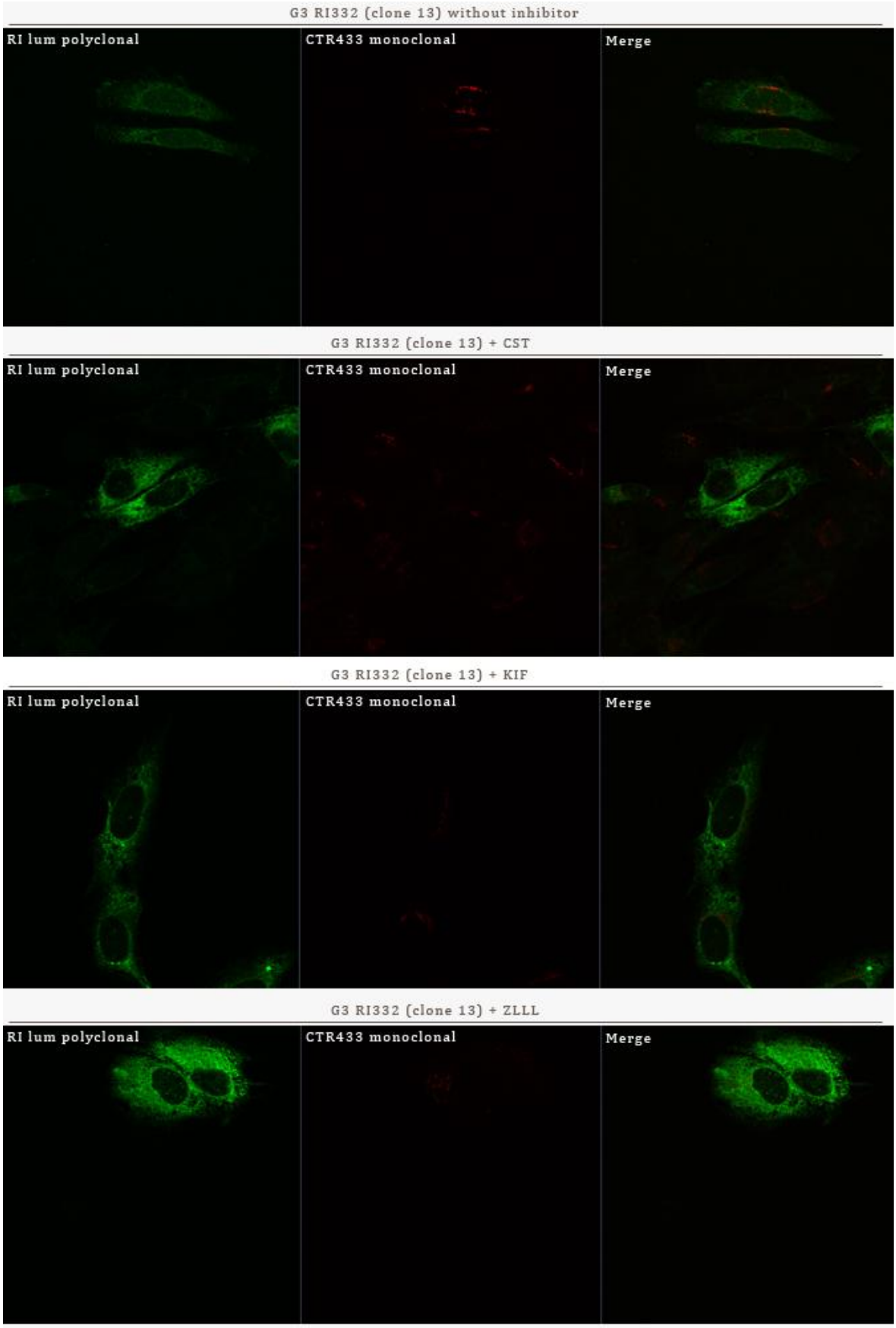

Figure 54. Double stainings of Golgi apparatus (CTR433 monoclonal) and ribophorin I / RI332 (RI lum polyclonal) in G3 cells (clone 13). Cells were grown in the absence of inhibitors, and in the presence of CST, KIF and ZLLL, respectively.

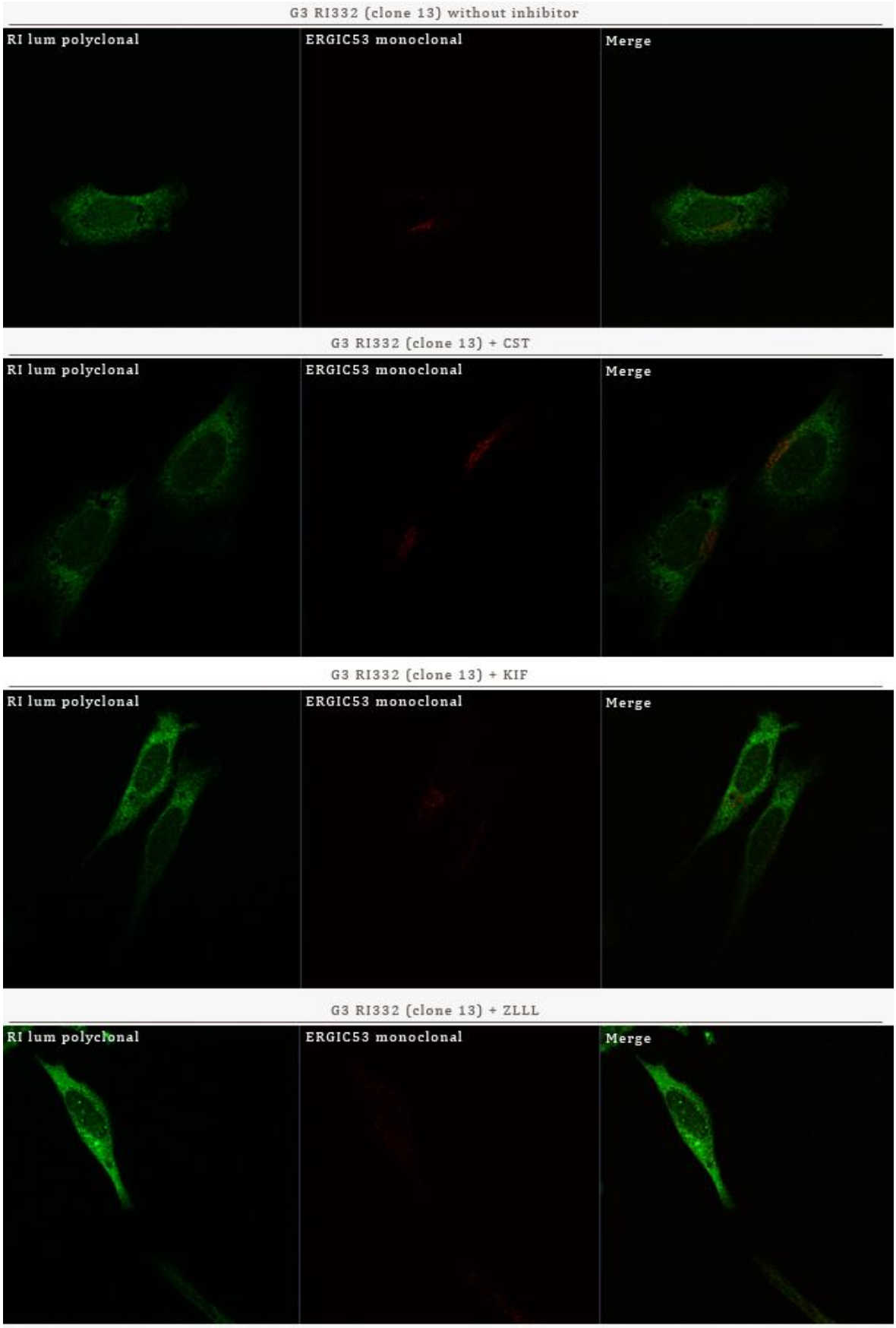

Figure 55. Double stainings of ERGIC (ERGIC53 monoclonal) and ribophorin I / RI332 (RI lum polyclonal) in G3 cells (clone 13). Cells were grown in the absence of inhibitors, and in the presence of CST, KIF and ZLLL, respectively.

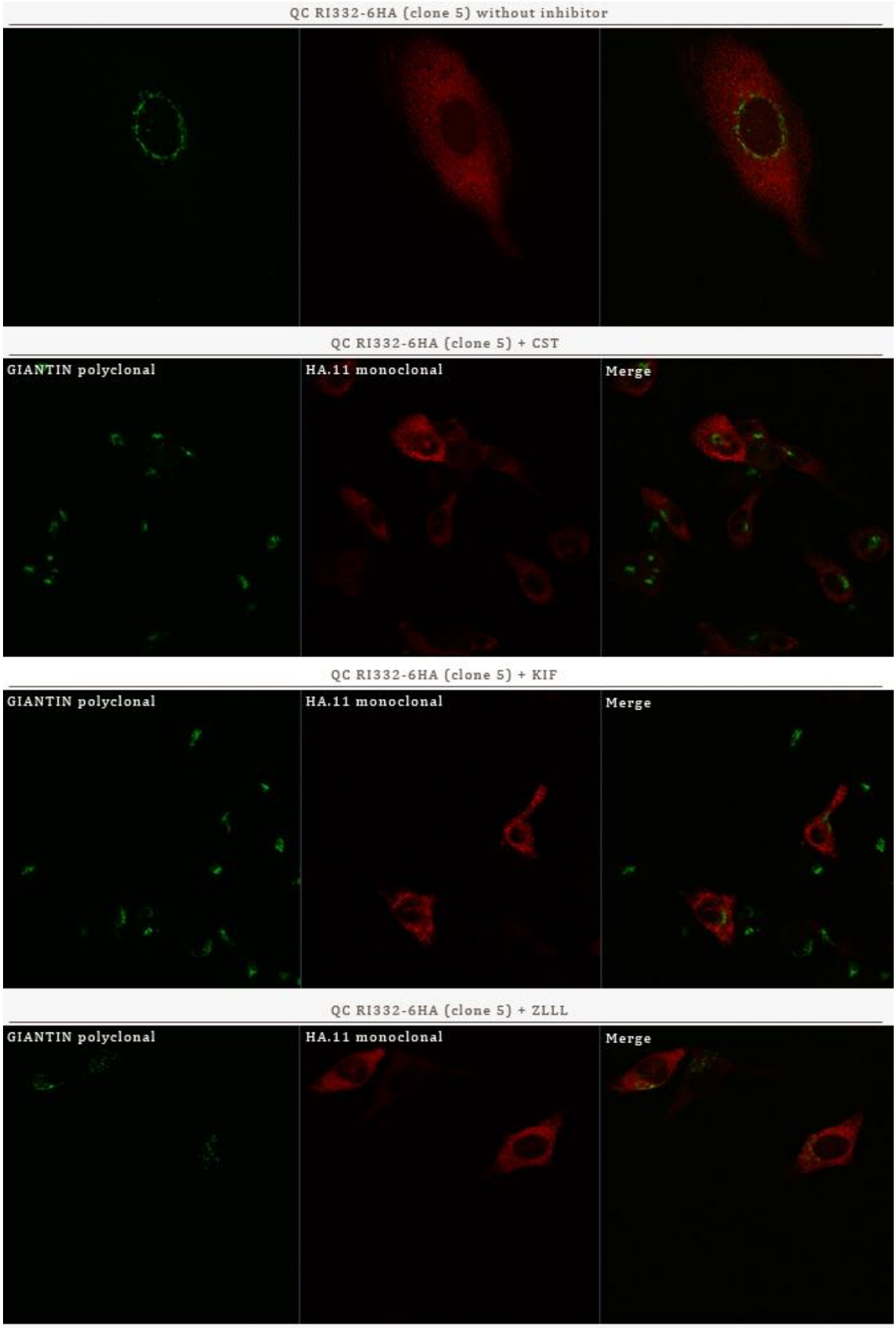

Figure 56. Double stainings of Golgi apparatus (GIANTIN polyclonal) and RI332-6HA (HA.11 monoclonal) in QC cells (clone 5). Cells were grown in the absence of inhibitors, and in the presence of CST, KIF and ZLLL, respectively.

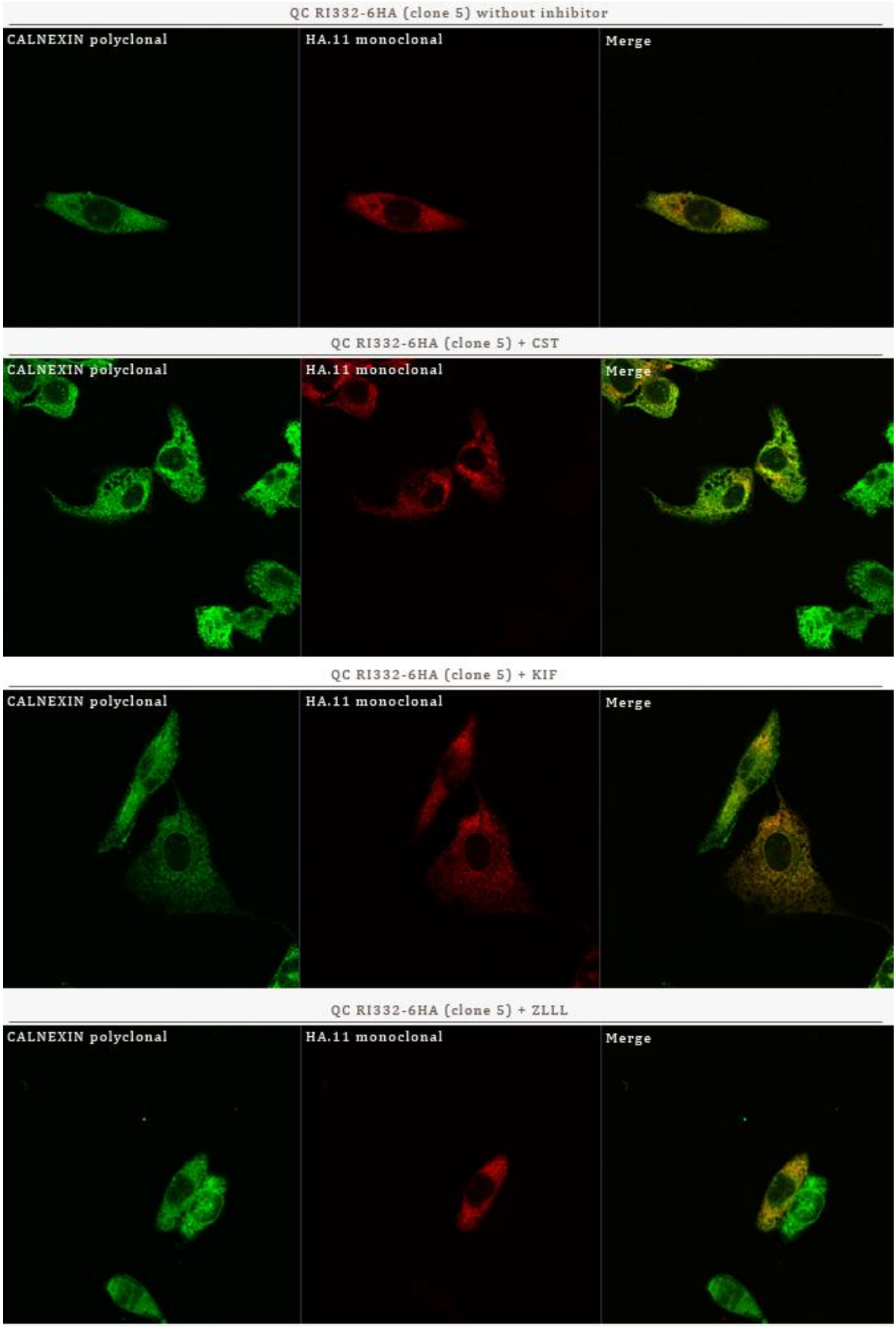

Figure 57. Double stainings of ER (CALNEXIN polyclonal) and RI332-6HA (HA.11 monoclonal) in QC cells (clone 5). Cells were grown in the absence of inhibitors, and in the presence of CST, KIF and ZLLL, respectively.

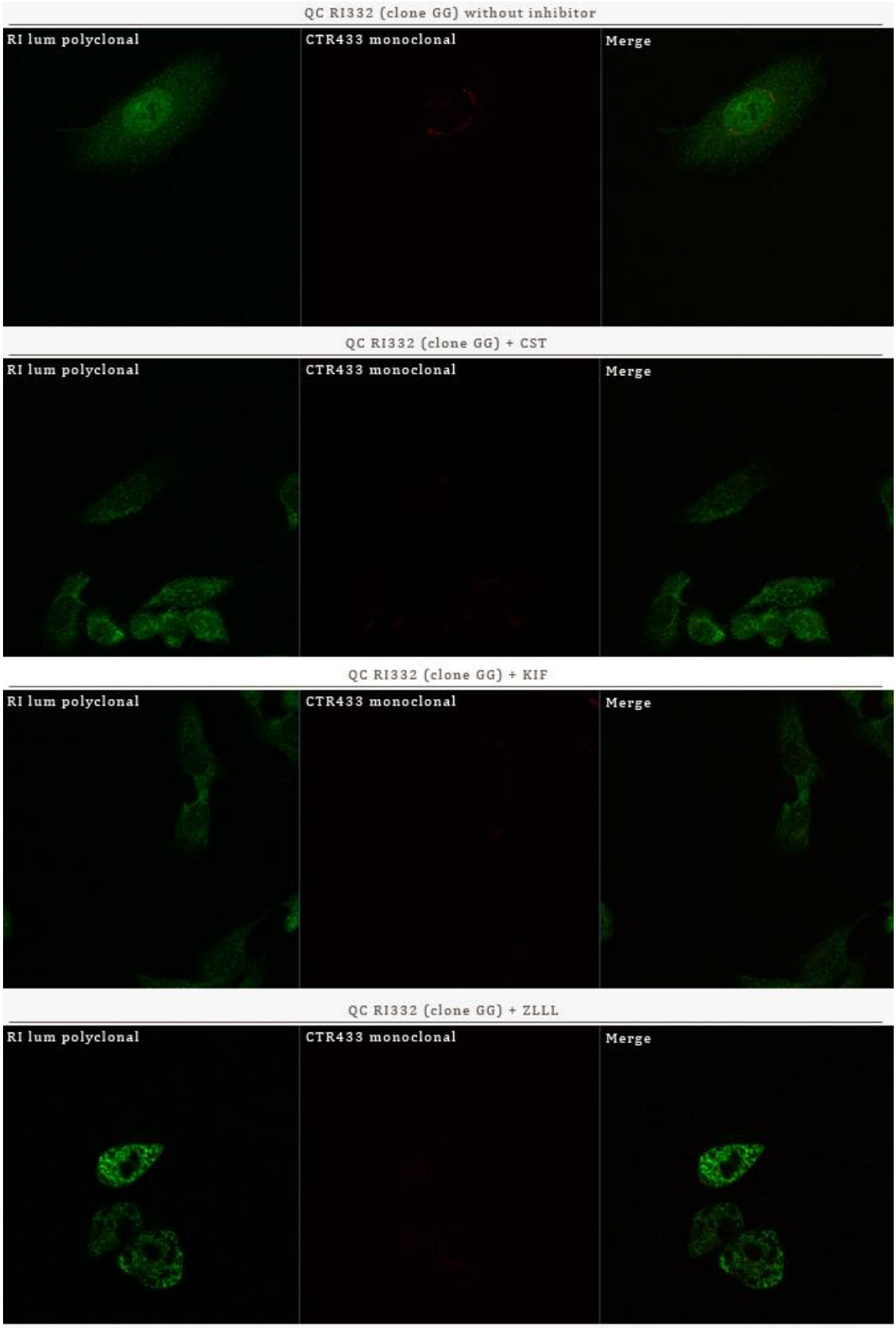

Figure 58. Double stainings of Golgi apparatus (CTR433 monoclonal) and ribophorin I / RI332 (RI lum polyclonal) in QC cells (clone GG). Cells were grown in the absence of inhibitors, and in the presence of CST, KIF and ZLLL, respectively.

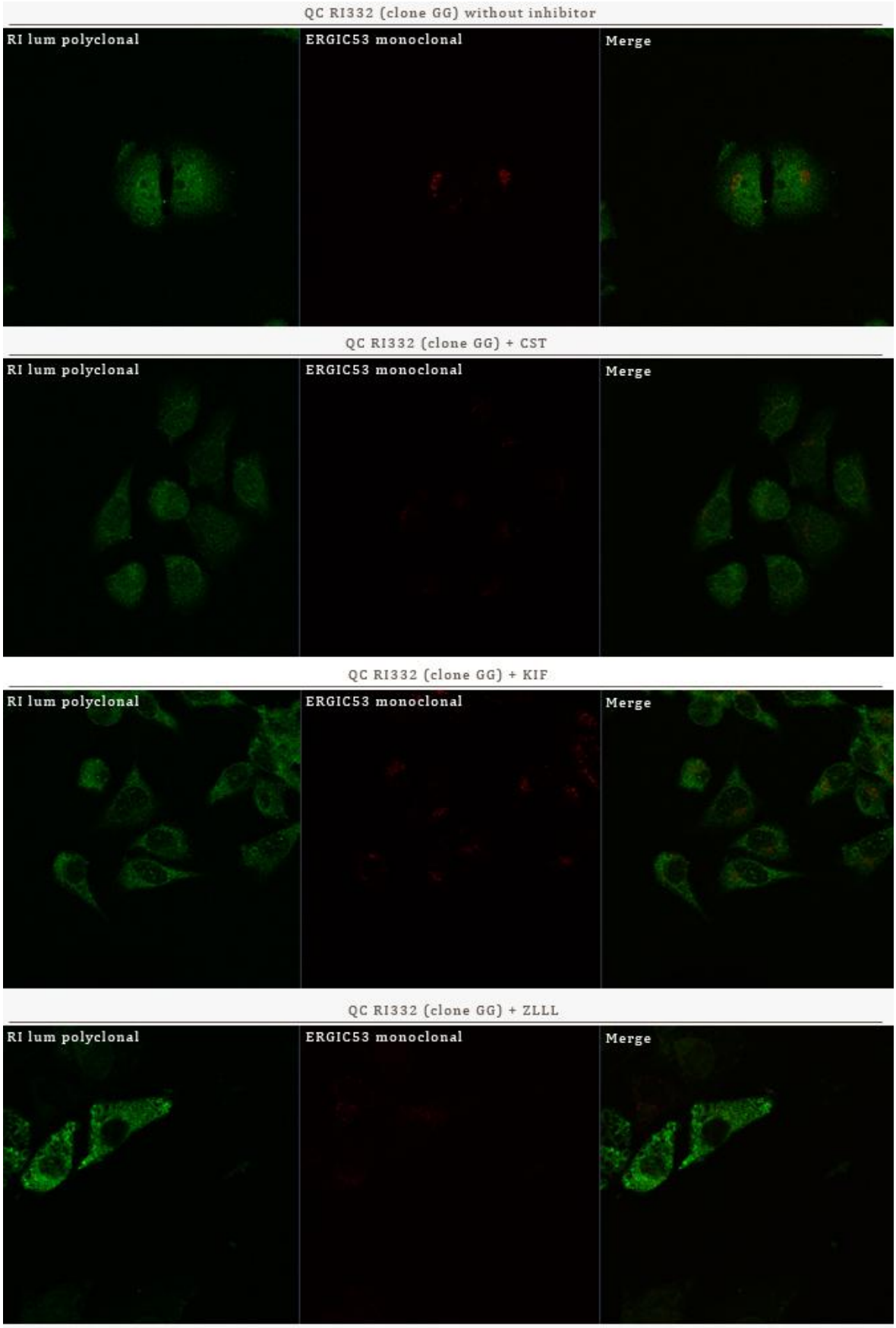

Figure 59. Double stainings of ERGIC (ERGIC53 monoclonal) and ribophorin I / RI332 (RI lum polyclonal) in QC cells (clone GG). Cells were grown in the absence of inhibitors, and in the presence of CST, KIF and ZLLL, respectively.

4.4.2. Statistical evaluation data of the colocalization assays

In the first part of this section (tables 12 to 17), the influence of inhibitors on the ERAD substrate localization will be analyzed. For the influence of CST in G3-RI332-6HA cells (clone 10), the original tables generated by SPSS are shown (tables 12 and 13). The original tables are in German language. Results from other t-tests for the inhibitor influence on the ERAD substrate localization are shown in tables 14 to 17. In the second part, t-tests for the co-localizations of the ERAD substrates with other compartments are shown in tables 18 to 22.

The first table generated by the SPSS software (table 12) gives information about the conditions (which inhibitor was used), number of samples (the average number of samples is between 10-15, but in some exceptions less samples were used for the statistical evaluation), mean value of the appropriate localization coefficients, the standard deviation and the standard error of the mean value. For each statistical evaluation, two different co-localization coefficients were used: i) co-localization coefficients with no respect to signal intensity (counts only how many signals of one channel overlap with signals of the other channel) and ii) co-localization coefficients with respect to signal intensities (weighted co-localization coefficients). The weighted coefficients are labeled with a "W" (in the example shown in tables 12 and 13, the coefficients with no respect to the intensities are called "CH3T2", and the weighted coefficients are named "CH3T2W").

Kanal	Condition	N	Mittelwert	Standardabweichung	Standardfehler des Mittelwertes
CH3T2	Control	11	,06082	,009293	,002802
	CST	12	,06233	,016827	,004858
CH3T2W	Control	11	,06936	,016812	,005069
	CST	12	,04558	,009150	,002641

Table 12. Group statistics

		Levene-Test		T-Test für die Mittelwertgleichheit						
		F	Sig.	T	df	Sig.	Mittlere Differenz	Standard-Fehler der Differenz	95% Konfidenzintervall der Differenz	
									Untere	Obere
CH3T2	Varianzen sind gleich	4,610	,044	-,264	21	,795	-,001515	,005745	-,013463	,010433
	Varianzen sind nicht gleich			-,270	17,417	,790	-,001515	,005608	-,013325	,010295
CH3T2W	Varianzen sind gleich	5,164	,034	4,265	21	,000	,023780	,005576	,012184	,035377
	Varianzen sind nicht gleich			4,160	15,152	,001	,023780	,005716	,011608	,035953

Table 13. Example of a t-test of independent samples

In the second table generated by SPSS (table 13), the results of the Levene test and the t-test of independent samples are shown. First of all, the significance of the Levene test has to be checked. If the significance is >0.05, then the t-test has to be read off in the column "Varianzen sind gleich" (variances are the same). If the significance of the Levene test is <0.05, the t-test has to be read off in the column "Varianzen sind nicht gleich" (variances are different). In the example shown in table 13, the variances (for the weighted and the non-weighted coefficients) of the Levene tests are less than 0.05. Therefore, the t-test will be read off in the column "Varianzen sind gleich").

The relevant information of the t-test is the significance (t-test significance). If the significance is >0.05, then no significant differences are present for the two groups. If the significance is <0.05, significant differences between the two groups are present.

All t-tests for the G3-RI332 and QC-RI332 cells (grown under different conditions) with the antibody combination RI lum vs. CTR433 are shown in table 14. The t-test for the same cells and conditions, but with the RI lum vs. ERGIC53 antibody combination is shown in table 15.

Cell line and antibodies	Channel	Condition	N	Mean value	Standard deviation	Levene test (sig.)	t-test (sig.)	Interpretation
G3-RI332 (clone 13) RI lum / CTR433	CH2T1	Control	10	0,0337	0,005282	0,136	**0,010**	*There is a significant difference*
		CST	6	0,0210	0,009274			
	CH2T1W	Control	10	0,0417	0,005559	0,049	**0,013**	*There is a significant difference*
		CST	6	0,0230	0,012522			
	CH2T1	Control	10	0,0337	0,005282	0,680	**0,253**	There is no significant difference
		KIF	7	0,0300	0,006245			
	CH2T1W	Control	10	0,0417	0,005559	0,889	**0,000**	*There is a significant difference*
		KIF	7	0,0271	0,005699			
	CH2T1	Control	10	0,0337	0,005282	0,068	**0,979**	There is no significant difference
		ZLLL	7	0,0336	0,009127			
	CH2T1W	Control	10	0,0417	0,005559	0,146	**0,608**	There is no significant difference
		ZLLL	7	0,0392	0,010849			
QC-RI332 (clone GG) RI lum / CTR433	CH2T1	Control	10	0,0448	0,006517	0,773	**0,000**	*There is a significant difference*
		CST	10	0,0123	0,005832			
	CH2T1W	Control	10	0,0604	0,10245	0,804	**0,000**	*There is a significant difference*
		CST	10	0,0156	0,10080			
	CH2T1	Control	10	0,0448	0,006517	0,109	**0,000**	*There is a significant difference*
		KIF	8	0,0235	0,004567			
	CH2T1W	Control	10	0,0604	0,010245	0,046	**0,000**	*There is a significant difference*
		KIF	8	0,0287	0,007146			
	CH2T1	Control	10	0,0448	0,006517	0,003	**0,000**	*There is a significant difference*
		ZLLL	6	0,0288	0,001941			
	CH2T1W	Control	10	0,0604	0,010245	0,000	**0,002**	*There is a significant difference*
		ZLLL	6	0,0415	0,001871			

Table 14. T-tests for the G3-RI332 (clone 13) and QC-RI332 (clone GG) cells, grown in the presence and absence of inhibitors; RI lum vs. CTR433 antibodies.

Cell line and antibodies	Channel	Condition	N	Mean value	Standard deviation	Levene test (sig.)	t-test (sig.)	Interpretation
G3-RI332 (clone 13) RI lum / ERGIC53	CH2T1	Control	10	0,0415	0,004860	0,009	**0,477**	There is no significant difference
		CST	9	0,0445	0,010853			
	CH2T1W	Control	10	0,0528	0,004059	0,004	**0,913**	There is no significant difference
		CST	9	0,0522	0,016262			
	CH2T1	Control	10	0,0415	0,004860	0,007	**0,600**	There is no significant difference
		KIF	7	0,0457	0,019345			
	CH2T1W	Control	10	0,0528	0,004059	0,002	**0,877**	There is no significant difference
		KIF	7	0,0544	0,025422			
	CH2T1	Control	10	0,0415	0,004860	0,000	**0,898**	There is no significant difference
		ZLLL	7	0,0430	0,028671			
	CH2T1W	Control	10	0,0528	0,004059	0,000	**0,888**	There is no significant difference
		ZLLL	7	0,0556	0,040759			
QC-RI332 (clone GG) RI lum / ERGIC53	CH2T1	Control	15	0,0682	0,013078	0,626	**0,000**	*There is a significant difference*
		CST	12	0,0377	0,010954			
	CH2T1W	Control	15	0,0895	0,019114	0,075	**0,000**	*There is a significant difference*
		CST	12	0,0377	0,012174			
	CH2T1	Control	15	0,0682	0,013078	0,338	**0,005**	*There is a significant difference*
		KIF	14	0,0497	0,018684			
	CH2T1W	Control	15	0,0895	0,018114	0,138	**0,016**	*There is a significant difference*
		KIF	14	0,0665	0,029070			
	CH2T1	Control	15	0,0682	0,013078	0,001	**0,855**	There is no significant difference
		ZLLL	7	0,0712	0,042145			
	CH2T1W	Control	15	0,0895	0,018114	0,012	**0,976**	There is no significant difference
		ZLLL	7	0,0901	0,049627			

Table 15. T-tests for the G3-RI332 (clone 13) and QC-RI332 (clone GG) cells, grown in the presence and absence of inhibitors; RI lum vs. ERGIC53 antibodies.

Cell line and antibodies	Channel	Condition	N	Mean value	Standard deviation	Levene test (sig.)	t-test (sig.)	Interpretation
G3-RI332-6HA (clone 10) HA.11 / CALNEXIN	CH3T2	Control	15	0,9952	0,004026	0,003	**0,002**	*There is a significant difference*
		CST	11	0,9991	0,001250			
	CH3T2W	Control	15	0,9983	0,001633	0,002	**0,006**	*There is a significant difference*
		CST	11	0,9997	0,000467			
	CH3T2	Control	15	0,9952	0,004026	0,261	**0,112**	There is no significant difference
		KIF	12	0,9975	0,003059			
	CH3T2W	Control	15	0,9983	0,001633	1,000	**0,802**	There is no significant difference
		KIF	12	0,9985	0,001784			
	CH3T2	Control	15	0,9952	0,004026	0,000	**0,004**	*There is a significant difference*
		ZLLL	14	0,9580	0,040053			
	CH3T2W	Control	15	0,9983	0,001633	0,000	**0,003**	*There is a significant difference*
		ZLLL	14	0,9769	0,022179			
QC-RI332-6HA (clone 5) HA.11 / CALNEXIN	CH3T2	Control	15	0,9920	0,015177	0,012	**0,100**	There is no significant difference
		CST	11	0,9990	0,001414			
	CH3T2W	Control	15	0,9958	0,005809	0,007	**0,072**	There is no significant difference
		CST	11	0,9997	0,000467			
	CH3T2	Control	15	0,9920	0,015177	0,026	**0,133**	There is no significant difference
		KIF	10	0,9984	0,002413			
	CH3T2W	Control	15	0,9968	0,005809	0,017	**0,097**	There is no significant difference
		KIF	10	0,9995	0,000850			
	CH3T2	Control	15	0,9920	0,015177	0,014	**0,069**	There is no significant difference
		ZLLL	9	0,9997	0,000441			
	CH3T2W	Control	15	0,9958	0,005809	0,007	**0,051**	There is no significant difference
		ZLLL	9	1,0000	0,000000			

Table 16. T-tests for the G3-RI332-6HA (clone 10) and QC-RI332-6HA (clone 5) cells, grown in the presence and absence of inhibitors; HA.11 vs. CALNEXIN antibodies.

Cell line and antibodies	Channel	Condition	N	Mean value	Standard deviation	Levene test (sig.)	t-test (sig.)	Interpretation
G3-RI332-6HA (clone 10) HA.11 / GIANTIN	CH3T2	Control	11	0,0608	0,009293	0,044	**0,790**	There is no significant difference
		CST	12	0,0623	0,016827			
	CH3T2W	Control	11	0,0693	0,016812	0,034	**0,001**	*There is a significant difference*
		CST	12	0,0455	0,009150			
	CH3T2	Control	11	0,0608	0,009293	0,110	**0,000**	*There is a significant difference*
		KIF	9	0,0362	0,005094			
	CH3T2W	Control	11	0,0693	0,06936	0,025	**0,000**	*There is a significant difference*
		KIF	9	0,0383	0,03833			
	CH3T2	Control	11	0,0608	0,009293	0,002	**0,004**	*There is a significant difference*
		ZLLL	11	0,0933	0,029090			
	CH3T2W	Control	11	0,0693	0,016812	0,029	**0,030**	*There is a significant difference*
		ZLLL	11	0,0970	0,034205			
QC-RI332-6HA (clone 5) HA.11 / GIANTIN	CH3T2	Control	16	0,0925	0,018323	0,574	**0,023**	*There is a significant difference*
		CST	8	0,0716	0,022379			
	CH3T2W	Control	16	0,0990	0,022238	0,372	**0,000**	*There is a significant difference*
		CST	8	0,0615	0,016767			
	CH3T2	Control	16	0,0925	0,018323	0,107	**0,123**	There is no significant difference
		KIF	10	0,1076	0,030034			
	CH3T2W	Control	16	0,0990	0,022238	0,021	**0,864**	There is no significant difference
		KIF	10	0,0963	0,039463			
	CH3T2	Control	16	0,0925	0,018323	0,094	**0,005**	*There is a significant difference*
		ZLLL	12	0,1215	0,031306			
	CH3T2W	Control	16	0,0990	0,022238	0,002	**0,001**	*There is a significant difference*
		ZLLL	12	0,6066	0,062571			

Table 17. T-tests for the G3-RI332-6HA (clone 10) and QC-RI332-6HA (clone 5) cells, grown in the presence and absence of inhibitors; HA.11 vs. GIANTIN antibodies.

Beside the statistical evaluation of the influence of inhibitors on the co-colocalization of RI332 (and RI332-6HA, respectively) with specific cellular compartments, also the co-localization coefficients of different antibody combinations were compared among themselves. For this purpose, only co-localization coefficients of cells grown in the absence of inhibitors were used (only one condition). The t-test results for all cell lines are shown in tables 18 to 22. The comparisons of the antibody combinations are shown below.

- HA.11/GIANTIN vs. HA.11/CALNEXIN
- HA.11/GIANTIN vs RI lum/CTR433
- HA.11/GIANTIN vs. RI lum/ERGIC53
- HA.11/CALNEXIN vs. RI lum/CTR433
- HA.11/CALNEXIN vs RI lum/ERGIC53

HA.11/GIANTIN vs. HA.11/CALNEXIN								
Cell line combinations	Channel	Antibodies	N	Mean value	Standard deviation	Levene test (sig.)	t-test (sig.)	Interpretation
G3-RI332-6HA vs. G3-RI332-6HA	CH2T1 (CH3T2)	HA_GIANTIN	11	0,0608	0,009293	0,028	**0,000**	*There is a significant difference*
		HA_CALNEXIN	15	0,9952	0,004026			
	CH2T1w (CH3T2w)	HA_GIANTIN	11	0,0693	0,016812	0,000	**0,000**	*There is a significant difference*
		HA_CALNEXIN	15	0,9983	0,001633			
G3-RI332-6HA vs. QC-RI332-6HA	CH2T1 (CH3T2)	HA_GIANTIN	13	0,0990	0,012800	0,997	**0,000**	*There is a significant difference*
		HA_CALNEXIN	15	0,9920	0,015177			
	CH2T1w (CH3T2w)	HA_GIANTIN	13	0,1062	0,017331	0,001	**0,000**	*There is a significant difference*
		HA_CALNEXIN	15	0,9968	0,005809			

Table 18. Comparison of HA.11/GIANTIN and HA.11/CALNEXIN co-localizations.

HA.11/GIANTIN vs. RI lum/CTR433								
Cell line combinations	Channel	Antibodies	N	Mean value	Standard deviation	Levene test (sig.)	t-test (sig.)	Interpretation
G3-RI332-6HA vs. G3-RI332	CH2T1 (CH3T2)	HA_GIANTIN	12	0,0570	0,007032	0,028	**0,021**	*There is a significant difference*
		RI_CTR433	8	0,0453	0,010836			
	CH2T1w (CH3T2w)	HA_GIANTIN	12	0,0643	0,013432	0,452	**0,056**	There is no significant difference
		RI_CTR433	8	0,0523	0,010070			
G3-RI332-6HA vs. QC-RI332	CH2T1 (CH3T2)	HA_GIANTIN	12	0,0616	0,013776	0,566	**0,063**	There is no significant difference
		RI_CTR433	7	0,0446	0,009292			
	CH2T1w (CH3T2w)	HA_GIANTIN	12	0,0709	0,021157	0,321	**0,482**	There is no significant difference
		RI_CTR433	7	0,0616	0,012097			
QC-RI332-6HA vs. G3-RI332	CH2T1 (CH3T2)	HA_GIANTIN	16	0,0925	0,018323	0,030	**0,000**	*There is a significant difference*
		RI_CTR433	7	0,0337	0,005282			
	CH2T1w (CH3T2w)	HA_GIANTIN	16	0,0990	0,022238	0,015	**0,000**	*There is a significant difference*
		RI_CTR433	7	0,0417	0,005559			
QC-RI332-6HA vs. QC-RI332	CH2T1 (CH3T2)	HA_GIANTIN	16	0,0925	0,018323	0,067	**0,000**	*There is a significant difference*
		RI_CTR433	7	0,0448	0,006517			
	CH2T1w (CH3T2w)	HA_GIANTIN	16	0,0990	0,022238	0,112	**0,013**	*There is a significant difference*
		RI_CTR433	7	0,0604	0,010245			

Table 19. Comparison of HA.11/GIANTIN and RI lum/CTR433 co-localizations.

HA.11/GIANTIN vs. RI lum/ERGIC53								
Cell line combinations	Channel	Antibodies	N	Mean value	Standard deviation	Levene test (sig.)	t-test (sig.)	Interpretation
G3-RI332-6HA vs. G3-RI332	CH2T1 (CH3T2)	HA_GIANTIN	11	0,0608	0,009293	0,183	**0,000**	*There is a significant difference*
		RI_ERGIC53	7	0,0415	0,004860			
	CH2T1w (CH3T2w)	HA_GIANTIN	11	0,0693	0,016812	0,008	**0,009**	*There is a significant difference*
		RI_ ERGIC53	7	0,0528	0,004059			
G3-RI332-6HA vs. QC-RI332	CH2T1 (CH3T2)	HA_GIANTIN	11	0,0608	0,009293	0,339	**0,158**	There is no significant difference
		RI_ ERGIC53	14	0,0677	0,013469			
	CH2T1w (CH3T2w)	HA_GIANTIN	11	0,0693	0,016812	0,516	**0,011**	*There is a significant difference*
		RI_ ERGIC53	14	0,0892	0,018772			
QC-RI332-6HA vs. G3-RI332	CH2T1 (CH3T2)	HA_GIANTIN	16	0,0925	0,018323	0,029	**0,000**	*There is a significant difference*
		RI_ ERGIC53	7	0,0415	0,004860			
	CH2T1w (CH3T2w)	HA_GIANTIN	16	0,0990	0,022238	0,009	**0,000**	*There is a significant difference*
		RI_ ERGIC53	7	0,0528	0,004059			
QC-RI332-6HA vs. QC-RI332	CH2T1 (CH3T2)	HA_GIANTIN	16	0,0925	0,018323	0,236	**0,000**	*There is a significant difference*
		RI_ ERGIC53	15	0,0682	0,013078			
	CH2T1w (CH3T2w)	HA_GIANTIN	16	0,0990	0,022238	0,568	**0,206**	There is no significant difference
		RI_ ERGIC53	15	0,0895	0,018114			

Table 20. Comparison of HA.11/GIANTIN and RI lum/ERGIC53 co-localizations.

HA.11/CALNEXIN vs. RI lum/CTR433								
Cell line combinations	Channel	Antibodies	N	Mean value	Standard deviation	Levene test (sig.)	t-test (sig.)	Interpretation
G3-RI332-6HA vs. G3-RI332	CH2T1 (CH3T2)	HA_CALNEXIN	15	0,9952	0,004026	0,693	**0,000**	*There is a significant difference*
		RI_ CTR433	7	0,0337	0,005282			
	CH2T1w (CH3T2w)	HA_ CALNEXIN	15	0,9983	0,001633	0,005	**0,000**	*There is a significant difference*
		RI_ CTR433	7	0,0417	0,005559			
G3-RI332-6HA vs. QC-RI332	CH2T1 (CH3T2)	HA_ CALNEXIN	15	0,9952	0,004026	0,036	**0,000**	*There is a significant difference*
		RI_ CTR433	7	0,0448	0,006517			
	CH2T1w (CH3T2w)	HA_ CALNEXIN	15	0,9983	0,001633	0,000	**0,000**	*There is a significant difference*
		RI_ CTR433	7	0,0604	0,010245			
QC-RI332-6HA vs. G3-RI332	CH2T1 (CH3T2)	HA_ CALNEXIN	15	0,9920	0,015177	0,149	**0,000**	*There is a significant difference*
		RI_ CTR433	7	0,0337	0,005282			
	CH2T1w (CH3T2w)	HA_ CALNEXIN	15	0,9968	0,005809	0,939	**0,000**	*There is a significant difference*
		RI_ CTR433	7	0,0417	0,005559			
QC-RI332-6HA vs. QC-RI332	CH2T1 (CH3T2)	HA_ CALNEXIN	15	0,9920	0,015177	0,292	**0,000**	*There is a significant difference*
		RI_ CTR433	7	0,0448	0,006517			
	CH2T1w (CH3T2w)	HA_ CALNEXIN	15	0,9968	0,99680	0,005	**0,000**	*There is a significant difference*
		RI_ CTR433	7	0,0604	0,06043			

Table 21. Comparison of HA.11/CALNEXIN and RI lum/CTR433 co-localizations.

HA.11/CALNEXIN vs. RI lum/ERGIC53								
Cell line combinations	Channel	Antibodies	N	Mean value	Standard deviation	Levene test (sig.)	t-test (sig.)	Interpretation
G3-RI332-6HA vs. G3-RI332	CH2T1 (CH3T2)	HA_CALNEXIN	15	0,9952	0,004026	0,630	**0,000**	*There is a significant difference*
		RI_ ERGIC53	7	0,0415	0,004860			
	CH2T1w (CH3T2w)	HA_ CALNEXIN	15	0,9983	0,001633	0,005	**0,000**	*There is a significant difference*
		RI_ ERGIC53	7	0,0528	0,004059			
G3-RI332-6HA vs. QC-RI332	CH2T1 (CH3T2)	HA_ CALNEXIN	15	0,9952	0,004026	0,008	**0,000**	*There is a significant difference*
		RI_ ERGIC53	15	0,0682	0,013078			
	CH2T1w (CH3T2w)	HA_ CALNEXIN	15	0,9983	0,001633	0,000	**0,000**	*There is a significant difference*
		RI_ ERGIC53	15	0,0895	0,018114			
QC-RI332-6HA vs. G3-RI332	CH2T1 (CH3T2)	HA_ CALNEXIN	15	0,9920	0,015177	0,148	**0,000**	*There is a significant difference*
		RI_ ERGIC53	7	0,0415	0,004860			
	CH2T1w (CH3T2w)	HA_ CALNEXIN	15	0,9968	0,005809	0,645	**0,000**	*There is a significant difference*
		RI_ ERGIC53	7	0,0528	0,004059			
QC-RI332-6HA vs. QC-RI332	CH2T1 (CH3T2)	HA_ CALNEXIN	15	0,9920	0,015177	0,886	**0,000**	*There is a significant difference*
		RI ERGIC53	15	0,0682	0,013078			
	CH2T1w (CH3T2w)	HA_ CALNEXIN	15	0,9968	0,005809	0,000	**0,000**	*There is a significant difference*
		RI_ ERGIC53	15	0,0895	0,018144			

Table 22. Comparison of HA.11/CALNEXIN and RI lum/ERGIC53 co-localizations.

5. Discussion

The majority of secretory proteins are N-linked glycoproteins. The complex N-linked oligosaccharide (Glc3Man9GlcNAc2) is extensively trimmed and modified in the ER and further compartments of the secretory pathway. The trimming is necessary in order to promote quality control of folding, maturation and assembling of the proteins (Lederkremer, 2009).

UDP-glucose (UDP-glc) plays a crucial role in the assembly of the N-linked glycan and in the quality control of glycoproteins. UDP-glc is a precursor of Dol-P-glucose which is a glucose donor for the N-linked glycan (Burda, et al., 1999). During the CNX cycle, UDP-glc is used by the central enzyme UDP-Glc:glycoprotein glucosyltransferase (GT) in order to reglucosylate unfolded and misfolded proteins *(see 1.5.2. CNX cycle)*.

During the first part of this diploma thesis, the degradation efficiency of two model proteins (ERAD substrates: RI332 and RI332-6HA) was investigated by pulse chase experiments. These proteins were expressed in two different cell lines, which had been originally generated from a Chinese hamster lung fibroblast cell line with a dective UDP-glucose pyrophosphorylase (Flores-Diaz, et al., 1997): i) G3 and ii) QC. The G3 cell line has a restored wild type phenotype, due to a stable transfection with a vector carrying the cDNA of the bovine UDP-glucose pyrophosphorylase gene. The QC cell line was transfected with an empty vector, resulting in the mutant phenotype. As a consequence, the QC cells have low levels of UDP-glc and thus glucosylation reactions are affected. Because of low levels of UDP-glc, the N-linked glycans are missing the three glucose molecules (S.E. Moore, unpublished observations). Consequently, the degradation of the ERAD substrates would be expected to be faster in the QC cells compared to G3 cells, because glycoproteins with N-linked glycans would be expected not to enter the CNX cycle which usually causes a temporary retention of glycoproteins in the ER *(see 1.5.2. CNX cycle)*.

In the second part of this diploma thesis, the interaction between the ERAD substrates and CNX was analyzed by sequential immunoprecipitation. It has already been described that terminally misfolded glycoproteins are guided by the CNX cycle to the ERAD pathway (Benyair, et al., 2011).

Finally, the last part of the diploma thesis was focused on the intracellular localization of the ERAD substrates. It was analyzed by indirect immunofluorescence and confocal laser scanning microscopy whether interfering with the ER quality control by using drugs that inhibit initial processing of the N-linked glycan or proteasomal degradation affects the localization of the two ERAD model substrates (RI332 and RI332-6HA). Furthermore, using a colocalization module of the microscope software *(see 4.5.2. Visualization)*, the colocalization coefficients of the ERAD substrates and designated cellular compartments were compared among themselves.

5.1. Half life determination of the ERAD substrates RI332 and RI332-6HA

Not surprisingly, the half lives of the two ERAD substrates RI332 and RI332-6HA are considerably shorter in the mutant cell lines QC-RI332 (RI332 $t_{1/2}$: 21,33±4,64 minutes) and QC-RI332-6HA (RI-332-6HA $t_{1/2}$: 18,84±6,86 minutes) rather than in the wild type cell lines G3-RI332 (RI332 $t_{1/2}$: 47,19±4,06 minutes) and G3-RI332-6HA (RI332-6HA $t_{1/2}$: 57,19±13,73 minutes) (see figures 15 to 18). Due to the mutation in UDP-glucose pyrophosphorylase, N-glucosylation is disturbed in QC cells. As a consequence, the proteins are not recognized by the players of the CNX cycle, which requires that glycoproteins are monoglucosylated (Williams, 2006). Therefore, RI-332 and RI-332-6HA appear to avoid the CNX cycle which at the end causes a faster retrotranslocaion to the cytosol, followed by proteasomal degradation.

The ERAD substrates in the G3 cell lines are properly glucosylated; they have first to be processed by glucosidases I & II in order to enter the CNX cycle (D'Alessio, et al., 2010; Pearse & Hebert, 2010). Once the proteins have entered the CNX cycle, they have to go through several cycles before they can be released. The release is initiated by the delayed action of ER mannosidase I (Bagola, et al., 2011; Benyair, et al., 2011).

In further experiments, inhibitors were used in order to interfere with the ER quality control. The ER quality control was disturbed by the inhibition of i) glucosidase I by CST, ii) ER mannosidase I by DMJ or KIF, and iii) the proteasome by ZLLL.

5.2. Effect of inhibitors on the ERAD substrate degradation

The first oligosaccharide trimming of properly N-glycosylated proteins occurs in the ER by glucosidases I & II. These two enzymes remove the two outermost glucose molecules of the oligosaccharide. By inhibiting their action, glycoproteins remain fully glucosylated. They are not recognized by CNX and CRT, which recognize only

monoglucosylated glycoproteins (Williams, 2006). According to expectations, these proteins should be retrotranslocated faster than in the normal situation when the glucose residues are cleaved off.

On the other hand, the inhibition of glucosidase I should not affect the destiny of non-glucosylated secretory proteins as they occur in QC cells. These proteins should not enter the CNX cycles at all.

As expected, the degradation of RI332 and RI332-6HA in the G3 cells becomes slightly faster in the presence of CST (RI332 half life decreases for approx. 33% and the RI332-6HA half life decreases for approx. 13%). This is perhaps an indication that the CNX cycle is at least partially avoided, because of the pre-incubation with CST that causes the inhibition of glucosidase I. However, the faster degradation is more apparent for the non-tagged ERAD substrate (RI332) (see figures 19 and 20).

Surprisingly, CST caused changes in the stability of the ERAD substrates in the QC cells. As seen in figures 21 and 22, RI332 and RI332-6HA are stabilized by the inhibition of glucosidase I (the half life of RI332 increased for approximately 220% and the half life of RI332-6HA increased for approximately 169%). This could be explained by a re-glucosylation of the ERAD substrates by UDP-glucose glycoprotein glucosyltransferase, and a prolonged interaction with CNX, which appears unlikely, however. An alternative explanation would be that the ERAD substrates enter an unknown degradation pathway in the QC cells.

Two different inhibitors of ER mannosidase I were used: i) KIF, a non-competitive inhibitor and ii) DMJ, a competitive inhibitor. By inhibiting ER mannosidases in the G3 cells, misfolded glycoproteins should retain trapped in the CNX cycle. In other words, the misfolded protein should be stabilized and retained in the ER. In QC cells, the inhibition of ER mannosidases should not affect the degradation of the ERAD substrates, since the ERAD substrates should not enter the CNX cycle.

As shown in figures 23, 24, 27 and 28, treatment of cells with both ER mannosidase inhibitors indeed increases the half lives of the ERAD substrates in G3 cells (DMJ increases the half life of RI332 for approx. 577% and of RI332-6HA for approx. 830%). The dramatic stabilisation is better shown in figure 35. In QC cells, the half life of the non-tagged ERAD substrate is only negligibly changed in the presence of both

inhibitors (DMJ increases the half life of RI332 for approximately 34%) (see figures 25 and 29). This finding confirms the assumption that the misfolded glycoproteins in QC cells partially avoid the CNX cycle. However, unexpectedly the tagged ERAD substrate (RI332-6HA) in the QC cells is stabilized by the ER mannosidases inhibitors (DMJ increases the half life of RI332-6HA for approx. 521%) (see figures 26 and 30). This suggests that the protein does enter the CNX cycle. It is possible that the 6HA tag changes the properties of the glycoprotein in an unknown way. Alternatively, ER mannosidase I or another ER mannosidase that is inhibited by KIF and DMJ may be involved in the degradation of the HA-tagged ERAD substrate in QC cells.

Finally, interfering with the ER quality control was also performed on the degradation level of ERAD itself. The proteasome was inhibited by ZLLL. The inhibition of the proteasome should stabilize all misfolded glycoproteins, independently of the glycosylation status and the cell line. As seen in figures 31 to 34, ZLLL treatment of cells indeed causes dramatic stabilization of both ERAD substrates in all cases (ZLLL increases the half life of RI332 in G3 cells for approx. 460% and in QC cells for approx. 415%. Similarly, ZLLL increases the half life of RI332-6HA in G3 cells for approx. 230% and in QC cells for approx. 990%).

Another observation in the fluorograms of cells grown in presence of ZLLL is that additional bands can be seen beneath the RI332 and RI332-6HA bands, respectively. Those bands represent accumulated glycoproteins with different trimming levels *(see also Kitzmüller et al., 2003)*. In the QC-RI332 cell line this observation is most extreme, but in the QC-RI332-6HA cell line it is inconspicuous. Similar differences exist also for the G3-RI332 and G3-RI332-6HA cell lines (for details see below).

5.3. Restoring the wild type phenotype in QC cells

In order to restore the wild type phenotype in the QC cells, the cells were incubated with an excess of galactose. It was described earlier that galactose is connected with a complex pathway that involves metabolites of galactose and glucose as well as a "cross-talk" between these two hexoses. Apparently, an excess of galactose can restore UDP-glucose levels and thus compensate the mutation in the UDP-glucose pyrophosphorylase gene (S.E. Moore, unpublished observations).

In regular glucose-containing medium, faster degradation of ERAD substrates is observed in QC cells when compared to G3 cells (figures 35 and 36). As seen in figures 37 to 41, the addition of galactose restores most effects seen in QC cells to those of wild type G3 cells (see above). Here, degradation becomes much slower in the presence of galactose – even slower than in G3 cells (see figure 41). Altered levels of sugar metabolites could be an explanation for this phenomenon. As seen in figure 42, the excess of galactose also restores the wild type fibroblast-like morphology of QC cells to that of G3 cells.

5.4. Interaction of ERAD substrates and CNX

In the previous part of the discussion, it became apparent that the ERAD substrates are degraded faster in QC cells than in G3 cells. It was postulated that the faster degradation is due to partial avoiding of the CNX cycle by the ERAD substrates in QC cells, which usually delays the retrotranslocation and subsequent degradation of misfolded proteins. In the following part, the results of the experiments analyzing the interaction between CNX and the model ERAD substrates *(see 4.3. ERAD substrate – calnexin association)* will be discussed.

In figure 51, it becomes obvious that the interaction between RI332/RI332-6HA and CNX is much stronger in the G3 cells than in the QC cells. This observation supports the hypothesis that the ERAD substrates in QC cells partially avoid entering the CNX cycle. It is also evident that the interactions are stronger at chase time point 5' than at chase time point 60'. This finding that is true for all cell lines is also plausible, since most of the misfolded proteins should have left the CNX cycle after the delayed activity of ER mannosidases. However, it is also discernible that the interaction between CNX and RI332-6HA lasts longer than the interaction between CNX and RI332 in the G3 cells. This would explain why less trimming variants of RI332-6HA are seen in the G3 cell line (figure 32), and why more trimming variants of RI332 are seen in the G3 cell line in the presence of ZLLL (figure 31). Due to prolonged interaction between RI332-6HA and CNX, the subsequent trimming reactions of RI332-6HA largely fail to appear.

From figures 43 to 50 it becomes evident that the efficiency of non-stringent co-immunoprecipitation is higher for the endogenous ribophorin I than for the soluble variants RI332 and RI332-6HA. Former studies have shown a preferential interaction

of the transmembrane protein CNX with membrane-bound substrates, whereas the soluble CRT is more frequently associated with substrates that are soluble in the lumen of the ER (Benyair, et al., 2011). This would explain the observations in figures 43 to 50 just described. However, no CRT antibody that worked in non-stringent IP was available to use instead of the CNX antibody to test this hypothesis.

In summary, the following conclusions can be drawn as to the degradation of the RI332 and RI332-6HA ERAD substrates in the Chinese hamster fibroblast cell lines G3 and QC:

- Faster degradation of the N-glycosylated ERAD substrates is observed in the QC cells compared to G3 cells under normal conditions (absence of inhibitors)
- Properly N-glycosylated ERAD substrates interact with CNX and enter the CNX cycle before they retrotranslocate to the cytosol where they are degraded by the proteasome
- Glycoproteins with three glucose molecules (G3 cells in the presence of CST) partially avoid entering the CNX cycle
- Degradation of ERAD substrates is accelerated in presence of glucosidase inhibitors in G3 cells, but not so in QC cells
- Degradation of ERAD substrates depends on mannosidase I in G3 cells, less so in QC cells
- Degradation of ERAD substrates depends on functional proteasomes
- The ERAD substrates interact stronger with CNX in G3 cells than in QC cells
- Galactose incubation of QC cells can restore the G3 phenotype

5.5. Intracellular localization of the ERAD substrates

The last section of the diploma thesis was dedicated to the intracellular localization of the ERAD substrates by indirect immunofluorescence and confocal laser scanning microscopy. Not only the localization of the two ERAD substrates (RI332 and RI332-6HA) under normal conditions in the cells was analyzed, but also whether interfering with the ER quality control by using drugs that inhibit initial processing of the N-linked glycan or proteasomal degradation affects the localization of the two ERAD model substrates.

Based on data from earlier publications, it could be well assumed that the ERAD substrates largely should show an ER localization, although (a) post-ER compartment(s) have been invoked in ERAD in the past. In the work of Lederkremer and colleagues, a so called quality control compartment that is a sub-compartment of the ER and contains a distinct set of ER chaperons has been postulated (Kamhi-Nesher, et al., 2001; Benyair, et al., 2011).

In this diploma thesis it should be tested whether the two ERAD substrates RI332 and RI332-6HA colocalize with markers of the ER, the ERIC and the Golgi apparatus using suitable antibodies for immunofluorescence. The analysis was based on sets of images for each condition that were evaluated using a colocalization software package from Zeiss followed by statistical analysis with SPSS; specifically two-sided t-tests of independent samples with appropriate colocalization coefficients were performed.

Just comparing the mean values of the appropriate colocalization coefficients, it became evident that there was very little colocalization between the ERAD substrates and the Golgi apparatus in all cell lines (mean values of less than 0,06; tables 14 and 17). Generally, the weighted colocalization coefficients gave even smaller numbers than the non-weighted ones. In contrast, there was considerable colocalization between the ERAD substrates ad the ER (mean values of more than 0,95; table 16), as would be expected. The colocalization between the ERAD substrates and the ERGIC was small (mean values of less than 0,009; table 15), comparable or perhaps only slightly above the colocalization between the ERAD substrates and the Golgi. Interestingly, there appears to be more colocalization between the ERAD substrates and the ERGIC in QC cells when compared to G3 cells (table 15; for a statistical comparison see below). This could indicate that the ER in the mutant QC cells is more “leaky” for glycoproteins than in G3 cells, perhaps due to the lack of glucosylation and thus the bypassing of the CNX cycle.

In table 14, the effects of CST (inhibitor of glucosidase I), KIF (inhibitor of ER mannosidase I) and ZLLL (inhibitor of the proteasome) on the colocalization of RI332 and Golgi apparatus in G3-RI332 and QC-RI332 cells are shown. Assuming that a t-test significance of less than 5% denotes a significant difference between the two

groups (control and inhibitor groups), a significant difference can be observed in the G3-RI332 cell line between the control group and the CST group (1% t-test significance for the non-weighted colocalization coefficients and 1,3% t-test significance for the weighted colocalization coefficients). As discussed earlier *(see 5.2. Effect of inhibitors on the ERAD substrate degradation)* the half life of RI332 decreases for approximately 33% in the presence of CST, which may be taken as an indication that the CNX cycle is partially avoided, because of the pre-incubation with CST. As a consequence, RI332 might be retrotranslocated to the cytosol faster in CST-treated cells which could account for the difference in colocalization of RI332 and the Golgi apparatus. A similar result was obtained with the tagged RI332-6HA, however, only for the weighted colocalization coefficient (0,1% t-test significance), whereas the non-weighted colocalization coefficient (79,0% t-test significance) appears to be an outlier in this case.

Surprisingly, the t-test significances of the non-weighted and weighted colocalization coefficient are not consistent for the colocalization of RI332 and the Golgi apparatus in KIF-treated G3 cells. A 25,3% t-test significance is notable for the non-weighted colocalization coefficient (no significant difference), whereas the t-test significance of the weighted colocalization coefficient is 0% (significant difference). No reasonable explanation is possible for this phenomenon.

Consistent statistical data are notable for the colocalization coefficients of RI332 and the Golgi in G3 cells in presence of ZLLL. The high values of the t-test (98% for the non-weighted and 61% for the weighted colocalization coefficients) indicate that there is no significant difference between these two groups (control and ZLLL group). This is the opposite observation than in the case of the control and CST group. A possible explanation for this observation could be that the RI332/Golgi apparatus colocalization is higher if the RI332 intracellular localization is extended in the ER (in absence of CST), but that its accumulation in the cytosol (in presence of ZLLL) does not affect the colocalization with the Golgi apparatus. This could be due to the relative close proximity of the Golgi apparatus and the ER in which RI332 is concentrated, whereas the retrotranslocated RI332 is more widespread in the cytosol.

Interfering with the ER quality control at all levels (inhibition of glucosidase I, ER mannosidase I and proteasome) causes a significant difference in the colocalization of RI332 and the Golgi apparatus. Plausible explanations for these observations are not easily possible.

Considering all other results (see tables 15 to 17), it is not possible to draw firm conclusions as to the influence of inhibitors on the intracellular localization of ERAD substrates in each case. The results concerning this part are not fully comprehensible, which could be due to methodical limitations (discussed below).

Similar observations are made in case of the colocalization coefficients for the comparisons of different antibody combinations among themselves. As expected, there is a significant difference between the HA.11/Giantin and HA.11/Calnexin combinations (see table 18). For all cell line comparisons (G3-RI332-6HA vs G3-RI332-6HA and G3-RI332-6HA vs. QC-RI332-6HA), this antibody combination shows 0% significance in the t-test (meaning that there is a significant difference). Such results were anticipated due to the fact that the Golgi apparatus is restricted to a small area, whereas the ER (Calnexin staining) is widely distributed. Different from this antibody combination, the combination of HA.11/Giantin and RI lum/CTR433 shows partially no significant difference. Ideally, no significant difference at all would be expected for this antibody combination, because both antibodies (Giantin and CTR433) specifically bind to the Golgi apparatus. However, the results shown in table 19 are not that obvious, because the data are not consistent. In two cell line combinations, the expected results appear (no significant differences). In other two cell line combinations, there is a significant difference between the two antibody combinations (with t-test significances of nearly 0%). CTR433 is a medial-Golgi marker (Birkeli, et al., 2003) and giantin can be also found in the cis-Golgi (Rodriguez-Gabin, et al., 2009), therefore it would be plausible to find no significant differences. Unfortunately, not all desirable comparisons of antibody combinations among themselves could be analyzed due to the lack of a suitable mouse monoclonal ER marker and a rabbit polyclonal ERGIC marker.

In all other antibody combination comparisons (see tables 20 to 22), the results are as anticipated. A significant difference is notable for i) the colocalization of

HA.11/Giantin vs. RI lum/ERGIC53 between all cell lines, ii) the colocalization of HA.11/Calnexin vs. RI lum/CTR433 between all cell lines, and iii) HA.11/Calnexin vs. RI lum/ERGIC53 between all cell lines.

It should be noted that the basis for stating colocalization or not is not entirely clear. This depends on several factors, apart from differences in background, varying signal intensities (that are widely compensated for in the so called weighted colocalization coefficients) certainly on the pixel size. Thus, a measure of "true" versus "coincidental" colocalization (the latter meaning that a "green" and a "red" signal are contained in the same pixel by coincidence, even though there is no colocalization) cannot be reliably given.

Taken together, the immunofluorescence and confocal laser scanning microscopy results clearly show a predominant ER localization of the ERAD substrates RI332 and RI332-6HA in G3 and QC cells. There is little colocalization with the ERGIC and perhaps even less with the Golgi apparatus. The effect of the inhibitors used on the localization of the ERAD substrates has not become entirely clear in each case during this study.

6. References

Alberts, B. et al., 2004. *Essential Cell Ciology.* 2nd edition, Gerland Science.

Alberts, B. et al., 2008. *Molecular Biology of the Cell.* 5th edition, Garland Science.

Anelli, T. & Sitia, R., 2008. Protein quality control in the early secretory pathway. *The EMBO journal,* Volume 28, pp. 315-327.

Avezov, E. et al., 2008. Endoplasmic Reticulum (ER) Mannosidase I Is Compartmentalized and Required for N-Glycan Trimming to Man5–6GlcNAc2 in Glycoprotein ER-associated Degradation. *Molecular Biology of the Cell,* Volume 19, pp. 216-225.

Bagola, K., Mehnert, M., Jarosch, E. & Sommer, T., 2011. Protein dislocation from the ER. *Biochimica et Biophysica Acta,* Volume 1808, pp. 925-936.

Beck, R., Ravet, M., Wieland, F. & Cassel, D., 2009. The COPI system: Molecular mechanisms and function. *FEBS Letters,* Volume 583, pp. 2701-2709.

Bedard, K., Szabo, E., Michalak, M. & Opas, M., 2005. Cellular Functions of Endoplasmic Reticulum Chaperones Calreticulin, Calnexin and ERp57. *International Review of Cytology,* Volume 245, pp. 91-121.

Benyair, R., Ron, E. & Lederkremer, G., 2011. Protein Quality Control, Retention, and Degradation at the Endoplasmic Reticulum. *International Review of Cell and Molecular Biology,* Volume 292, pp. 197-280.

Bethune, J., Wieland, F. & Moelleken, J., 2006. COPI-mediated Transport. Volume 211, pp. 65-79.

Birkeli, K. et al., 2003. Endosome-to-Golgi Transport Is Regulated by Protein Kinase A Type IIa. *The Journal of Biological Chemistry,* Volume 17, pp. 1991-1997.

Brodsky, J. & Skach, W., 2011. Protein folding and quality control in the endoplasmic reticulum: Recet lessons from yeast and mammalian cell systems. *Current Opinion in Cell Biology,* Volume 23, pp. 464-475.

Burda, P. et al., 1999. Ordered assembly of the asymmetrically branched lipid-linked oligosaccharide in the endoplasmic reticulum is ensured by the substrate specificity of the individual glycosyltransferases. *Glycobiology,* Volume 9, pp. 617-625.

Buxbaum & Engelbert, 2007. *Fundamentals of Protein Structure and Function.* 1st edition, Springer.

Caramelo, J. & Parodi, A., 2008. Getting In and Out from Calnexin/Calreticulin Cycles. *The Journal of Biological Chemistry,* Volume 283, pp. 10221-10225.

Chakrabarti, A., Chen, A. & Varner, J., 2011. A Review of the Mammalian Unfolded Protein Response. *Biotechnology and Bioengineering,* Volume 108, pp. 2777-2793.

Chotwiwatthanakun, Ngopon, Unajak & Jitrapakdee, 2008. The ribophorin I from Penaeus mondon shrimp: cDNA cloning, expression and phylegenetic analysis. *Comparative Biochemistry and Physiology,* Volume 150, pp. 331-337.

Dalbey, R. & Von Heijne, G., 2002. *Protein Targeting Transport & Translocation.* 1st edition, Academic Press.

D'Alessio, C., Caramelo, J. & Parodi, A., 2010. UDP-GlC: glcoprotein glucosyltransferase-glucosidase II, the ying-yang of the ER quality control. *Seminars in Cell & Developmental Biology,* Volume 21, pp. 491-499.

de Virgilio, M., Weninger, H. & Ivessa, N. I., 1998. Ubiquitination is required for the retro-translocation of a short-lived luminal endoplasmic reticulum glycoprotein to the cytosol for degradation by the proteasome. *The journal of biological chemistry,* Volume 273, pp. 9734-9743

Diehl, A., Fuchs, S. & Koumenis, C., 2011. The Cell Biology of the Unfolded Protein Response. *Gastroenterology,* Volume 141, pp. 38-41.

Ellgaard, L. & Frickel, E., 2003. Calnexin, Calreticulin, and ERp57: teammates in glycoprotein folding. *Cell Biochemistry and Biophysics,* Volume 39, pp. 223-247.

Ellgaard, L. & Helenius, A., 2003. Quality Control in the Endoplasmic Reticulum. *Molecular Cell Biology,* Volume 4, pp. 181-191.

Ermonval, M. et al., 2001. N-glycan structure of a short-lived variant of ribophorin I expressed in the MadIA214 glycosylation-defective cell line reveals the role of a mannosidase that is not ER mannosidase I in the process of glycoprotein degradation. *Glycobiology,* Volume 11, pp. 565-576.

Fei, W. et al., 2009. Conditions of endoplasmic reticulum stress stimulate lipid droplet formation in Saccharomycescerevisiae. *Biochemical Journal,* Volume 424, pp. 61-67.

Flores-Diaz, M. et al., 1997. Cellular UDP-glucose deficiency caused by a single point mutation in the UDP-glucose pyrophosphorylase gene. *The Journal of Biological Chemistry,* Volume 272, pp. 23784-23791.

Flores-Diaz, M. et al., 2004. A cellular UDP-glucose deficiency causes overexpression of glucose/oxygen-regulated proteins independent of the endoplasmic reticulum stress elements. *The Journal of Biological Chemistry,* Volume 279, pp. 21724-21731.

Freeze, H., 2007. Congenital Disorders of Glycosylation: CDG-I, CDG-II, and Beyond. *Current Molecular Medicine,* Volume 7, pp. 389-396.

Freeze, H. & Aebi, M., 2005. Altered glycan structures: the molecular basis of congenital disorders of glycosylation. *Current opinion in structural biolog,* Volume 15, pp. 490-498.

Freeze, H., Eklund, E., Ng, B. & Patterson, M., 2012. Neurology of inherited glycosylation disorders. *The Lancet Neurology,* Volume 11, pp. 453-466.

Frenkel, Z., Gregory, W., Kornfeld, S. & Lederkremer, G., 2003. Endoplasmic Reticulum associated degradation of Mammalian Glycoproteins Involves Sugar Chain Trimming to Man6-5GlcNAc2. *The Journal of biological chemistry,* Volume 278, pp. 34119-34124.

Gauss, R., Sommer, T. & Jarosch, E., 2006. The Hrd1p ligase complex forms a linchpin between ER-lumenal substrate selection and Cdc48p recruitment. *The EMBO Journal,* Volume 25, pp. 1827-1835.

Gerdes, H.-H., 2008. Membrane traffic in the secretory pathway. *Cellular and Molecular Life Sciences,* Volume 65, pp. 2779-2780.

Gilmore, R., 2011. Structural biology: Porthole to catalysis. *Nature,* Volume 474, pp. 292-293.

Glick, B., 2002. The Secretory Pathway. In: *Protein Targetin, Transporti & Translocation.* Academic Press.

Haeuptle, M. & Hennet, T., 2009. ongenital Disorders of Glycosylation: An Update on Defects Affecting the Biosynthesis of Dolichol-Linked Oligosaccharides. *Human Genome Variation Society,* Volume 30, pp. 1628-1641.

Hebert, D., Bernasconi, R. & Molinari, M., 2009. ERAD substrates: Which way out?. *Seminars in Cell & Developmental Biology,* Volume 21, pp. 526-532.

Hennet, T., 2012. Diseases of glycosylation beyond classical conenital disorders of glycosylation. *Biochemica et Biophysica Acta,* Volume 1820, pp. 1306-1307.

High, S. & Wilson, C., 2007. Ribophorin I acts as a substrate-specific facilitator of N-Glycosylation. *Journal of Cell Science,* Volume 120, pp. 648-657.

Hosokawa, N., Kamiya, Y. & Kato, K., 2010. The role of MRH domain-containing lectins in ERAD. *Glycobiology,* Volume 20, pp. 651-660.

Hosokawa, N. et al., 2007. Stimulation of ERAD of misfolded null Hong Kong α1-antitrypsin by Golgi α1,2-mannosidases. *Biochemical and Biophysical Research Communications,* Volume 362, pp. 626-632.

Hsu, V. & Yang, J.-S., 2009. Mechanisms of COPI vesicle formation. *FEBS Letters,* Volume 583, pp. 3758-3763.

Hughes, H. & Stephens, D., 2008. Assembly, organization, and function of the COPII coat. *Histochem Cell Biology,* Volume 129, pp. 129-151.

Jaeken, J., 2011. Congenital disorders of glycosylation (CDG): it's (nearly) all in it!. *Journal of inherited metabolic disease,* Volume 34, pp. 853-858.

Jaeken, J., Hennet, T., Matthijs, G. & Freeze, H., 2009. CDG nomenclature: Time for a change!. *Bichemica et Biophysica Acta - Molecular Basis of Disease,* Volume 1729, pp. 825-826.

Jessop, C. et al., 2009. Substrate Specificity of the Oxidoreductase ERp57 Is Determined Primarily by Its Interaction with Calnexin and Calreticulin. *The journal of biological chemistry,* Volume 284, pp. 2194-2202.

Kamhi-Nesher, S. et al., 2001. A novel quality control compartment derived from endoplasmic reticulum. *Molecular Biology of the Cell,* Volume 12, pp. 1711-1723.

Kampmann, M. & Blobel, G., 2009. Nascent Proteins Caught in the Act. *Science,* Volume 326, pp. 1352-1353.

Kartberg, F. et al., 2005. Commuting between Golgi cisternae—Mind the GAP!. *Biochimica et Biophysica Acta,* Volume 1744, pp. 351-363.

Kaser, A., Flak, M., Tomczak, M. & Blumberg, R., 2011. The unfolded protein response and its role in intestinal homeostasis and inflammation. *Experimental Cell Research,* Volume 317, pp. 2772-2779.

Kitzmüller, C. et al., 2003. Processing of N-linked glycans during endoplasmic-reticulum-associated degradation of a short lived variant of ribophorin I. *The Biochemical Journal,* Volume 376, pp. 687-696.

Kleizan, B. & Braakman, I., 2004. Protein folding and quality control in the endoplasmic reticulum. *Current Opinion in Cell Biology,* Volume 16, pp. 343-349.

Lederkremer, G., 2009. Glycoprotein folding, quality control and ER-associated degradation. *Current Opinion in Structural Biology,* Volume 19, pp. 515-523.

Lodish, H., Berk, A. & Matsudaira, P., 2004. *Molecular Cell Biology.* 5th edition, Palgrave Macmillan.

Lynes, E. & Simmen, T., 2011. Urban planning of the endoplasmic reticulum (ER): how diverse mechanisms segregate the many functions of the ER. *Biochemica et Biophysica Acta,* Volume 1813, pp. 1893-1905.

Määttänen, P., Gehring, K., Bergeron, J. & Thomas, D., 2010. Protein quality control in the ER: The recognition of misfolded proteins. *Seminars in Cell & Developmental Biology,* Volume 21, pp. 500-511.

Michalak, M. et al., 2009. Calreticulin, a multi-process calcium-buffering chaperone of the endoplasmic reticulum. *Biochem Journals,* Volume 417, pp. 651-666.

Mohorko, E., Glockshuber, R. & Aebi, M., 2011. Oligosaccharyltransferase: the central enzyme of N-linked protein glycosylation. *Journal of inherited metabolic disease,* Volume 34, pp. 869-878.

Murshid, A. & Presley, J., 2004. ER-to-Golgi transport and cytoskeletal interactions in animal cells. *Cellular and Molecular Life Science,* Volume 61, pp. 133-145.

Ng, W. et al., 2007. Characterization of the proteasome interaction with the Sec61 channel in the endoplasmic reticulum. *Journal of Cell Science,* Volume 120, pp. 682-691.

Nsibu, N. et al., 2008. Clinical and biochemical features in a Congolese infant with conenital disorder of glucosylation (CDG)-IIx. *European Journal of Paediatric Neurology,* Volume 12, pp. 257-261.

Olzmann, J. & Kopito, R., 2011. Lipid droplet formation is dispensable for endoplasmic reticulum associated degradation. *The journal of biological chemistry,* Volume 286, pp. 27872-27874.

Pearse, B. & Hebert, D., 2010. Lectin chaperones help direct the maturation of glycoproteins in the endoplasmic reticulum. *Biochimica et Biophysica Acta,* Volume 1803, pp. 684-693.

Pucadyil, T. & Schmid, S., 2009. Conserved Functions of Membrane Active GTPases in Coated Vesicle Formation. *Science,* Volume 325, pp. 1217-1220.

Raasi, S. & Wolf, D., 2007. Ubiquitin receptors and ERAD: A network of pathways to the proteasome. *Seminars in cell & developmental biology,* Volume 18, pp. 780-791.

Reynaud, E. & Simpson, J., 2002. Navigating the secretory pathway. *EMBO reports,* Volume 3, pp. 828-833.

Rodriguez-Gabin, A., Yin, X. & Larocca, J., 2009. Transport of mannose-6-phosphate receptors from the trans-Golgi network to endosomes requires Rab31. *Experimentall Cell Research,* Volume 315, pp. 2215-2230.

Schröder, M. & Kaufman, R., 2005. ER stress and the unfolded protein response. *Fundamental and Molecular Mechanisms of Mutagenesis,* Volume 569, pp. 29-63.

Schwarz, F. & Aebi, M., 2011. Mechanisms and principles of N-linked protein glycosylation. *Current Opinion in Structural Biology,* Volume 21, pp. 576-582.

Sharma, V. et al., 2011. Phosphomannose Isomerase Inhibitors Improve N-Glycosylation in Selected Phosphomannomutase-deficient Fibroblasts. *The Journal of Biological Chemistry,* Volume 286, pp. 39431-39439.

Smith, M., Ploegh, H. & Weissman, J., 2011. Road to ruin: Targeting Proteins for Degradation in the Endoplasmic Reticulum. *Science,* Volume 334, pp. 1086-1090.

Spang, A., 2008. The life cycle of a transport vesicle. *Cellular and Molecular Life Sciences,* Volume 65, pp. 2781-2789.

Stigliano, I. et al., 2011. Glucosidase II and N-glycan mannose content regulate the half lives of monoglucosylated species in vivo. *Molecular Biology of the Cell,* Volume 22, pp. 1810-1823.

Stolz, A. & Wolf, D., 2010. Endoplasmic reticulum associated protein degradation: A chaperone assisted journey to hell. *Biochimica et Biophysica Acta,* Volume 1803, pp. 694-705.

Tsai, Y. & Weissman, A., 2011. Ubiquitylation in ERAD: Reversing to go forward?. *PLoS Biology,* Volume 9, pp. 1-5.

Ushioda, R. & Nagata, K., 2011. The Endoplasmic Reticulum-Associated Degradation and Disulfide Reductase ERdj5. *Methods in Enzymology,* Volume 490, pp. 235-258.

Vembar, S. & Brodsky, J., 2008. One step at a time: endoplasmic reticulum-associated degradation. *Nature,* Volume 9, pp. 944-957.

Walter, P. & Ron, D., 2011. The Unfolded Protein Response: From Stress Pathway to Homeostatic Regulation. *Science,* Volume 9, pp. 1081-1086.

Wang, W.-A., Groenendyk, J. & Michalak, M., 2012. Calreticulin signaling in health and disease. *The International journal of Biochemistry & Cell Biology,* Volume 44, pp. 842-846.

Williams, D., 2006. Beyond lectins: the calnexin/calreticulin chaperone system of the endoplasmic reticulum. *Journal of Cell Science,* Volume 119, pp. 615-623.

Wilson, C. & High, S., 2007. Ribophorin I acts as a substrate-specific facilitator of N-glycosylation. *Journal of Cell Science,* Volume 120, pp. 648-657.

Wilson, C. & Roebuck, Q. H. S., 2008. Ribophorin I regulates substrate delivery to the oligosaccharyltransferase core. *PNAS,* Volume 105, pp. 9534-9539.

Woods, A., Woods, C. & Snow, T., 2012. Congenital disorders of glycosylation. *Avances in Neonatal Care,* Volume 12, pp. 90-95.

Yu, X., Breitman, M. & Goldberg, J., 2012. A Structure-Based Mechanism for Arf1-Dependent Recruitment of Coatomer to Membranes. *Cell,* Volume 148, pp. 530-542.

7. Abstract

7.1. Abstract - English version

During the journey of secretory proteins from the cytosol to their final destinations, they must pass a number of cellular compartments in which folding, modification and assembly occurs. The endoplasmic reticulum (ER) is not only an organelle in the secretory pathway where folding, modification and assembly occur, but also a compartment in which quality control (ERQC) of protein folding takes place.

Of central importance for the ER quality control is the so-called calnexin cycle (CNX cycle). Unfolded and misfolded glycoproteins enter the CNX cycle which may allow them to fold properly. Only glycoproteins with specific oligosaccharide motifs can enter and leave this cycle. Trimming of the oligosaccharides determines the destiny of the glycoproteins, making glycosylation essential for the fate of the secretory proteins.

This diploma thesis is focused on understanding the importance of glycosylation (more precise glucosylation) for ERQC and especially ER-associated degradation (ERAD). For this purpose, the destiny of two potential ERAD substrates (RI332 and RI332-6HA) was analyzed in two different Chinese hamster fibroblast cell lines. One cell line (G3) has a fully operative glycosylation, while the other cell line (QC) is not able to glucosylate the glycoproteins.

Results obtained during this diploma thesis clearly point to the importance of glucosylation in context of ERAD. Misfolded glycoproteins which are not glucosylated are partially able to avoid the CNX cycle. As a consequence, the ERAD substrates enter the degradative pathway faster and thus have a half life that is two- to three- times shorter. It could be further shown that the ERAD substrates are dramatically stabilized when mannose trimming of the oligosaccharide is prevented in G3 cells, thus keeping the glycoproteins in the CNX cycle. Stabilization is also observed when the proteasome is inhibited.

The results of this diploma thesis demonstrate a stronger interaction of mono-glucosylated glycoproteins with CNX as compared to non-glucosylated glycoproteins,

and that this interaction is limited in time. In addition, it could be shown that galactose is able to revert the glucosylation deficiency in QC cells.

In the last part of this diploma thesis, the intracellular localization of the two model ERAD substrates was analyzed. For this purpose, the immunolabeled RI332 and RI332-6HA proteins were visualized by microscopy, and their relative colocalization with cellular compartments (ER, ER – Golgi - intermediate compartment (ERGIC) and Golgi apparatus) was determined. Both ERAD substrates are predominantly located in the ER, and interfering with the ER quality control seems to affect their localization in a not fully coherent way.

7.2. Abstract (Zusammenfassung) - German version

Während des Transports von sekretorischen Proteinen vom Zytosol zu deren endgültigen Destinationen, durchqueren sie mehrere zelluläre Kompartimente, in denen die Proteine gefaltet, modifiziert und assembliert werden. Das endoplasmatische Retikulum (ER) ist nicht nur das Organell, wo die Faltung, Modifizierung und Assemblierung von Proteinen stattfindet, sondern auch das Kompartiment, wo die Qualitätskontrolle (ERQC) erfolgt.

Von zentraler Bedeutung für die ERQC ist der sog. Calnexin Zyklus (CNX Zyklus). Ungefaltete und missgefaltete Proteine gelangen in den CNX Zyklus, der ihnen Zeit gibt sich richtig zu falten. Den CNX Zyklus können nur Proteine mit spezifischen Oligosaccharid Motiven betreten und verlassen. Das Trimmen des Oligosaccharids entscheidet über die Zukunft des Glycoproteins, wodurch die Glykosylierung von großer Bedeutung für das Schicksal sekretorischer Glykoproteine ist.

Diese Diplomarbeit befasst sich mit der Rolle der Glykosylierung (bzw. der Glukosylierung) in der ERQC, und vor allem für den ER- assoziierten Proteinabbau (ERAD). Dazu wurde das Schicksal von zwei potentiellen ERAD Substraten (RI332 und RI332-6HA) in zwei unterschiedlichen Zelllinien von Chinesischen Hamster Fibroblasten analysiert. Die G3 Zelllinie besitzt eine voll funktionsfähige Glykosylierung, während die QC Zelllinie in der Glukosylierung defekt ist.

Die während dieser Diplomarbeiten erhaltenen Resultate deuten klar auf die Wichtigkeit der Glukosylierung im Kontext von ERAD hin. Missgefaltete Glykoproteine, die nicht glukosyliert werden, können teilweise den CNX Weg umgehen. Als Konsequenz gelangen diese ERAD Substrate schneller in den Abbauweg, wodurch sie um das Zwei- bis Dreifache kürzere Halbwertszeiten haben. Es konnte weiters gezeigt werden, dass die ERAD substrate dramatisch stabilisiert werden, wenn das Mannose – Trimming des Oligosaccharids in G3 Zellen blockiert wird, wodurch die Glykoproteine im CNX Zyklus gebunden bleiben. Stabilisierung erfolgt auch nach Inhibierung des Proteasoms. Die Resultate der Diplomarbeit deuten auch auf eine stärkere, aber zeitlich begrenzte, Interaktion von mono-glukosylierten Proteinen mit CNX hin, im Unterschied zur praktisch fehlenden Interaktion von nicht glukosylierten Proteinen mit CNX. Weiteres konnte gezeigt

werden, dass ein Überschuss an Galaktose den Glukosylierungs- Defekt in QC Zellen kompensieren kann.

Im letzten Teil der Diplomarbeit wurde die intrazelluläre Lokalisierung der zwei ERAD Substrate analysiert. Dafür wurden die mit Antikörpern markierten Substrat-Proteine (RI332 und RI332-6HA) mikroskopisch visualisiert, und die relative Colokalisierung mit zellulären Kompartimenten ermittelt (ER, ER – Golgi – Intermediär – Kompartiment (ERGIC) und Golgi – Apparat). Die beiden ERAD – Substrate lokalisieren überwiegend zum ER und ein Einfluss der pharmakologischen Interventionen von ERQC auf die Lokalisierung war nicht in jedem Fall eindeutig erkennbar.

8. Acknowledgment

Primarily, I want to express my gratitude to Ervin N. Ivessa for giving me the opportunity to work on this project, for his tireless support and help along the way. Equally, I extend my thanks to Anette and Wolfgang Hagemann, whose grant made my studying in Vienna possible at all.

I also want to thank my colleagues at the Max F. Perutz Laboratories for their support and advice. A note of thanks goes also to the laboratory of Peter Ambros at the Children's Cancer Research Institute for having been sympatethic about my unfinished diploma work and the opportunity to start my PhD project.

Last but not least, I owe my utmost gratitude to my wife Edina and my parents Tima and Nedim for their unswerving understanding, support, encouragement, inspiration and love.

9. Curriculum vitae

9.1. Personal data

First name / Surname:	Fikret Rifatbegović
Adress:	Juchgasse 32/7, 1030 Vienna
E-Mail adress:	f.rifatbegovic@gmail.com
Nationality:	Bosnia and Herzegovina
Date and place of birth:	06.05.1984 in Brčko, Bosnia and Herzegovina
Gender:	Male

9.2. Education

August 2012 – running	PhD study at the Children's Cancer Research Institute (CCRI) in Vienna
April 2011 – April 2012	Diploma thesis: "Absence of glucosylation on N-linked glycans: consequences for ER-associated degradation (ERAD)" under supervision of Ao. Univ.-Prof. DI Dr. N. Erwin Ivessa at MAX F. PERUTZ LABORATORIES (MFPL), University of Vienna & Medical University of Vienna (MUW).
October 2005 – April 2011	Molecular Biology diploma study (A490) at the University of Vienna
September 2000 – May 2004	Grammar School, Sarajevo, Bosnia and Hercegovina
1996 – 2000	Elementary school, Sarajevo, Bosnia and Hercegovina
1992 – 1996	Elementary school, Germany

9.3. Work experience

May 2012 – July 2012	Student apprentice at St. Anna Kinderkrebsforschung (Children's cancer research institute), group of Prof. Ambros
February 2011 – April 2011	Student apprentice at St. Anna Kinderkrebsforschung (Children's cancer research institute), group of Prof. Ambros
Sept. 2010–Nov. 2010	Student apprentice at Max F.Perutz Laboratories (MFPL), University of Vienna, Group of Prof. Ivessa
March 2010 – April 2010	Student apprentice at the Vienna Institute of Biotechnology, BOKU, under supervision of Dr. Guadalupe Pinar